UNIVERSITÀ DELLA CALABRIA

UNIVERSITA' DELLA CALABRIA

Dipartimento di Fisica

Dottorato di Ricerca in

Scienze e Tecnologie Fisiche, Chimiche e dei Materiali

CICLO

XXXII

TITOLO TESI

Current anomalies and signatures of zero-energy excitations in onedimensional superconducting systems

Settore Scientifico Disciplinare FIS07

Coordinatore: Ch.ma Prof. ssa Gabriella Cipparrone

Firma ____ Firma oscurata in base alle linee guida del Garante della privacy

Supervisore/Tutor: Ch.mo Prof. Domenico Giuliano

Firma___ Firma oscurata in base alle linee guida del Garante della privacy

Dottorando: Dott./ssa Rosa Giuliano

Firma . Firma oscurata in base alle linee guida del Garante della privacy

Current anomalies and signatures of zero energy excitations in onedimensional superconducting systems

Abstract:

I sistemi monodimensionali superconduttivi sono terreno fertile sia per lo studio teorico di fenomeni esotici, sia per le innumerevoli applicazioni ingegneristiche a cui possono dare luogo.

In questo lavoro di tesi, l'attenzione sarà posta verso questo genere di sistemi dal punto di vista teorico, approfondendo ed analizzando due tipi diversi di superconduttività (in onda s ed in onda p) in sistemi monodimensionali con simmetrie differenti.

Nel primo argomento trattato, si propone un modello di superconduttore in onda p, con simmetria ad anello ed attraversato da un flusso magnetico. In condizioni particolari, osservando lo spettro energetico del sistema, si nota la comparsa di modi ad energia zero, i cosiddetti Modi di Majorana, ad oggi grande argomento di studio nella fisica della materia condensata per le loro possibili implementazioni in qbit e porte logiche e perché non abbiamo ancora evidenze sperimentali della loro presenza (nonostante vi siano diversi esperimenti in atto) nella fisica delle alte energie. Il device così presentato diventa quindi uno strumento utilissimo per la rilevazione e lo studio di questi modi ad energia zero, utilizzando come quantità misurabile la corrente persistente indotta dal flusso magnetico. Infatti, essendo la corrente la derivata dell'energia dello stato fondamentale, le informazioni che si sono ottenute guardando allo spettro energetico, vengono automaticamente tradotte e ricalcate nella forma della corrente, la quale, quando si manifestano i Modi di Majorana nel sistema, presenta delle evidentissime discontinuità. Nel lavoro di tesi, oltre a fornire una possibile applicazione sperimentale, in cui basta usare un magnetometro per effettuare la misura in modo non invasivo, è stato proposto un modello analitico per ottenere una formula per la corrente persistente utilizzando la matrice di trasferimento del sistema. Ovviamente, la manifestazione dei modi ad energia zero in un sistema finito-dimensionale non è banale e si manifesta solo per speciali valori del flusso magnetico che attraversa l'anello. Il modello quindi proposto diviene decisamente comodo per le implementazioni sperimentali. Va notato, tuttavia, che nei casi reali i sistemi non sono mai perfettamente aderenti al modello teorico che si propone. Per questo motivo, il passo successivo è stato quello di studiare lo stesso modello in presenza di disordine. Quello che è emerso dall'analisi è che per una quantità di disordine moderata, è ancora possibile rilevare i Modi di Majorana nel sistema attraverso la corrente persistente. Effettuando un'analisi statistica del sistema, è stato inoltre possibile fornire un diagramma di fase in cui riportiamo i valori che può assumere l'ampiezza del disordine al variare del potenziale chimico del sistema per mantenere la presenza dei modi ad energia zero.

Nella seconda parte della tesi, l'attenzione si volge invece ai superconduttori in onda s e, in particolare, a giunzioni di metalli superconduttori-normali-superconduttori (SNS). In sistemi con questa simmetria, è previsto che scorra una corrente, detta corrente Josephson, anche in assenza di differenza di potenziale ai capi del filo. Questo fenomeno, che ad oggi trova largo spazio tra le implementazioni ingegneristiche, è legato alla differenza di fase tra il metallo superconduttore e quello normale. Allo stesso modo, si può manifestare anche tra due superconduttori che hanno una differenza di fase diversa da zero. Tuttavia, in particolari condizioni (quale la presenza dello spin-orbita e dell'effetto Zeeman), si può avere un'anomalia nella corrente ed avere, anche con differenza di fase nulla, una certa quantità di corrente che fluisce nel sistema. Questo effetto prende il nome di corrente Josephson anomala. Per studiarla ed ampliare le conoscenze su questo fenomeno, è stato pensato un sistema SNS in cui nella zona normale (N) sono presenti interazione spin-orbita, effetto Zeeman ed un confinamento armonico. L'approccio utilizzato è stato quello del formalismo della matrice di scattering per ottenere le equazioni che sono state poi risolte numericamente variando i parametri del sistema. In questo modo, non solo possiamo studiare l'anomalia della corrente Josephson, che risulterà essere evidente dai risultati riportati dai grafici di densità presenti nel lavoro di tesi, ma anche ciò che accade nel caso in cui si considerino più canali di scattering. Ciò che è emerso, alla fine dell'analisi, è che quando si considera un numero di canali di scattering maggiore di 1, la corrente, oltre a presentare la sua anomalia, presenta anche una asimmetrizzazione nella sua forma. Ciò implica che il movimento delle particelle da sinistra a destra è diverso dal moto opposto che queste hanno nella giunzione. Se ne conclude che un sistema così strutturato consente la prototipazione di un diodo superconduttivo.

Contents

Chapter 1

Introduction

Superconductivity was discovered in 1911 by Heike Kamerlingh Onnes, who was studying the resistance of solid mercury at cryogenic temperatures using the recently produced liquid helium as a refrigerant. At the temperature of 4.2 K, he observed that the resistance abruptly disappeared (1). In the subsequent decades, superconductivity was observed in several other materials: in 1913, lead was found to superconduct at 7 K, and in 1941, niobium nitride was found to superconduct at 16 K. What was before then observed experimentally is that the electrical resistance of a metallic conductor decreases gradually as temperature is lowered.

In ordinary conductors, such as copper or silver, this decrease is limited by impurities and other defects. Even near 0 K, a real sample of a normal conductor shows some resistance. In a superconductor, the resistance drops abruptly to zero when the material is cooled below a certain temperature T_C, called critical temperature, which varies from material to material. An electric current through a loop of superconducting wire can persist indefinitely with no power source. But the great efforts have been devoted to finding out the properties of superconductors. The important step occurred in the 30s, when Meissner and Ochsenfeld discovered that superconductors expelled applied magnetic fields, a phenomenon which has come to be known as the Meissner effect (2). The occurrence of this effect indicates that superconductivity cannot be understood simply as the idealization of perfect conductivity in classical physics. Afterwards, Fritz and Heinz London showed that the Meissner effect was a consequence of the minimization of the electromagnetic free energy carried by superconducting current (3).Thas was the first theory for superconductivity with which we can obtain the dependence of the magnetic field inside the superconductor on the distance to the surface.

During the 1950s, the interest in the phenomena of superconductivity led to the study and formulation of different theories. In those years, what we call now "conventional superconductors" were fully understood. Even today, the most significant and important models for superconductors are the phenomenological Ginzburg-Landau theory and the microscopic BCS theory (4; 5). The first one (6), which combined Landau's theory of second-order phase transitions with a Schrödinger-like wave equation, had great success in explaining the macroscopic properties of superconductors.

In particular, Abrikosov showed that Ginzburg-Landau theory predicts the division of superconductors into the two categories now referred to as Type I and Type II, based on their response to the applied magnetic fields. In the same years, Maxwell and Reynolds found that the critical temperature of a superconductor depends on the isotopic mass of the constituent element (7; 8).This important discovery pointed to the electron-phonon interaction as the microscopic mechanism responsible for superconductivity. The second theory was finally proposed in 1957 by Bardeen, Cooper and Schrieffer (9). This BCS theory explained the superconducting current as a superfluid of Cooper pairs, pairs of electrons interacting through the exchange of phonons. Abrikosov, Ginzburg, Landau, Bardeen, Cooper and Schrieffer were awarded the Nobel Prize for their work.

Generalizations of BCS theory for conventional superconductors form the basis for understanding of the phenomenon of superfluidity, because they fall into the lambda transition universality class. The extent to which such generalizations can be applied to unconventional superconductors is still controversial. For all the superconductors discovered so far, the flux quantization experiments have, indeed, provided strong evidence that the superconductivity arises from the formation of Cooper pairs by electrons. However, the mechanism for glueing electrons depends on the material which we are considering. In a conventional superconductor, the Cooper pairs are, as we have already illustrated, mediated by the lattice vibrational modes, the phonons; in this case, we have the so-called "$s-wave$" pairing. Alternately,in unconventional superconductors, they are mediated via the fluctuations of electron spins and we can have "$p, d, f-wave$" superconducting pairing. Accordingly to this, the pairing potential that describes the Cooper pairs orbital motion can be different. As we will see, indeed, different kinds of superconductivity rise up different and exotic behaviour and states of matter. Unconventional superconductors can be interesting because they include high-temperature cuprates, heavy fermion inter-metallic compounds, and iron-based superconductors. This kind of materials are accompanied with multiple electronic phases, a typical feature of strong correlated matter. Although the BCS theory was originally developed for conventional superconductors, we can use it also for the unconventional ones. This is the important basic assumption for the Bogolioubov- de Gennes (BdG) approach to superconductivity. This formalism relies on the assumption there exist well-defined quasi-particles in the superconductor. It has the advantage to provide information about the one-particle excitations of the system. The quasi particle excitation spectrum, indeed, can be derived together with the corresponding quasi-particle amplitudes. The BdG formalism is essentially correct in the weak-coupling regime, but also yields qualitative results in situations of very strong coupling. The interest in microscopic electronic structure calculations of this type was revived by low-temperature scanning-tunneling-microscopy (STM) experiments which provided extremely detailed, spatially resolved, excitation spectra around a single impurity, near the interfaces of superconductors' junctions or near their surfaces, or around a vortex core in the presence of an Abrikosov flux lattice.

In recent years, superconductivity has become increasingly popular. As the experimental realization became more and more achievable , the various properties of the

superconductors began to appeal to industries. For this reason, the demand for superconducting metals and devices has increased. A typical use of superconductors is to build magnet coils: the use of superconducting cables greatly reduces their size, weight and energy consumption for the same magnetic field strength. Obviously the construction and operation of a superconducting magnet is much more expensive, requiring it to be kept at a temperature lower than the critical temperature. A typical application of this type concerns the construction of the large toroids of clinical nuclear magnetic resonance systems. Superconductors have been used in experimental conditions even on a large scale in large machines such as CERN accelerators, they have been used in LEP conductor cables and currently in the LHC where it is necessary to have very intense magnetic fields (about $9T$). Potentially, the possible developments are enormous in fields such as accumulation and transmission of energy, electric motors and realization of large magnetic fields.

However, the use of superconductors in a trivial way is only the tip of the iceberg. Various studies have revealed more and more remarkable properties of the superconductors that have brought them even more in vogue.

For example, after the discovery of Josephson junctions (18; 19), there was been a real revolution in the field of superconductor applications. The extreme sensitivity, precision and speed of transmission due to the presence of electro-magnetic fields is used in these devices to give extremely precise measurements of these fields, or to obtain localized switching to superconducting (or from superconducting to normal) extremely sensitive and fast; given the nanometric (and quantum) nature of the device the switching times are extremely short (picoseconds). For example, the junctions are used in the realization of devices for measuring the magnetic field (SQUID) capable of measuring infinitesimal magnetic field values and used, also in the medical field, for some types of analysis. These junctions are also used in particle detectors to detect very small temperature changes caused by interaction with the particle to be detected. When a particle passes through the detector, it gives it energy that causes a temperature rise. By measuring the change in resistance of the detector, which is kept near the critical temperature, it can be detected when a particle crosses the sensor.

Moreover, in very recent times, the first quantum processor based on Josephson junctions was announced (21; 22; 23; 24). Indeed, as we will see, Josephson junctions can be used to made prototypes for electronic components, such as diodes or transistors. Examples of circuits using Josephson junctions include digital circuits based on superconducting logic (i.e. a class of logic circuits or logic gates that use the unique properties of superconductors, including zero-resistance wires, ultrafast Josephson junction switches, and quantization of magnetic flux (fluxoid)), superconducting quantum computing circuits, superconducting analog circuits, and so on (20).

However, the properties of superconductors do not only reduce to the Josephson or zero resistance current. As mentioned above, there are different types of superconductivity and a special consideration must be made for p-wave superconductors, since they reserve very interesting physical and applicative properties. Indeed, in 2001 Kitaev proposed a one-dimensional p-superconductive model in which zero-energy modes

emerged (142), the Majorana modes (10). The toy-model has become a starting point for countless research and experimental realizations in search of further proof of the existence of the Majorana modes.

The research on Majorana modes arise after his proposal in 1937, when, trying to complete the standard model, he proposed a kind of particles that were antiparticles of themselves (10). Although today there are several experiments that attempt to prove the existence of Majorana fermions through double beta decay (such as GERDA and NEMO-3), assuming neutrinos to potential candidates, there are no experimental proofs in the field of high-energy physics. However, starting from Kitaev formulation, an experimental measurement of the equivalent of Majorana fermions in condensed matter (precisely, Majorana modes) was proposed in the last years (51). This measure is currently subject to various criticisms from the scientific community, but unquestionably remains a valuable starting point. Advances in experimental realizations of such Majorana modes were facilitated by various proposals which involved superconductor-topological insulator interfaces, proximity-induced superconductivity in spin-orbit coupled wires, ferromagnetic atoms in proximity to superconductor. Several reports of experiments show highly suggestive evidence of the existence of the Majorana modes in these systems (56). Moreover, conclusive evidence of their existence is of great interest from the perspective of topological quantum computing given their non-Abelian braiding statistics (57; 58) and that they form a natural basis for topological qubits. The theoretical prediction that the combination of spin-orbit coupling, Zeeman spin splitting, and ordinary s-wave superconductivity could lead to an effective topological superconducting phase under appropriate (and experimentally achievable) conditions has led to an explosion of theoretical and experimental activities in semiconductor nanowires (InSb or InAs) in proximity to a superconductor (NbTi or Al) in the presence of an external magnetic field. The experimental finding of a zero-bias peak (ZBP) (59; 60; 61; 62; 63), in precise agreement with the theoretical predictions in the differential tunneling conductance of an InSb nanowire (in contact with a NbTiN superconducting substrate) at a finite external magnetic field ($B \sim 0.1 - 1\ T$), followed by independent corroborative observation of such ZBP both in InSb and InAs nanowires in contact with superconducting Nb and Al by several groups, has created excitement in the condensed matter physics community as well as the broader scientific community as perhaps the first direct evidence supporting the existence of the exotic, the elusive, and the emergent Majorana bound states in solids.

So, the study of superconducting systems, and in particular of the physics that emerges from them (Majorana modes, anomalous currents, and so on), is today one of the major topics of debate and research. The proposal of the first quantum computer recently made by Google is not indifferent (25; 26).

In this thesis, we will propose a model for the study of the anomalous Josephson current and in particular of its asymmetry under specific conditions. Moreover, using a ring symmetry, we will propose a way to measure the presence of the Majorana modes in a completely non-invasive way and their resistance to disorder. Specifically, the work is divided as follows:

- In Chapter 2 we will examine the Josephson current in superconducting-normal-superconducting (SNS) junctions. Here we introduce the history, the engineering uses and the theoretical treatment of the Josephson current and the anomalous phenomenon. To easily calculate the current, as we will show, we will present a formalism based on the classic BTK approach and the Scattering matrix. Once the technique used is exposed, we will use it to calculate the anomalous Josephson current in systems in which spin-orbit interaction and the Zeeman effect are present.

- In Chapter 3 we will analize hybrid superconducting rings pierced by a magnetic flux to obtain informations about Majorana modes through the persistent current. We will see, through a numerical approach, how, when the system is in the topological phase condition, it is possible to highlight the presence of the Majorana modes in the system through the discontinuities of the current. This kind of signature will allow us to study the robustness of the Majorana modes with respect to a certain amount of disorder applied to the system.

- In Chapter 4 we propose an analytical technique to calculate the persistent current in the superconducting hybrid rings through the calculation of the transfer matrix of the system. Specifically, the concept of transfer matrix will be depth and it will be shown how it is linked to the secular equation of the system. Next, we will show how it is possible to use an integration technique on the complex plane to facilitate the calculation of the current. The analytical study of the current will also allow us to provide an exhaustive formal proof of the presence of the Majorana modes in the ring.

- Finally, in Chapter 5 we will provide a brief discussion of the major results obtained in the previous chapters and provide our conclusions.

Chapter 2

The anomalous Josephson current in Spin-Orbit superconducting-normal-superconducting junctions

The Josephson effect is the flow of current through two superconductors, or a superconducting-normal-superconducting metal junction (SNS junctions), due to the phase difference φ of the superconducting pairing between them. This current, as we wills see in the following, is a periodic function of φ. Usually, when there is no phase difference between the two superconducting metals that make up the junction, the Josephson current is zero. However, under certain conditions, the current can be zero when φ is equal to a certain value φ_0. This phenomenon is called Anomalous Josephson effect. Nowaday, Josephson junctions have important applications in quantum-mechanical circuits, such as SQUIDs, which are very sensitive magnetometers used to measure extremely subtle magnetic fields, superconducting qubits, that that big technology companies, like Google (25; 26; 12) , Microsoft (13) , IBM (14) and Rigetti (15) , today want to use for the realization of quantum computers, and RSFQ digital electronics. The NIST (National Institute of Standards and Technology) standard for one volt is achieved by an array of 20208 Josephson junctions in series. Moreover, as will be explicitly shown below, the anomaly of the Josephson current and its possible asymmetries can be exploited for the construction of electronic components, such as, for example, diodes and transistors. Anomalous Josephson current and the asimmetry of the current will be the main protagonists of this chapter.

Drawing inspiration from what has just been said, we will focus, in the following sections, our attention on the calculation of the Josephson current in SNS junctions in which the normal region can present several peculiarities (i.e. the presence of barriers, spin interaction orbit, etc.). As we will see in detail, through a scattering matrix formalism, it will be possible, in the short junction limit (i.e. when the coherence length of the superconductor ξ is smaller than the length of the normal region), to reduce the

calculation of the Josephson current to the resolution of a scattering problem in the normal region. The purpose of the chapter, in addition to providing details on the technique used to compute analytically and numerically the Josephson current, is to highlight the conditions under which the parameters choice of the SNS junction brings out not only the anomaly, but also an asymmetry in the current. We find that in the case of one open channel in the normal region (the nanowire) φ_0 can deviate substantially from zero but the critical current does not show any direction dependence, contrary to the case in which we have two (or more) transport channels. In both case we find the anomaly in the current, i.e. a finite φ_0 for sufficiently strong spin-orbit interaction and magnetic field but, as we will show below, we observe a substantially different behaviour of the junction.

The chapter is structured as follows:

- In Section 2.1 we will give a brief description of the Josephson effect and introduce the anomalous Josephson current, underlying the dependence of the current of the phase difference φ.
- In Section 2.2 we introduce the Scattering matrix approach to the computation of the Andreev bound states and, consequently, of the Josephson current in SNS junctions. Here, we will discuss the case of a SNS junction in which a delta-like potential barrier is introduced in the normal region (it can be seen as an impurity in the system) and we will do some indication to improve the Scattering matrix approach in the presence of more scattering channel (for more details about this topic, we refer to Appendix E).
- In Section 2.3 we discuss a SNS junction in which Rashba spin orbit interaction and Zeeman effect are introduced into the normal region. This, as we will see, will cause anomaly and an asymmetry in the current. In addition, density plots will be presented to highlight the dependence of asymmetry and anomaly on the varying intensity of the spin-orbit interaction on the applied magnetic field.

2.1 The Josephson current

We know from the BCS theory that superconductivity is a result of the correlated motion of electrons in the superconducting solid. Part of this correlation is the formation of pairs of electrons called Cooper pairs. According to Josephson (18; 19) , under certain circumstances these Cooper pairs move from one superconductor to the other across the thin insulating layer. Generally, when two (or more) superconducting wires form a contact, there will be a motion of Cooper pairs due to the fact that the pairings $\Delta = |\Delta|e^{i\varphi}$ can have different order parameter phase φ. Such motion of pairs of electrons constitutes what we call Josephson current, and the process by which the pairs cross the insulating layer is called Josephson tunneling. Before Josephson's prediction, it was only known that normal electrons can flow through an insulating barrier,

by means of quantum tunneling. Josephson was the first to predict the tunneling of superconducting Cooper pairs.

Consider two pieces of superconductor, that we will index as "1" and "2", with a junction between them. The respective superconducting phases are defined as φ_1 and φ_2, the coupling of the junction between the two superconductors is κ, while μ_1 and μ_2 are the chemical potentials of the respectively regions. To derive the Josephson equations, we start introducing ψ_1 and ψ_2, the quantum mechanical wavefunction of the superconducting state in the left and the right superconductor, respectively. The dynamics of the two wavefunctions are then determined by the following coupled Schrödinger equations:

$$\begin{aligned} i\hbar\frac{\partial\psi_1}{\partial t} &= \mu_1\psi_1 + \kappa\psi_2 \\ i\hbar\frac{\partial\psi_2}{\partial t} &= \mu_2\psi_2 + \kappa\psi_1 \end{aligned} \tag{2.1}$$

We make the ansatz that the wavefunctions can be written as:

$$\begin{aligned} \psi_1 &= \sqrt{\nu_1}e^{i\varphi_1} \\ \psi_2 &= \sqrt{\nu_2}e^{i\varphi_2} \end{aligned} \tag{2.2}$$

where $\nu_i, i = 1, 2$ are the density of the Cooper pairs in the two regions. Substituting Eqs.(2.2) in Eqs.(2.1), we find that:

$$\begin{aligned} \hbar\frac{\partial\nu_1}{\partial t} &= -\hbar\frac{\partial\nu_2}{\partial t} = 2\kappa\sqrt{\nu_1\nu_2}\sin(\varphi) \\ -\hbar\frac{\partial\varphi}{\partial t} &= \mu_2 - \mu_1 \end{aligned} \tag{2.3}$$

where $\varphi = \varphi_2 - \varphi_1$. Eqs.(2.3) are the governing equations for the Josephson effect, but they can be written in a more compact way. At first, the time derivative of the density of Cooper pairs describes a charge transport and thus:

$$I = \frac{\partial\nu_1}{\partial t} \tag{2.4}$$

If a voltage $V(t)$ is applied between the junctions the energy levels will shift according to:

$$2eV(t) = \mu_2 - \mu_1 \tag{2.5}$$

where e is the electron charge. If we define $I_0 = 2\kappa\sqrt{\nu_1\nu_2}$, the Josephson junction equations become:

$$\frac{d\varphi}{dt} = \frac{e}{\hbar}V(t) \quad (2.6)$$
$$I(\varphi) = I_0 \sin(\varphi) \quad (2.7)$$

where $I(\varphi)$ is called Josephson current and I_0, which is called "critical current", states the maximum value of the supercurrent. The critical current is an important phenomenological parameter of the device that can be affected by temperature as well as by an applied magnetic field.

The weak link can consist of a thin insulating barrier (known as a superconductor−insulator−superco junction, or SIS), a short section of non-superconducting metal (SNS junctions), or a physical constriction that weakens the superconductivity at the point of contact (SsS junctions) (16). Moreover, Josephson junctions exhibit a variety of phenomena, such as the DC Josephson effect, which is a constant current flow in the absence of any voltage biases between the different superconductors; the AC Josephson effect which is, instead, an alternating current flow in the presence of constant voltage biases, and the Shapiro steps, which appear as plateaus in plots of the average voltage versus average current when the currents are made periodical. The physics of such junctions is known to rely crucially on the pairing symmetry of its constituent superconductors. For example, a junction of two p-wave superconductors exhibits a fractional Josephson effect (27; 17) which manifests itself in a fractional Josephson frequency $\omega J = eV/\hbar$ or the absence of odd-integer Shapiro steps. The latter property of such junctions has been used experimentally for the detection of Majorana modes (17; 104). Furthermore, a junction of two superconducting wires of $s-$ and $p-wave$ symmetriesis known to generate a magnetic moment at the interface whose time variation can be controlled by an external applied voltage (27; 28). Multiple junctions with $s-wave$ superconductors have been studied using a scattering matrix formalism (104; 86; 93; 29; 30; 31; 32; 101) ,and voltage-induced Shapiro steps have been studied in a junction of threes-wave superconductors(33) . However, no such studies have been carried out for multiterminal junctions involving unconventional superconductors. The discovery of the supercurrent, as we will see in details in the following, helped to the realization of digital logic circuitry, that can be used as ultrafast computers using Josephson logic. Josephson junctions can also be involved into circuits called SQUIDs, an acronym for Superconducting QuantUm Interference Device. These devices are extremely sensitive and very useful in constructing extremely sensitive magnetometers and voltmeters. For example, one can make a voltmeter that can measure picovolts.

2.1.1 The Anomalous Josephson current

The Josephson effect, as we have just seen, is traditionally expressed by a current-phase relation of the form $I(\varphi) = I_0 \sin(\varphi)$ with φ the phase difference of the order parameter

of the two superconducting leads. A priori the current-phase relation could also be of the form:

$$I(\varphi) = I_0 \sin(\varphi + \varphi_0) \tag{2.8}$$

that allows a non-zero current even when the two superconducting leads have the same phase (i.e. $\varphi = 0$) and it can be shown that several symmetries can enforce φ_0 to be strictly zero. Despite this, as we shall see, it may be interesting for engineering applications the study of the cases in which φ_0 has a finite non-zero value; this is the Anomalous Josephson effect. To observe this effect in the current, is necessary to break the time reversal symmetry, by introducing into the system a magnetic field B, and spin-rotation (chiral) symmetry, by means introduce a spin orbit interaction (SOI).

In the last years, to observe the anomalous Josephson effect, several possibilities have been addressed. In particular, for superconducting-normal junctions, we can improve the time-reversal and spin-rotational-simmetry breaking in the normal region. To realize such kind of system, we can consider, for example, a magnetic normal metal (34; 35; 36; 37; 38) , a one-dimensional quantum wire, a quantum dot (39; 40) , a multichannel system with a barrier or a quantum point contact (41; 42) , or, a semiconducting nanowire (43; 44) . Anomalies of the Josephson current have also been predicted in presence of Coulomb interactions and SOI for a wire (45; 46) or a quantum dot (40) contacted with conventional s-wave superconductors. More recent proposals suggest the possibility of realizing a non-coplanar ferromagnetic junction (47) . Most interestingly in other systems the anomalous Josephson effect (AJE) can be exploited to discern topological versus conventional superconductivity (48; 49; 50) . Recently, the anomalous Josephson current has been demonstrated in an experiment using gate defined quantum dot in a $InSb$ nanowire embedded in a superconducting quantum interferometer (51) . Moreover advances in the fabrication of nanowires of $InAs$ have made materials with a large g-factor and a strong spin-orbit (SO) interaction available.

2.2 Scattering Matrix approach to compute the Josephson current in SNS junctions

As we already seen, the Josephson current is a periodic function of the phase difference φ. However, we need a simple way to compute the Josephson current in more complicated systems. To do this, we remind that the current can be obtained from the ground state energy $E_{gs}(\varphi)$ at zero temperature by the thermodynamic relation :

$$I(\varphi) = \frac{2e}{\hbar} \frac{dE_{gs}}{d\varphi} \tag{2.9}$$

This equation makes a relation between the equilibrium current and the derivative of the ground state energy E_{gs} with respect to the phase difference. To apply this relation we need to know how to obtain E_{gs} from the Bogoliubov- de Gennes equations. The

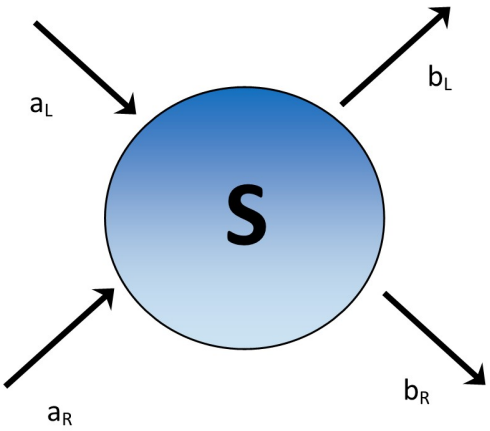

Figure 2.1: Sketch of the scattering matrix S.

required formula was derived from the Green's function expression for E_{gs} (94).Now the problem is shifted to the evaluation of the spectrum of the system, that we can carry out through a scattering matrix approach.

To introduce the concept of scattering matrix, let us consider a simple localized one-dimesional barrier problem. So, we have a positive-energy electron with energy E which comes from the left to the right and scatters along the barrier $V(x)$. The solution of Schrödinger's equation outside the potential barrier are plane waves given by:

$$\psi_L(x) = a_L e^{ikx} + b_L e^{-ikx} \tag{2.10}$$
$$\psi_R(x) = a_R e^{ikx} + b_R e^{-ikx} \tag{2.11}$$

where L/R stand, respectively, for left and right and idicate the left side of the barrier and the right one, while k is the particle momentum:

$$k = \sqrt{\frac{2mE}{\hbar^2}} \tag{2.12}$$

where m is the mass of the particle. The term with coefficient a_L represents the incoming wave, whereas term with coefficient b_R represents the outgoing wave. b_L stands for the reflecting wave. Since we set the incoming wave moving in the positive direction (coming from the left), the coeffcient a_R is zero and can be omitted. The transition overlap of the outgoing waves with the incoming waves is a linear relation which define the scattering matrix S (see Fig.2.1) as:

$$\begin{bmatrix} b_L \\ b_R \end{bmatrix} = S \begin{bmatrix} a_L \\ a_R \end{bmatrix} \tag{2.13}$$

where:

$$S = \begin{pmatrix} s_{11} & s_{12} \\ s_{21} & s_{22} \end{pmatrix} = \begin{pmatrix} r_L & t_R \\ t_L & r_R \end{pmatrix} \tag{2.14}$$

Here, the coefficients $r_{L/R}$ and $t_{L/R}$ are, respectively, the reflection and transmission amplitudes from the left or the right of the barrier $V(x)$. We can say, then, that the scattering matrix binds the states entering the barrier with the outgoing ones, so that:

$$(out) = S(in) \tag{2.15}$$

where (out) represent the outgoing waves and (in) the incoming ones. The scattering matrix just defined, is unitary. This is a consequence of its relation to the transmission and reflection coefficients, of which we know that the sum of the square modules of $r_{L/R}$ and $t_{L/R}$ is equal to 1.

We note that in the metal also occur scattering processes which involve holes. However, since there is no process that links the propagation of the hole and the particle, we can treat the propagation problems separately. What follows is that the hole processes are symmetrical to those of the particle with $E \to -E$. Note that the scattering matrix can also describe multichannel processes, i.e. when scattering can occur at different energies. To generalize the matrix S, we have to take into account that $r_{L/R}$ and $t_{L/R}$ are $N \times N$ matrices, where N is the number of open channels. In the following description and in the entire section we will discuss matrices with only one open channel. In the next section, instead, we will see an application of multichannel scattering for the description of a system with harmonic confinement potential.

So, we consider, now, a superconducting-normal (SN) junction and a positive-energy particle that comes from the left (see Fig.2.2) along the normal region and scatters through the junction to get to the superconductive region. The spectrum of a superconductor, as we have already seen (see Appendix D), has a gap. This, which varies from metal to metal, takes the place of the potential barrier $V(x)$ seen in the normal case. The substantial difference is, however, in the fact that the ground state of the superconductor is formed by Cooper pairs. For this reason, during scattering, particles can be involved in processes that are much more complex than those exposed so far. Here, indeed, an incoming positive-energy particle can be reflected (r_{ee}) or transmissed (t_{ee}) as a positive-energy particle, or, due to the superconducting metal, can be reflected (r_{eh}) or transmissed (t_{eh}) as a positive-energy hole; these phenomena are called Andreev scattering processes (55).

The left/right-side wavefunctions take now the form:

$$\begin{aligned} \psi_L(x) &= a_{e,L}e^{iq_e x} + a_{h,L}e^{-iq_h x} + b_{e,L}e^{-iq_e x} + b_{h,L}e^{iq_h x} \\ \psi_R(x) &= a_{e,R}e^{iq_e x} + a_{h,R}e^{-iq_h x} + b_{e,R}e^{-iq_e x} + b_{h,R}e^{iq_h x} \end{aligned} \tag{2.16}$$

where the indices e/h stands, respectively, for particle and hole and $q_{e/h}$ are the momenta:

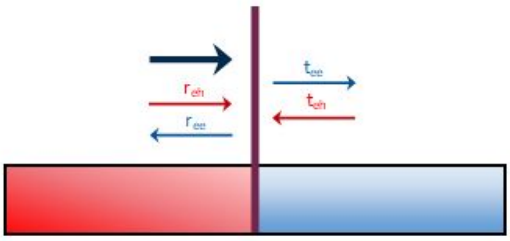

Figure 2.2: Sketch of a scattering process in an SN junction. Here the red region indicates the normal metal, while the blue part the superconducting one. The dark arrow is the incoming positive-energy particle, the light-blue arrows report the particle-particle processes, while the reds the particole-hole ones. Finally, the importance of the junction, which provides a potential barrier, is highlighted by the purple line.

$$q_{e/h} = \sqrt{\frac{2m}{\hbar^2}(\epsilon_F \pm \alpha\sqrt{(E^2 - \Delta^2)})} \tag{2.17}$$

where α is equal to 1 for the particle and -1 for the hole, Δ is the superconducting pairing, E the energy and ϵ_F the Fermy energy level of the system. In addiction, $a_{e,L}$ is the coefficient for the incoming particle, $a_{h,L}$ for the reflected hole, $b_{e,L}$ for the reflected particle, $b_{e,R}$ for the transmitted particle, while $b_{h,R}$ for the transmitted hole. Because of we are considering the particular case of an incoming positive-energy particle, the other coefficients are zero. Due the Andreev reflection (55), as we will see in the following, we can not divide the propagation problem of the particles and the holes (that, instead, as we have already seen, it is possible in the case of scattering between normal metals). We can, however, as we have previously done, define the scattering matrix S as:

$$\begin{pmatrix} a_{e,L} \\ a_{e,R} \\ a_{h,L} \\ a_{h,R} \end{pmatrix} = S \begin{pmatrix} b_{e,L} \\ b_{e,R} \\ b_{h,L} \\ b_{h,R} \end{pmatrix} \tag{2.18}$$

where S takes now the form:

$$S = \begin{pmatrix} s_{11} & s_{12} & s_{13} & s_{14} \\ s_{21} & s_{22} & s_{23} & s_{24} \\ s_{31} & s_{32} & s_{33} & s_{34} \\ s_{41} & s_{42} & s_{43} & s_{44} \end{pmatrix} = \begin{pmatrix} r_{ee,L} & t_{ee,R} & r_{eh,L} & t_{eh,R} \\ t_{ee,L} & r_{ee,R} & t_{eh,L} & r_{eh,R} \\ r_{he,L} & t_{he,R} & r_{hh,L} & t_{hh,R} \\ t_{he,L} & r_{he,R} & t_{hh,L} & r_{hh,R} \end{pmatrix} \tag{2.19}$$

where the $r_{eh,L/R}, r_{he,L/R}, t_{eh,L/R}$ and $t_{he,L/R}$ are the Andreev reflection and transmission coefficients. Because of the particle-hole simmetry, S can be represented as a scattering block for particles (S_{ee}), a scattering block for holes (S_{ee}) and two mixed scattering blocks and written as:

$$S = \begin{pmatrix} S_{ee} & S_{eh} \\ S_{he} & S_{hh} \end{pmatrix} \tag{2.20}$$

where:

$$S_{hh}(E) = S^*_{ee}(-E) \tag{2.21}$$
$$S_{he}(E) = -S^*_{eh}(-E) \tag{2.22}$$

Now that we have introduced the scattering matrix, let's see how it can be used to calculate the Josephson current.

2.2.1 The Andreev bound states and the scattering matrix

First of all, we have to show how to relate the excitation spectrum of Bogoliubov quasiparticles to the scattering matrix of normal electrons (95). Let us consider an SNS junction with the normal region confined in $\frac{L}{2} > x > -\frac{L}{2}$ and a superconducting paring $\Delta e^{i\varphi}$. We already know that the wave function in the normal region takes the form:

$$\psi_N(x) = a_{e/h} e^{ikx} + b_{e/h} e^{-ikx} \tag{2.23}$$

while in the superconducting ones:

$$\begin{aligned} \psi_{SL}(x) &= a_{e,L} e^{iq_e x} + a_{h,L} e^{-iq_h x} + b_{e,L} e^{-iq_e x} + b_{h,L} e^{iq_h x} \\ \psi_{SR}(x) &= a_{e,R} e^{iq_e x} + a_{h,R} e^{-iq_h x} + b_{e,R} e^{-iq_e x} + b_{h,R} e^{iq_h x} \end{aligned} \tag{2.24}$$

with k and $q_{e,h}$ defined as in Eq.(2.12) and Eq.(2.17). If we want to compute the quasiparticle current through a lead of the system we have to calculate the integral:

$$I = \int dy \int dx \; j_x = -i\frac{\hbar}{m} \Re \left(u^* \frac{\partial u}{\partial x} - v^* \frac{\partial v}{\partial x} \right) \tag{2.25}$$

where j is the current density, m is the quasiparticles mass, while u and v are the solutions of the wavefunctions (cfr Appendix D). Since, for solutions of propagative wave, the momenta k and $q_{e,h}$ are real numbers, we can show that the wave functions in the normal and in the superconductive regions carries the same amount of quasiparticle current $|I|$. However, the wave functions do not carry the same amount of charge current I_c:

$$I = -ie\frac{\hbar}{m} \Re \left(u^* \frac{\partial u}{\partial x} + v^* \frac{\partial v}{\partial x} \right) \tag{2.26}$$

This, of course, does not contradict the unitarity of the S-matrix constructed from these wavefunctions. To simplify the notation, we can introduce the incoming and outcoming vectors by defining:

$$a_{in} = (a_{e,N}, a_{e,R}, a_{h,L}, a_{h,R}) \tag{2.27}$$
$$b_{out} = (b_{e,N}, b_{e,R}, b_{h,L}, b_{h,R}) \tag{2.28}$$

The scattering matrix S_N in the normal region takes the block form:

$$b_{out} = \begin{pmatrix} S_{ee} & 0 \\ 0 & S_{hh} \end{pmatrix} a_{in} \tag{2.29}$$

By using the particle-hole simmetry, we can write Eq.(2.29) as:

$$b_{out} = \begin{pmatrix} S_0(E) & 0 \\ 0 & S_0^*(-E) \end{pmatrix} a_{in} \tag{2.30}$$

where S_0 is the scattering matrix defined as in Eq.(2.14). For energies $0 < E < \Delta$ there are no propagating modes in the superconducting leads. In this regime the only possible process is the normal and the Andreev reflection; however, since $\Delta \ll E_F$, where E_F is the Fermi energy of the system, we may ignore normal reflections at the SN interface: this is called Andreev approximation (55). We can, then, define an Andreev scattering matrix S_A for the scattering on the SN interface (95):

$$S_A = \alpha \begin{pmatrix} 0 & r_A \\ r_A^* & 0 \end{pmatrix} \tag{2.31}$$

where $\alpha = e^{-i \arccos(E/\Delta)}$, while r_A is:

$$r_A = \begin{pmatrix} e^{i\frac{\varphi}{2}}\mathbf{1} & 0 \\ 0 & e^{-i\frac{\varphi}{2}}\mathbf{1} \end{pmatrix} \tag{2.32}$$

Andreev reflection transforms a particle into an hole, without change the mode index. The transformation is accompanied by a phase shift, which consists of two parts:

- A phase shift $-\arccos(E/\Delta)$ due to the penetration of the wavefunction into the superconductor.
- A phase shift equal to plus or minus the phase of the pair potential in the superconductor (plus for reflection from hole to electron, minus for the reverse process).

For energy $E > \Delta$, by matching the wavefunctions for $x = \pm L/2$ and doing some algebric computations, we can define the S matrix of the whole SNS junction as:

$$S = U^{-1} \left(\mathbf{1} - M\right)^{-1} \left(\mathbf{1} - M^\dagger\right) S_N U \tag{2.33}$$

where:

$$U = \begin{pmatrix} r_A & 0 \\ 0 & r_A^* \end{pmatrix}^{\frac{1}{2}} \tag{2.34}$$

and:

$$M = \alpha S_N \begin{pmatrix} 0 & r_A \\ r_A & 0 \end{pmatrix} \tag{2.35}$$

We are now ready to relate the excitation spectrum of the Josephson junction to the S-matrix of the normal region. First the discrete spectrum. The condition $a_{in} = S_A S_N a_{in}$ for a bound state implies that $\det \mathbf{1} - S_A S_N$. By using the folding identity:

$$\det \begin{pmatrix} a & b \\ c & d \end{pmatrix} = \det \left(ad - aca^{-1}b \right) \tag{2.36}$$

where a, b, c and d are square matrices and $\det a \neq 0$, and Eqs.(2.33), we can write:

$$\det \left[\mathbf{I} - r_{ph} S_h \left(-\epsilon \right) r_{hp} S_p \left(\epsilon \right) \right] = 0 \tag{2.37}$$

which determines the discrete spectrum. The density of states of the continuous spectrum is related to S by the general relation (96):

$$\rho = \frac{1}{2\pi i} \frac{\partial}{\partial E} \ln \det S + const \tag{2.38}$$

where *const* indicates a φ-independent term. Putting together what we have got so far, we obtain:

$$\frac{\partial \rho}{\partial \varphi} = -\frac{1}{\pi} \frac{\partial^2}{\partial \varphi \partial E} \ln \det \left(\mathbf{I} - r_{ph} S_h \left(-\epsilon \right) r_{hp} S_p \left(\epsilon \right) \right. \tag{2.39}$$

which determines the φ-dependence of the continuous spectrum. In the case where the length of the normal region is smaller than the coherence length, i.e. when $L < \xi$, the continuum states tend to zero and become negligible for calculation purposes. For this reason, it becomes convenient to work in the short junction limit, where the contribution of the superconducting zones is brought only by the Adreev matrices. The calculations made below, as we shall see, are carried out in the short junction limit.

At this point, it becomes important to emphasize that the calculation of the Josephson current, as we set it, is reduced to the calculation of the matrix S_N. In the following, we will show how to compute the Josephson current in superconducting-normal-superconducting junctions in presence of a delta-like barrier in the normal region and in the presence of Rashba spin-orbit and Zeeman interaction, reducing, from time to time, the problem to the simple calculation of the scattering matrix in the normal region.

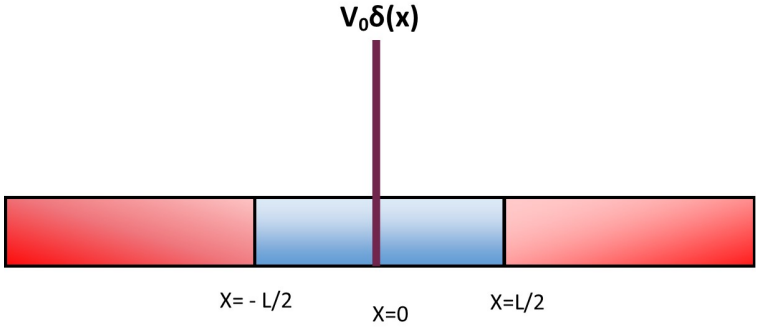

Figure 2.3: Sketch of a SNS junction with a δ-like potential barrier in $x = 0$. Here we represent the superconducting metal in red and the normal metal in blue.

2.2.2 Josephson current and Andreev bound states in a SNS junction with a delta potential in $x = 0$

Now, we show how to compute the Andreev Bound states for $T = 0$ in an hybrid SNS one-dimensional system. Our device is composed by a superconductor region for $x < -\frac{L}{2}$, a normal region for $|x| \leq \frac{L}{2}$ and another superconductor region for $x > \frac{L}{2}$. We assume that in the normal region there is a scattering center $V(x) = V_0\delta(x)$ at $x = 0$ and that the system has only one scattering channel (see Fig. 2.3).

Let us start from the equations:

$$\begin{pmatrix} H_0 & \Delta(x) \\ \Delta^*(x) & -H_0 \end{pmatrix} \begin{pmatrix} u_\sigma^{(a)}(x) \\ v_\sigma^{(a)}(x) \end{pmatrix} = \epsilon \begin{pmatrix} u_\sigma^{(a)}(x) \\ v_\sigma^{(a)}(x) \end{pmatrix} \tag{2.40}$$

where $\sigma = \uparrow, \downarrow$ indicates the spin polarization, $u_\sigma^{(a)}(x)$ and $v_\sigma^{(a)}(x)$ are, respectively, the particle and the hole-like solutions for a fixed spin polarization, a indicates the region (i.e.superconducting or normal), and H_0 is the free-fermion hamiltonian:

$$H_0 = -\frac{\hbar^2}{2m}\frac{d^2}{dx^2} + V(x) - \epsilon_F \tag{2.41}$$

a indicates the region which we are considering, $\Delta(x)$ the superconducting pairing defined as:

$$\Delta(x) = \begin{cases} \Delta_0 e^{i\frac{\phi}{2}} & for\ x < -\frac{L}{2} \\ 0 & for\ |x| \leq \frac{L}{2} \\ \Delta_0 e^{-i\frac{\phi}{2}} & for\ x > \frac{L}{2} \end{cases} \tag{2.42}$$

and ϵ_F the Fermi energy. We note that $V(x)$ is zero everywhere except for $x = 0$. Then, by combining Eqs.(2.40,2.41,2.42), we find the energy relation dispersions and the solutions for the normal ($-\frac{L}{2} < x < \frac{L}{2}$) and the superconducting ($|x| \geq \frac{L}{2}$)

regions (we have solved and discussed the BdG equations for the continuum model in Appendix(D)).

The spectrum of this kind of system consists of a finite set of bound states (Andreev levels) with energy $|\epsilon| < \Delta_0$, and a continuum of states with $|\epsilon| > \Delta_0$. We remind that the current can be obtained from the ground state energy $E_{gs}(\varphi)$ at zero temperature by the thermodynamic relation

$$I(\varphi) = \frac{2e}{\hbar}\frac{dE_{gs}}{d\varphi} \tag{2.43}$$

In the short junction limit only the subgap Andreev states contribute to the Josephson current (in the long-junction limit, one can use the technique developed in Refs.(86; 125) to exactly account for contributions from all the states, to leading order in the inverse junction length). Thus, one obtains

$$I(\varphi) = \frac{e}{\hbar}\sum_{n}{}' \frac{\partial E_n(\varphi)}{\partial \varphi} \tag{2.44}$$

In Eq.(2.44) "n" labels the Andreev states, the primed sum means that only negative energy (occupied) Andreev states are considered. Notice that a factor of 2 difference with the usual relation found in literature because spin degeneracy is lifted here.

The calculation of the Andreev states in a quasi one dimensional system can be conveniently done using a scattering matrix approach (114; 120) . Let us consider the short junction limit, that is that the normal region is short compared to the superconducting coherence length ξ; in such a case the Josephson current is fully determined by the Andreev subgap states (114; 120) ;moreover, we assume that for energies below the superconducting gap Δ_0 at the interface between the normal and the superconducting regions only intra-channel Andreev scattering takes place where a hole (electron) with spin σ is reflected as an electron (hole) with spin $-\sigma$.

Now, because we have not spin-flip processes, we can separate the problem and consider a fixed value of σ. To compute the Andreev bound states, we use the scattering matrix approach described in (52) . We have that in the first superconducting region (and similarly in the second one):

$$S_A \begin{pmatrix} a_{e,L} \\ a_{e,R} \\ a_{h,L} \\ a_{h,R} \end{pmatrix} = \begin{pmatrix} b_{e,L} \\ b_{e,R} \\ b_{h,L} \\ b_{h,R} \end{pmatrix} \tag{2.45}$$

where S_A is the Andreev scattering matrix. On considering $|\epsilon| \leq \Delta_0$, we have that at the interfaces between normal and superconducting regions only intra-channel Andreev scattering take place. Assuming one scattering channel, we have that S_A can be written under the Andreev approximation and takes the form:

$$S_A = \begin{pmatrix} 0 & r_{ph} \\ r_{hp} & 0 \end{pmatrix} \tag{2.46}$$

where r_{ph} and r_{hp} are the Andreev-reflection matrices defined as:

$$r_{ph} = e^{-i\gamma} \begin{pmatrix} e^{-i\frac{\varphi}{2}} & 0 \\ 0 & e^{i\frac{\varphi}{2}} \end{pmatrix} \tag{2.47}$$

$$r_{hp} = e^{-i\gamma} \begin{pmatrix} e^{i\frac{\varphi}{2}} & 0 \\ 0 & e^{-i\frac{\varphi}{2}} \end{pmatrix} \tag{2.48}$$

and:

$$\gamma = \arccos\left(\frac{\epsilon}{\Delta_0}\right) \tag{2.49}$$

In the normal region, instead, Andreev scattering processes are not allowed. Because of the absence of the superconducting pairing, the scattering matrix takes the form:

$$S_N \begin{pmatrix} a_{e,L} \\ a_{e,R} \\ a_{h,L} \\ a_{h,R} \end{pmatrix} = \begin{pmatrix} b_{e,L} \\ b_{e,R} \\ b_{h,L} \\ b_{h,R} \end{pmatrix} \tag{2.50}$$

where S_N is the block-diagonal matrix:

$$S_N = \begin{pmatrix} S_p(\epsilon) & 0 \\ 0 & S_h(\epsilon) \end{pmatrix} \tag{2.51}$$

Now, to find the Andreev bound states, we have to solve the equation:

$$\det\left[\mathbb{I} - r_{ph} S_h(-\epsilon)\, r_{hp} S_p(\epsilon)\right] = 0 \tag{2.52}$$

Because of we already known who are r_{ph} and r_{hp}, is clear that to solve Eq.(2.52) we have to compute S_N. By separating the problem for particles and holes, we find:

$$\psi_{p,NL} = a_{e,L} e^{ik_{p,N}x} + b_{e,L} e^{-ik_{p,N}x} \tag{2.53}$$

$$\psi_{p,NR} = a_{e,R} e^{ik_{p,N}x} + b_{e,R} e^{-ik_{p,N}x} \tag{2.54}$$

for the particle and

$$\psi_{h,NL} = a_{h,L} e^{-ik_{h,N}x} + b_{h,L} e^{ik_{h,N}x} \tag{2.55}$$

$$\psi_{h,NR} = a_{h,R} e^{-ik_{h,N}x} + b_{h,R} e^{ik_{h,N}x} \tag{2.56}$$

for the hole. Let us focus the attention to the particle scattering problem (the derivation of the hole one is analogous). On imposing that the wave function must be continuous at $x = 0$, we find the condition:

$$a_{e,R} + b_{e,R} - a_{e,L} - b_{e,L} = 0 \tag{2.57}$$

We can not impose any conditions on the derivative of the wave function because of the delta potential $V(x)$, but we can avoid this problem integrating from $-\eta$ to η both sides of the Schrödinger equation and to the limit for $\eta \to 0$. We obtain the condition:

$$i\frac{k_{p,N}}{2m}\left(-a_{e,R} + b_{e,R} - a_{e,L} + b_{e,L}\right) + V_0\left(a_{e,R} + b_{e,R}\right) = 0 \tag{2.58}$$

By comining Eqs.(2.57,2.58), we obtain the scattering matrix:

$$\begin{pmatrix} a_{e,R} \\ a_{e,L} \end{pmatrix} = S_p(\epsilon) \begin{pmatrix} b_{e,R} \\ b_{e,L} \end{pmatrix} \tag{2.59}$$

where:

$$S_p(\epsilon) = \begin{pmatrix} r_{11}^p & t_{12}^p \\ t_{21}^p & r_{22}^p \end{pmatrix} = \begin{pmatrix} -i\frac{A}{1+iA} & \frac{1}{1+iA} \\ \frac{1}{1+iA} & -i\frac{A}{1+iA} \end{pmatrix} \tag{2.60}$$

and:

$$A = \frac{mV_0}{\hbar^2 k_{N,p}} \tag{2.61}$$

In the same way, we obtain the hole scattering matrix:

$$\begin{pmatrix} a_{h,R} \\ a_{h,L} \end{pmatrix} = S_h(\epsilon) \begin{pmatrix} b_{h,R} \\ b_{h,L} \end{pmatrix} \tag{2.62}$$

where:

$$S_h(\epsilon) = \begin{pmatrix} r_{11}^h & t_{12}^h \\ t_{21}^h & r_{22}^h \end{pmatrix} = \begin{pmatrix} i\frac{B}{1-iB} & \frac{1}{1-iB} \\ \frac{1}{1-iB} & i\frac{B}{1-iB} \end{pmatrix} \tag{2.63}$$

and:

$$B = \frac{mV_0}{\hbar^2 k_{N,h}} \tag{2.64}$$

In the limit of short junction, we can disregard the energy-dependence of the scattering matrix, obtaining that $S_h^*(-\epsilon) = S_p(\epsilon) \approx S_p(0)$ and Eq.(2.52) becomes:

$$\det\left[\mathbb{I} - r_{ph} S_p(0)\, r_{hp} S_p^*(0)\right] = 0 \tag{2.65}$$

By multiplying both sides of Eq.(2.65) by $\det S_0$ and using the unitary and symmetry properties of the scattering matrix, we find that the ABSs are simply determined by the equation:

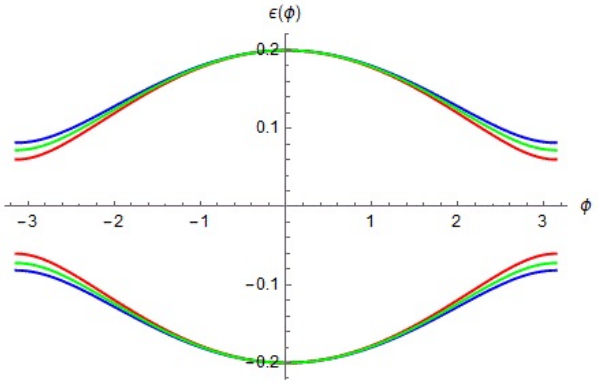

Figure 2.4: Andreev Bound states as a function of φ. For each curve we set $\Delta_0 = 0.2$, $k_F = m = 1$; we obtain the green curve setting $V_0 = 0.15$; instead, in the red curve $V_0 = 0.1$; finally, the blue curve is obtained putting $V_0 = 0.2$.

$$\det\left[\left(1-\frac{\epsilon^2}{\Delta_0^2}\right)\mathbb{I} - t_{12}t_{12}^{\dagger}\sin^2\left(\frac{\phi}{2}\right)\right] = 0 \tag{2.66}$$

where t_{12} is the transmission matrix. In our case (i.e. one scattering channel), the transmission matrix is the coefficient $\frac{1}{1+iA}$; then $t_{12}^{\dagger} = t_{12}^{*}$ and Eq.(2.66) becomes:

$$1-\frac{\epsilon^2}{\Delta_0^2} - \frac{1}{1+A^2\left(k_F\right)}\sin^2\left(\frac{\varphi}{2}\right) = 0 \tag{2.67}$$

Obtaining:

$$\epsilon = \pm\Delta_0\sqrt{1-\left(\frac{\hbar^2k_F^2}{\hbar^2k_F^2+m^2V_0^2}\right)\sin^2\left(\frac{\varphi}{2}\right)} \tag{2.68}$$

In Fig. 2.4 we plot Eq.(2.68) as a function of ϕ on varying the amplitude of the delta potential V_0.

This kind of approach,as we will see in the following, can be generalized and applied to many kind of systems in which the normal region has some impurities or more scattering channels are allowed. More details about the application of multichannel scattering matrix to the computation of the ABS and the Josephson current are shown in Appendix(E).

2.3 Anomalous Josephson Effect in Spin-Orbit Nanowires

Now we consider a SNS junction in which the normal region (—x—¡L$\overline{2)hasRashbaandZeemaninteraction.Moreover,u}$

$$H = \frac{p_x^2}{2m} + \frac{p_y^2}{2m} + \frac{1}{2}m\omega^2y^2 + \frac{\alpha(x)}{\hbar}(\sigma_x p_y - \sigma_y p_x) + g\mu_B B\sigma_y + \frac{i}{2}\partial_x\alpha(x)\sigma_y \tag{2.69}$$

with $\alpha(x) = \alpha[\Theta(x + \frac{L}{2}) - \Theta(x - \frac{L}{2})]$, α being the strength of the Rashba spin-orbit interaction, B is the applied magnetic field. Notice that the last term in Eq.(2.69) is necessary to preserve the hermicity of the Hamiltonian operator in case of a position-dependent SOI. Due to the presence of the transverse confinement potential, it is natural to employ a multi-channel scattering approach to the problem. Indeed in the superconducting leads one can define transverse modes, so that the electron wave functions in the x-direction are characterized by a band and a spin index. Here, we do the short junction limit, by means of the scattering matrix formalism we calculate the Josephson current studying how the minimum of the free energy φ_0 and the direction dependence of the critical current evolve as a function of the spin-orbit interaction and the applied magnetic field. We assume no spin-orbit interaction in the leads as we want to focus on the non-topological phase. Moreover due to a large g factor in the semiconducting region, a strong Zeeman spin splitting can be recovered, even for weak values of the magnetic field which, in turn, does not affect the superconductors and is accordingly neglected in the leads. Orbital effects of the magnetic field do not need to be taken into account as we consider a magnetic field oriented in the plane of the nanowire.

We look for solutions of the Bogoliubov-de Gennes equations:

$$\begin{pmatrix} H - \epsilon_F & \Delta \\ \Delta^\dagger & -(H^* - \epsilon_F) \end{pmatrix} \begin{pmatrix} u(x,y) \\ v(x,y) \end{pmatrix} = E \begin{pmatrix} u(x,y) \\ v(x,y) \end{pmatrix} \tag{2.70}$$

where E measures the energy with respect to the Fermi level ϵ_F, while $u(x,y)$ and $v(x,y)$ are respectively the electron and hole spinors in the Nambu representation. Notice that the spin structure is not explicit at this level. We take the pairing potential to be:

$$\hat{\Delta} = \Delta(x) \begin{pmatrix} 0 & -1 \\ 1 & 0 \end{pmatrix} \tag{2.71}$$

with

$$\Delta(x) = \Delta_0 \left[\Theta(-x - L)e^{-i\varphi/2} + \Theta(x - L)e^{i\varphi/2}\right] \tag{2.72}$$

and we take a symmetric phase difference φ between the two superconductors. $\Theta(x)$ is the Heaviside step function. The spectrum of Eq.(2.70) consists, as we have already seen before, of a finite set of bound states, the Andreev levels, with energy $|\epsilon| < \Delta_0$, and a continuum of states with $|\epsilon| > \Delta_0$.

Again, in the short junction limit, we can compute the Josephson current by starting from Eq.(2.44). As we did before, we can use a scattering matrix approach; in particular we start from Eqs.(2.45,2.46), when, now, we have that the Andreev-reflection coefficients must take in account a spin-orbit and multichannel interaction. Indeed, we have:

$$\hat{r}_{eh} = i\, e^{-i\gamma} \begin{pmatrix} \hat{1} \otimes \hat{\sigma}_y e^{-i\varphi/2} & 0 \\ 0 & \hat{1} \otimes \hat{\sigma}_y e^{+i\varphi/2} \end{pmatrix} \tag{2.73}$$

and

$$\hat{r}_{he} = -i\, e^{-i\gamma} \begin{pmatrix} \hat{1} \otimes \hat{\sigma}_y e^{+i\varphi/2} & 0 \\ 0 & \hat{1} \otimes \hat{\sigma}_y e^{-i\varphi/2} \end{pmatrix} \tag{2.74}$$

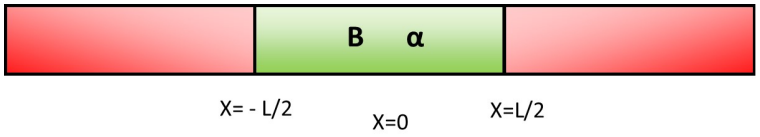

Figure 2.5: Sketch of an SNS junction with magnetic (B) and spin-orbit (α) interaction in the normal region (green region of the scheme).

In Eq.(2.74) $\hat{1}$ is the identity matrix in the channel space, the $\hat{\sigma}_y$ Pauli matrix acts in the spin space and $\gamma = \arccos(\epsilon/\Delta)$. In the normal region Andreev scattering processes are not allowed, which permit us to write

$$\begin{pmatrix} b_{eL} \\ b_{eR} \\ b_{hL} \\ b_{hR} \end{pmatrix} = \begin{pmatrix} S_e(\epsilon) & \mathbf{0} \\ \mathbf{0} & S_h(\epsilon) \end{pmatrix} \begin{pmatrix} a_{eL} \\ a_{eR} \\ a_{hL} \\ a_{hR} \end{pmatrix} \tag{2.75}$$

Again, by solving the secular equation:

$$\det\left[\hat{1} - \hat{r}_{eh}\hat{S}_h(-\epsilon)\hat{r}_{he}\hat{S}_e(\epsilon)\right] = 0 \tag{2.76}$$

we can find the Andreev bound states. We already know that, in the short-junction limit one can disregard the energy dependence of the scattering matrix and take $\hat{S}_h^*(-\epsilon) = \hat{S}_e(\epsilon) \simeq \hat{S}_e(0)$. Therefore in order to solve Eq.(2.76), we have to calculate the scattering matrix of the normal region at the Fermi energy.

We want, now, to show how to compute the normal scattering matrix in presence of Spin-orbit and Zeeman interaction. We address the case of one open channel with two spin orientations. However, our method is easily generalised to two or more open channels.

As a first step, we solve the Schroedinger equation within the L-lead ($x < -\frac{L}{2}$) and the R-lead ($x > \frac{L}{2}$) (assuming no superconductivity), as well as in the central region SO with spin-orbit interaction ($x < |\frac{L}{2}|$) (Fig.2.5) . Therefore, we derive the scattering matrix by matching the solutions at the interfaces between the three regions.The band structure is strongly influenced by the presence of the spin orbit coupling and, interestingly enough, depending on the position of the Fermi level, the number of open channels of the leads and the central region can be different.

To obtain a reliable approximation for the eigenfunctions and eigenvectors in the spin-orbit region, we exactly diagonalize the Hamiltonian in the basis of the wave functions $\{e^{i\kappa x}\chi_m(y)\phi_\sigma\}$, with $\{\chi_m(y)\}$ being the eigenfunctions of the harmonic oscillator and ϕ_σ the eigenfunctions of σ_z, by considering a finite number l of transverse modes $\{\chi_m(y)\}$, $m \in \{1, ..., l\}$. The above basis functions are eigenfunctions in the right (R) and left (L) regions. Such an approximation is indeed expected to provide a good description of the scattering dynamics of the system at energies small compared to the

energy of the last transverse mode considered. In our calculation we find that the low energy properties of our system are well described if we truncate the basis at $l = 6$.

Therefore, the problem is now reduced to finding the eigenvalues and the eigenfunction of the corresponding $2l \times 2l$-dimensional Hamiltonian matrix $\mathcal{H}(\kappa)_{m,\sigma;m',\sigma'}$. For a given energy E the allowed κ_i are the solution of

$$det\left[\mathcal{H}(\kappa_i) - E\right] = 0. \tag{2.77}$$

For each value of the energy we have κ_i $(i = 1, .., 4l)$ solutions, and the generic eigenfunction is:

$$\psi_{so}(x, y; E) = \sum_{i=1}^{4l} b_i^{so} e^{i\kappa_i x} \sum_{m\sigma} c_{m,\sigma}^{(i)} \chi_m(y)\phi_\sigma \tag{2.78}$$

where the coefficients $c_{m,\sigma}^{(i)}$ have to be determined numerically (the coefficients b_i^{so} are determined by imposing the matching conditions listed below). The number of real $\{\kappa_i\}$ in the SO region may vary according to the value of the Fermi energy. As we will show later, changing the number of real $\{\kappa_i\}$ without affecting the number of propagating channels in the leads, greatly affects the conductance of the system when it is in the normal state, and in turn the Josephson current when the leads are superconducting.

We now consider values of the Fermi energy such that one or two channels (each twice spin degenerate) are propagating in the leads. In order to obtain the total S-matrix, one has to compute all the reflection and transmission coefficients, by matching the wave function in Eq.(2.78) with the one in the leads for any possible choice of scattering boundary conditions. For instance, let us consider explicitly the case of a spin-up particle incoming from the left-hand side. In this case the wave functions within L and R are respectively given by:

$$\psi_L(x, y; E) = e^{ik_1 x}\chi_1(y)\phi_\uparrow + r_{1\uparrow,1\uparrow}^L e^{-ik_1 x}\chi_1(y)\phi_\uparrow + r_{1\downarrow,1\uparrow}^L e^{-ik_1 x}\chi_1(y)\phi_\downarrow + \sum_{\sigma=\uparrow,\downarrow;i=2,..,n} d_{i,\sigma}^L\, e^{k_i x}\chi_i(y)\phi_\sigma \tag{2.79}$$

$$\psi_R(x, y; E) = t_{1\uparrow,1\uparrow}^{RL} e^{ik_1 x}\chi_1(y)\phi_\uparrow + t_{1\downarrow,1\uparrow}^{RL} e^{ik_1 x}\chi_1(y)\phi_\downarrow + \sum_{\sigma=\uparrow,\downarrow;i=2,..,n} d_{i,\sigma}^R\, e^{-k_i x}\chi_i(y)\phi_\sigma \tag{2.80}$$

with $k_1 = [2m(E - \hbar\omega/2)]^{1/2}/\hbar$ and $k_i = [2m(\hbar\omega(i + 1/2) - E)]^{1/2}/\hbar$ for $\{i = 2, ..., l\}$.

The wave function at $x = \pm\frac{L}{2}$ must be continuos, its derivative with respect to x must be, in general, discontinuous to account the non perfect transparency at the interfaces and the SO interaction (cfr. Eq.(2.69)). Projecting the equations corresponding to the matching conditions onto the basis states $\chi_m(y)\phi_\sigma$ $(m = 1, ..., l; \sigma = \uparrow, \downarrow)$ we obtain the following set of equations:

$$\int_{-\infty}^{+\infty} \chi_m^*(y)\phi_\sigma^\dagger \left[\psi_L(-\frac{L}{2}, y) - \psi_{so}(-\frac{L}{2}, y)\right] dy = 0, \tag{2.81}$$

$$\int_{-\infty}^{+\infty} \chi_m^*(y)\phi_\sigma^\dagger \left[\psi_R(\frac{L}{2}, y) - \psi_{so}(\frac{L}{2}, y)\right] dy = 0. \tag{2.82}$$

$$\int_{-\infty}^{+\infty} \chi_m^*(y)\phi_\sigma^\dagger \Big\{ \partial_x \psi_{so}(-\frac{L}{2}, y) - \partial_x \psi_L(-\frac{L}{2}, y) - \frac{im}{\hbar^2}\alpha\sigma_y\psi_{so}(-\frac{L}{2}, y) \Big\} dy = 0, \quad (2.83)$$

$$\int_{-\infty}^{+\infty} \chi_m^*(y)\phi_\sigma^\dagger \Big\{ \partial_x \psi_R(\frac{L}{2}, y) - \partial_x \psi_{so}(\frac{L}{2}, y) + \frac{im}{\hbar^2}\alpha\sigma_y\psi_{so}(\frac{L}{2}, y) \Big\} dy = 0. \quad (2.84)$$

Therefore, we have a set of $8l$ equations which we solve numerically to determine the corresponding S matrix elements. Repeating the calculation for each possible incoming channel we construct the complete scattering matrix S_e as function of the energy E which we set to E_F in the following as we are interested only in on-shell scattering matrices.

2.3.1 Current anomaly analysis and phase diagrams

Having calculated the scattering matrix of the normal region, we can evaluate the Andreev spectrum, and eventually the Josephson current. What we obtain is shown in Fig.2.6: here we plot the current to underline the dependence of the anomaly as a function of the spin-orbit and Zeeman interaction. Now, by having this results, we can use them to do some density plot to observe the properties of the anomaly in the current and to define under what system parameters conditions we can have also an asimmetry in the maximum and the minimum of the current.

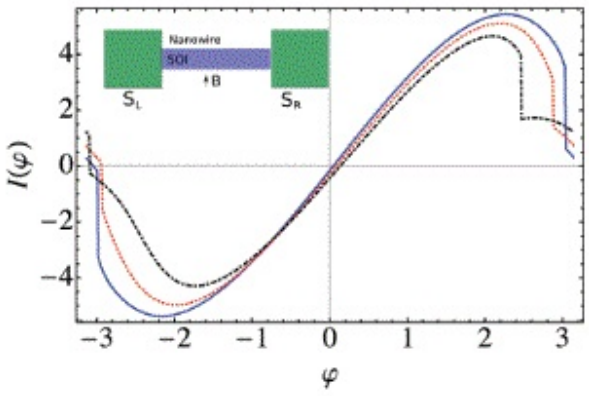

Figure 2.6: Here, we show plots of the Josephson current for several values of the magnetic field and fixed strength of the spin-orbit interaction. The current is plotted in units of $e\Delta/\hbar$.We set the Fermi energy to $\epsilon_F/E_\omega = 3.5$ (i.e. two open channels),$\alpha = 0.6 l_\omega m/\hbar^2$ and$Bg\mu_B/E_\omega$ =0.25(blue),0.50(red),0.75(black).A scheme of the studied device is in the inset (93).

In Fig. 2.7 we present a density plot of φ_0, i.e. the phase at which the free energy has a minimum, as a function of the Rashba spin-orbit interaction and of the applied magnetic field. For the sake of the simplicity of the computation, we introduce the dimensionless quantities $\alpha' = \alpha l_\omega m/\hbar^2$ and $B' = g\mu_B B/E_\omega$. In this case, while for

sufficiently large spin orbit interaction and magnetic field φ_0 can be different from 0 (or π when the magnetic field is strong enough to induce a π-transition), the asymmetry is identically zero.

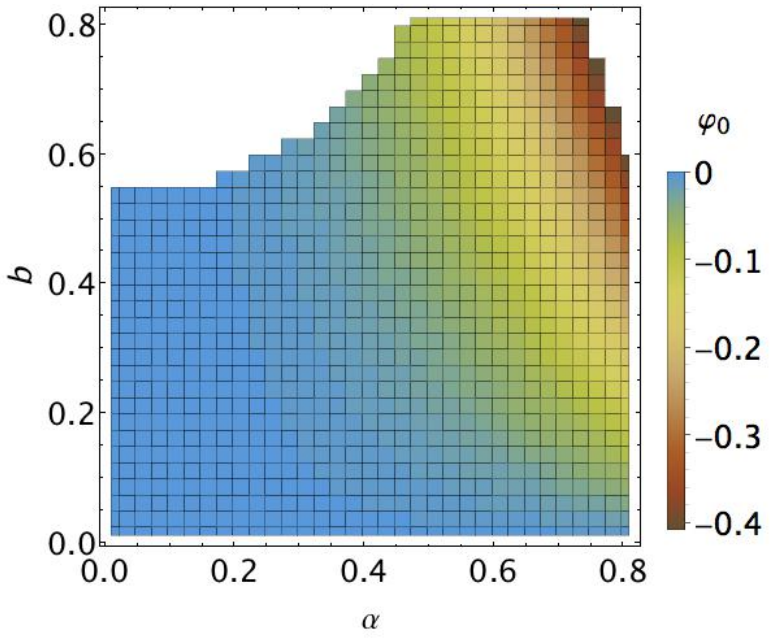

Figure 2.7: Here, we show a density plot of φ_0 in the case of one open channel as a function of the applied magnetic field and the Rashba spin-orbit interaction. On the axes, we introduce the dimensionless quantities $B' = g\mu_B B/E_\omega$ and $\alpha' = \alpha l_\omega m/\hbar^2$.We set the Fermi energy $\epsilon_F/E_\omega = 1.5$, the length of the normal section $L = 2l_\omega$, the number of transverse bands $l = 4$,where $E_\omega = \hbar\omega/2$ and $\omega = \sqrt{\hbar/m\omega}$. Notice that the upper left part of the plot corresponds to values of φ_0 close to π and, hence, not showed for convenience (93).

After this, now we change the Fermi energy E_F to values such that two open channels, corresponding to four Andreev states, are available. In Fig. 2.8 we show, again, a density plot of the phase-anomaly in the current as a function of the applied magnetic field and the spin orbit interaction. In Fig. 2.9 , instead,we show the computed value of the visibility $\aleph = (I_{0+} - I_{0-})/(I_{0+} + I_{0-})$, with I_{0+} (I_{0-}) the maximum (minimum) amplitude of the Josephson current in the positive (negative) direction. In analogy to the previous case we observe that for large enough α' and B', the value of φ_0 deviates substantially from 0 (or π). Most importantly, in contrast to what has been observed in the previous case, the visibility $\aleph$ can take values as large as 0.2. Such effect, being tuned, for instance by varying the magnetic field, may have useful application for superconducting circuits: for example, circuits with an efficiency as high as 50% are required to realize a proper superconducting diode. However, by properly engineering the interfaces and the materials we expect to achieve a wider tuneability of this value

up to experimentally relevant scales. Nonetheless, we believe that the present analysis can be taken as a first example for further studies in this direction.

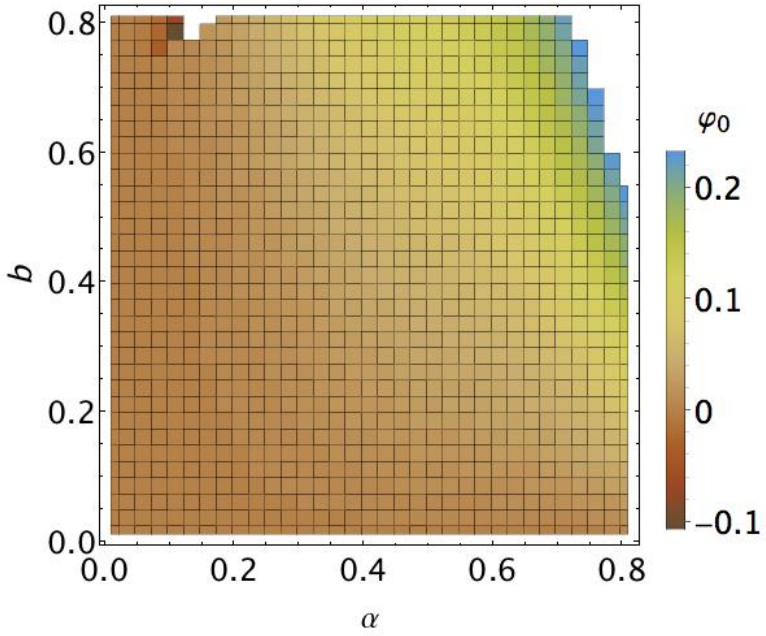

Figure 2.8: Here, we show a density plot of φ_0 in the case of two open channels as a function of the applied magnetic field and the Rashba spin orbit interaction. We set the Fermi energy $\epsilon_F/E_\omega = 3.5$, where as the remaining parameters are the same as in Fig.2.3.1. Notice that in the one-channel case, one obtains a larger deviation of φ_0 from 0, given the same spin orbit and magnetic-field parameters (93).

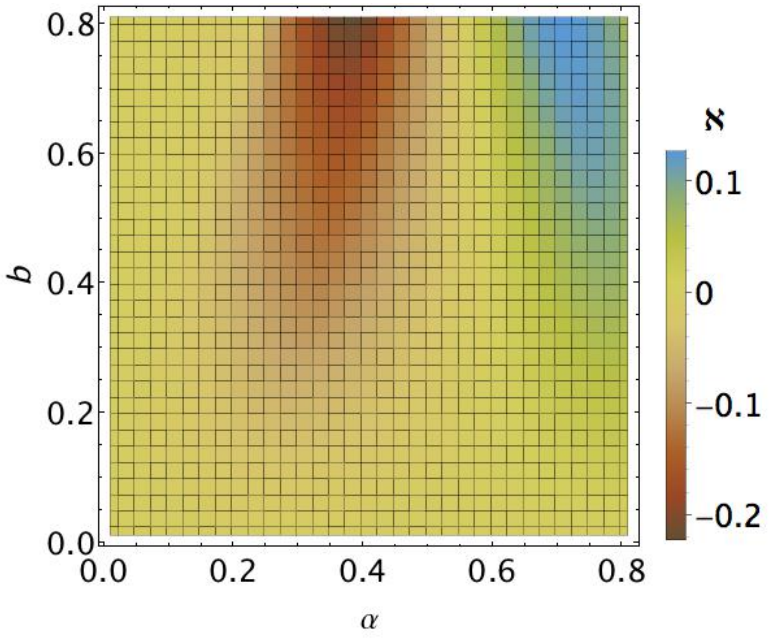

Figure 2.9: Here we show a density plot of $\aleph = (I_{0+} - I_{0-})/(I_{0+} + I_{0-})$ as a function of $alpha'$ and B'; the choice of parameters is the same of Fig.2.3.1 and we have set the Fermi energy $\epsilon_F/E_\omega = 3.5$ (93).

Chapter 3

Majorana Modes against effects of disorder in superconducting $p-$wave rings

Recent progresses in the fabrication of nanostructures made it possible to engineer hybrid devices, in between normal and superconducting rings (NS hybrid rings - NSHRs), in which superconductivity is induced by e.g. proximity effect only in part of the system (139). Realizing NSHRs opens the way to the possibility of exploring a number of remarkable physical regimes. For instance, one may think of looking at the persistent current across the ring while varying the lengths of the two regions and keeping the length of the normal region ℓ_N lower than the phase coherence length ξ. In this way, one may therefore monitor the crossover between the normal mesoscopic regime towards the complementary Josephson-junction regime, in which $\ell_S \gg \xi_0$ (140). Moreover, it is also expected to see the predicted crossover between the Φ_0 periodicity if Φ, which is appropriate for a mesoscopic normal ring, in which the current flow is mainly supported by electron transport, to the Φ_0^*-periodicity in the Josephson regime, in which the current flow is mainly due to tunneling of Andreev quasiparticles (88; 140).

The focus of this chapter is, however, the use of hybrid superconducting rings to obtain informations about the presence and the characteristics of zero-energy Majorana modes. Indeed, as we will see in detail in the development of the chapter, when we have an hybrid ring or a SQUID, in which the superconducting metal is in the topological phase, the spectrum of the system will present an energy level-crossing on varying of Φ. The crossing in the spectrum, which occurs when the magnetic flux which pierces the ring is equal to a certain value $\Phi = \Phi_0$, is a signature of the presence of zero-energy modes in the system and it is a function of the parameters which characterize the ring itself. Because of the system we are considering is a ring crossed by a magnetic field, we can think of verifying the consequences of the level crossing in the persistent current.

As predicted by electromagnetism, when a conductive system is crossed by an electromagnetic flux, a current $I(\Phi)$ is established in it, as a function of the flux. As we will see, the current $I(\Phi)$ can be computed differentiating the energy of the fundamen-

tal state of the system $E_{GS}(\Phi)$, which, when level crossing appears, presents cusps at $\Phi = \Phi_0$. Once derived, the presence of the cups implies discontinuities in the current $I(\Phi)$. The jumps of the current represent an experimentally visible way to test the presence of Majorana Modes in the system. Moreover, to mesure $I(\Phi)$, one can use a non-invasive tecnique based on magnetomers. As a counter-proof, we will see how in the case of s-wave systems, in which there cannot be a topological phase, there is no level crossing and the current does not therefore present any discontinuity.

The system that we are going to study, permits us not only to have informations about Majorana modes. Indeed, by using a numerical analysis, we can introduce a white noise in the ring and study the effects of disorder on these modes. Beyond topological aspects alone, the disordered one-dimensional p-wave superconducting wire has been actively studied for more than a decade under symmetry classification of D-class due to its localization-delocalization properties characteristics. One of the highlighting features of this system is the existence of a delocalised multi-fractal wavefunction at a critical point and the surrounding 'Griffiths phase'. In this phase a proliferation of the low energy bulk states into the superconducting gap causes the density-of-states to diverge at zero energy. This critical point indeed separates the topological and trivial phases; the delocalized state at the critical point provides a channel for the Majorana end mode in the topological phase to vanish in the trivial phase. By performing an ensemble statistic on the system, and looking at the discontinuities of the current on varying the chemical potential μ, we can obtain informations on how Majorana modes are robust against disorder, creating, once the parameters that characterize the system have been established on the topological phase, a map of the chemical potential vs the intensity of the disorder itself. This, as we shall see, will allow us to obtain informations on the consequences of disorder on the topological phase.

In the following, we will describe how it is possible to obtain the persistent current and and how to introduce disorder into the system. In particular, we will study the case of a topological superconductor and a topological-non topological junction and we will compare the obtained results with the $s-$wave case. What we will see throught the analysis is that a few amount of disorder does not affect the topological phase, which is, indeed, stabilized thanks to the localization effects; while a big amount of disorder destroys the Majorana modes.

The chapter is divided as follows:

- In Section 3.1 we will deal with the treatment of the persistent current from a classical to a quantum approach, introducing the Peierls's substitution in the case of lattice-modeled Hamiltonian. Moreover we will see how the persistent current of a system can be obtained through the calculation of the groundstate energy
- In Section 3.2 we introduce the Hamiltonian of the superconducting hybrid ring starting from the Kitaev model. Then we give the Hamiltonian of the system, describing its properties, we calculate the persistent current using numerical techniques and present the results obtained in the "clean" case.

- In Section 3.3 we will analyze the effects of disorder in the system and on the topological phase. Then, we describe the trend of the DOS (density of states) of the states below the system's gap and how they vary with the increase in disorder, linking it to the persistent current. By using these results, we get a graph of the chemical potential versus the intensity of the disorder: this will be a map with which we can get information on the topological phase of the system as these parameters change.

3.1 Persistent current

Onnes (89) discovered during an experiment that, piercing a superconductive ring by a magnetic flux even if the field ceases to act on the system, it continues to flow for an infinite time lapse. In particular we have,the Lenz law:

$$-\Sigma \frac{\partial B(t)}{\partial t} = RI(t) + L\frac{\partial I(t)}{\partial t} \tag{3.1}$$

where $B(t)$ is the magnetic-flux density, Σ is the ring area, R is the ring resistance and $I(t)$ the inducted current. Now, if we set $B(t) = 0$, we can simply solve the differential equation for $I(t)$:

$$I(t) = I(t_0)\ e^{-\frac{Rt}{L}} \tag{3.2}$$

which, considering a superconductive material that has $R = 0$, gives a first result:

$$I(t) = I(t_0) \tag{3.3}$$

The materials in which the persistent current can be observed are in thermal equilibrium and in the absence of an external excitation. The observability of persistent currents in normal metal rings was not trivial to imagine and it was first considered as a only-superconducting phenomenon since it was first predicted in 1983 by Buttiker (88) . Subseqently, these persistent currents have been studied experimentally several times but with conflicting results for the superconductive cases, due in part to the difficulty of the measurements, but we actually have some interesting results for homogeneous normal rings (89; 90; 91; 92) . The normal state persistent current that we are going to study is an equilibrium property of the system. Then we attempt to describe broadly the theory relevant to mesoscopic persistent currents introducing the Aharonov-Bohm phase (87) .

Let us consider quantum mechanical charged particles living on a one- dimensional closed loop. Let us assume that a magnetic flux Φ pierces the ring, corresponding to a uniform magnetic field perpendicular to the plane of the ring (see Fig.3.1). To such a magnetic field is associated a vector potential A, that is point-by-point directed along the tangent to the ring, and whose strength is given by the relation

$$A = \frac{\Phi}{L}$$

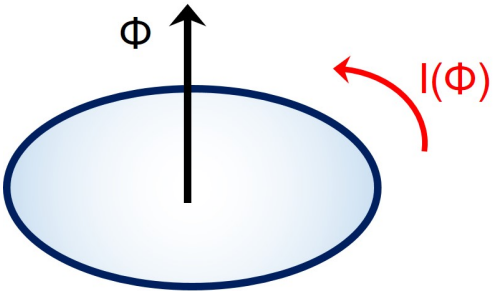

Figure 3.1: Metallic ring pierced by a magnetic flux Φ and the induced current $I(\Phi)$.

where L is the length of the ring. Accounting for the additional magnetic flux amounts, in a continuum quantum mechanical model to trade the momentum p for the covariant momentum $p - eA$, in a lattice model to perform the Peierls substitution, that is, in trading the single electron hopping amplitude

$$J_{j,j+1} \to J e^{-i\frac{ea}{\hbar}A_j} \tag{3.4}$$

where a is the lattice step and the exponential $e^{-i\frac{ea}{\hbar}A_j}$ is the consequence of the gauge-invariance imposition and is known as Aharonov-Bohm phase (87) . Focusing on the lattice model, we see that, on setting $\frac{ea}{\hbar}A_j \to \varphi_j$, the microscopic current operator on ring $j \to j+1$ j_j is given by:

$$j_j = e\frac{\partial H}{\partial \varphi_j} \tag{3.5}$$

H being the system Hamiltonian. Therefore, if $|\mathrm{GS}\rangle$ denotes the system's groundstate, the groundstate persistent current at $T = 0$ in the case in which φ_j is independent of j in a uniform system will be given by:

$$I = -\frac{e}{\ell}\frac{\partial}{\partial \varphi}\langle \mathrm{GS}|H|\mathrm{GS}\rangle = -\frac{e}{\ell}\frac{\partial \mathcal{E}_0[\varphi]}{\partial \varphi} \tag{3.6}$$

with $\mathcal{E}_0[\varphi]$ being the groundstate energy as a function of the applied (dimensionless) flux φ. From a thermodynamic point of view, at temperature $T \neq 0$, the persistent current $I[\varphi : T]$ can be obtained from the free energy (114) $\mathcal{F}[\varphi; T]$ as :

$$I[\varphi; T] = e\partial_\varphi \mathcal{F}[\varphi; T] \tag{3.7}$$

Then, during the discussion of this chapter, we will consider only the case in which the temperature is $T = 0$, in which Eq.(3.7) becomes:

$$\mathcal{F}[\varphi; 0] = E_{\mathrm{GS}}[\varphi] \tag{3.8}$$

with $E_{\mathrm{GS}}[\varphi]$ being the total groundstate energy of the system, $E_{\mathrm{GS}}[\varphi]$. Therefore, in terms of the quasiparticle excitation of $H[\Phi]$, $\{\epsilon_n[\varphi]\}$, one obtains:

$$I[\varphi] = e\partial_\varphi E_{\rm GS}[\varphi] = e\partial_\varphi \sum_{\epsilon_n<0} \epsilon_n[\varphi] \tag{3.9}$$

with the sum taken, as specified, over negative-energy single-quasiparticle states.

By now, there is a large amount of literature about persistent current in normal mesoscopic ring addressing a number of issues such as, for instance, the effect of disorder in the ring with consequent possible halving in the period of the current (133; 134), the role of the spin degree of freedom (135), the consequences of the electronic interaction, with and without impurity scattering (136), the presence of spin-orbit interaction (137), etc. Nevertheless, after the recent measurements presented in Ref.(132), it appears that the experimental data can be well fitted by employing a simple quantum mechanical noninteracting model of diffusive electrons (132). While this corresponds to the length scale of the ring being much lower than the electronic phase coherence length in the system, the fact that in semiconducting materials the electronic mean free path is comparable with the phase coherence length (138) makes it in principle possible to realize ballistic rings, in which a fully ballistic propagation takes the place of the diffusive dynamics of the electrons (139).

3.2 Majorana Bound States and topological phase transition in a p-wave disordered ring

In this section, we discuss at first in detail the derivation of the exact wavefunction of sub-gap states in an open Kitaev chain, of finite length ℓ_S. While, for finite-ℓ_S, we find a single Dirac fermion level, which can be either empty, or occupied, with a corresponding finite energy gap E_M, as $\ell_S \to \infty$, the states become degenerate in energy at the Fermi level, and appropriate linear combinations of the corresponding wavefunctions become localized at the two endpoints of the chain, eventually corresponding to the two zero-energy Majorana solutions of Kitaev's model (142). Finally, we will show the effects of disorder on a one-dimensional p-wave superconducting ring, focusing our attention to the properties of Majorana Bound States (MBSs) in the persistent current on increasing disorder. Let us start by describing the "clean" case, i.e. the system in absence of disorder.

3.2.1 Exact wavefunctions for sub-gap states for a finite-length Kitaev chain

Let us consider an homogeneous finite-lenght Kitaev-chain (142) (see Fig.3.2). We can describe it with the Hamiltonian:

$$H = -w \sum_{i=1}^{\ell-1} \left\{ c_j^\dagger c_{j+1} + c_{j+1}^\dagger c_j \right\} + \mu \sum_{i=1}^{\ell} c_j^\dagger c_j + \Delta \sum_{i=1}^{\ell-1} \left\{ c_j c_{j+1} + c_{j+1}^\dagger c_j^\dagger \right\} \tag{3.10}$$

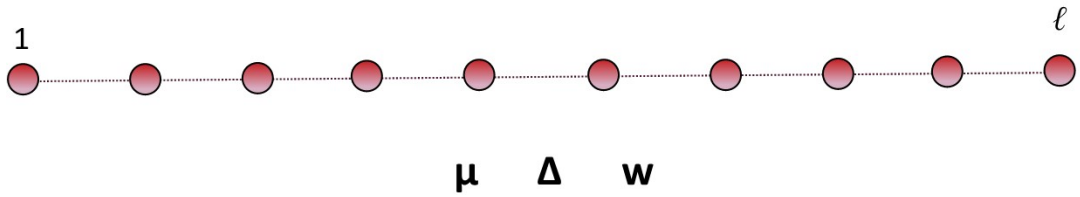

Figure 3.2: Sketch of an homogeneous finite-lenght Kitaev chain

where w is the hopping energy from the $j-t$h site to the $j+1$-one, μ is the chemical potential, Δ is the superconducting pairing and c_j and $c_j^\dagger$ are, respectively, fermionic annihilation and creation operators . From Eq.(3.10) we can derive the BdG equation and the energy dispersion relation for the system (see Appendix B). Now, in order to compute the exact wavefunctions for sub-gap states for the finite-length Kitaev chain, we start from the dispersion relation in Eqs.(B.10) which, for sub-gap solutions ($|E|<\Delta_w$) yields the allowed values of the (complex conjugate) particle- and hole-momenta defined by:

$$\begin{aligned}\cos(k_p) &= -\frac{w\mu}{2(w^2-\Delta^2)} - \frac{i}{2}\sqrt{\frac{\Delta_w^2-E^2}{w^2-\Delta^2}} \\ \cos(k_h) &= -\frac{w\mu}{2(w^2-\Delta^2)} + \frac{i}{2}\sqrt{\frac{\Delta_w^2-E^2}{w^2-\Delta^2}}\end{aligned} \tag{3.11}$$

Eqs.(3.11) are readily solved by setting $k_p=\pi-q_R+iq_I$ and $k_h=(k_p)^*=\pi-q_R-iq_I$, with

$$\begin{aligned}\cos(q_R)\cosh(q_I) &= \frac{w\mu}{2(w^2-\Delta^2)} \\ \sin(q_R)\sinh(q_I) &= \frac{1}{2}\sqrt{\frac{\Delta_w^2-E^2}{w^2-\Delta^2}}\end{aligned} \tag{3.12}$$

As a result, the general formula for a subgap solution will be given by:

$$\begin{aligned}\begin{bmatrix} u_j \\ v_j \end{bmatrix} &= (-1)^j \Bigg\{ A_{(p,+)} \begin{bmatrix} u \\ v \end{bmatrix} e^{-iq_Rj} e^{-q_Ij} + A_{(p,-)} \begin{bmatrix} u \\ -v \end{bmatrix} e^{iq_Rj} e^{q_Ij} \\ &+ A_{(h,+)} \begin{bmatrix} u^* \\ v^* \end{bmatrix} e^{iq_Rj} e^{-q_Ij} + A_{(h,-)} \begin{bmatrix} u^* \\ -v^* \end{bmatrix} e^{-iq_Rj} e^{q_Ij} \Bigg\}\end{aligned} \tag{3.13}$$

with u, v solutions of the algebraic system :

$$\begin{aligned}\{E+2w\cos(k_p)+\mu\}u - 2i\Delta\sin(k_p)v = 0 \\ 2i\Delta\sin(k_p)u + \{E-2w\cos(k_p)-\mu\}v = 0\end{aligned} \tag{3.14}$$

The actual energy eigenstates are determined as nontrivial solutions such as the one in Eq.(3.13) satisfying the boundary conditions $\left[\begin{array}{c} u_0 \\ v_0 \end{array} \right] = \left[\begin{array}{c} u_{\ell+1} \\ v_{\ell+1} \end{array} \right] = 0$. It is therefore straightforward to verify that this implies the equation for the energy eigenvalues given by:

$$[\Im m(uv^*)]^2 \sinh^2[q_I(\ell+1)] = [\Re e(uv^*)]^2 \sin^2[q_R(\ell+1)] \tag{3.15}$$

Eqs.(3.13,3.14,3.15) can be used to estimate the energy of the sub-gap levels and the corresponding wavefunction for any value of μ. Indeed, we use them to numerically estimate the energy gap and to accordingly infer the overlap scale between the localized Majorana modes at given values of the system's parameters. Specifically, one is only interested in the low-energy physics of a finite-size one-dimensional topological superconductor coupled to normal conductors at each of its endpoints, the whole topological superconductor can be traded for an effective Hamiltonian involving only the low-energy sup-gap degrees of freedom discussed above, with parameters effectively determined by the actual system parameters. To illustrate how the procedure works, let us focus onto the simple case $\mu = 0$, ℓ even. In this case, k_p and k_h are simply given by:

$$\begin{array}{rcl} k_p & = & \frac{\pi}{2} + i\lambda(E) \\ k_h & = & \frac{\pi}{2} - i\lambda(E) \quad , \end{array} \tag{3.16}$$

with:

$$\sinh[\lambda(E)] = \frac{1}{2}\sqrt{\frac{4\Delta^2 - E^2}{w^2 - \Delta^2}} \tag{3.17}$$

As a result, Eq.(3.13) can now be presented as:

$$\begin{array}{rcl} \left[\begin{array}{c} u_j \\ v_j \end{array} \right] & = & A_{(p,+)} \left[\begin{array}{c} u \\ v \end{array} \right] i^j e^{-\lambda[E]j} + A_{(p,-)} \left[\begin{array}{c} u \\ -v \end{array} \right] i^{-j} e^{\lambda[E]j} \\ & + & A_{(h,+)} \left[\begin{array}{c} u^* \\ v^* \end{array} \right] i^{-j} e^{-\lambda[E]j} + A_{(h,-)} \left[\begin{array}{c} u^* \\ -v^* \end{array} \right] i^j e^{\lambda[E]j} \end{array} \tag{3.18}$$

with:

$$\left[\begin{array}{c} u_p \\ v_p \end{array} \right] = \frac{1}{\sqrt{2}} \left[\begin{array}{c} e^{\frac{i}{2}\mathrm{sgn}(E)\vartheta} \\ i\mathrm{sgn}(E) e^{-\frac{i}{2}\mathrm{sgn}(E)\vartheta} \end{array} \right] \quad ; \quad \left[\begin{array}{c} u_h \\ v_h \end{array} \right] = \frac{1}{\sqrt{2}} \left[\begin{array}{c} -i\mathrm{sgn}(E) e^{-\frac{i}{2}\mathrm{sgn}(E)\vartheta} \\ e^{\frac{i}{2}\mathrm{sgn}(E)\vartheta} \end{array} \right] \tag{3.19}$$

and:

$$\vartheta = \mathrm{atan}\left[\frac{2w \sinh[\lambda(E)]}{|E|} \right] \tag{3.20}$$

It is straightforward, though tedious, to show that the secular equation for the sub-gap energy eigenvalues is now given by:

$$(\ell+1)\lambda[E] = \pm \sinh^{-1}\left[\frac{2w}{E}\sinh[\lambda(E)]\right] \tag{3.21}$$

which is solved by setting:

$$|E| = \epsilon = 2\Delta\left[\frac{\cosh[\lambda[E]]}{\cosh[(\ell+1)\lambda[E]]}\right] \approx 2\Delta e^{-\ell\lambda[E]} \approx 2\Delta\exp\left\{-\ell\sinh^{-1}\left[\frac{\Delta}{\sqrt{w^2-\Delta^2}}\right]\right\} \tag{3.22}$$

Therefore, from Eq.(3.22) we readily estimate that the hybridization length scale between the Majorana modes, ℓ_M, is given by:

$$\ell_M \sim \left\{\sinh^{-1}\left[\frac{\Delta}{\sqrt{w^2-\Delta^2}}\right]\right\}^{-1} \tag{3.23}$$

From Eq.(3.13) we may therefore construct the wavefunctions corresponding to the positive- and to the negative-energy sub-gap solutions. As a result, one obtains for the positive- sub-gap energy solution of the BdG equations:

$$\begin{aligned}\left[\begin{array}{c} u_j \\ v_j \end{array}\right]_+ &= c\Bigg\{e^{\frac{\xi}{2}}\left[\begin{array}{c} e^{\frac{i}{2}\vartheta} \\ ie^{-\frac{i}{2}\vartheta}\end{array}\right] i^j e^{-j\lambda[E]} + ie^{-\frac{\xi}{2}}\left[\begin{array}{c} e^{\frac{i}{2}\vartheta} \\ -ie^{-\frac{i}{2}\vartheta}\end{array}\right] i^{-j}e^{j\lambda[E]} \\ &+ e^{\frac{\xi}{2}}\left[\begin{array}{c} -ie^{-\frac{i}{2}\vartheta} \\ -e^{\frac{i}{2}\vartheta}\end{array}\right] i^{-j}e^{-j\lambda[E]} - ie^{-\frac{\xi}{2}}\left[\begin{array}{c} -ie^{-\frac{i}{2}\vartheta} \\ e^{\frac{i}{2}\vartheta}\end{array}\right] i^{j}e^{j\lambda[E]}\Bigg\}\end{aligned} \tag{3.24}$$

with:

$$c = \frac{1}{4}\sqrt{\frac{2\sinh[\lambda[E]]}{\sinh[\xi[E]-\lambda[E]]}} \tag{3.25}$$

and $\xi[E] = \sinh^{-1}\left[\frac{2w}{E}\sinh[\lambda(E)]\right]$. Similarly, one obtains for the negative- sub-gap energy solution of the BdG equations:

$$\begin{aligned}\left[\begin{array}{c} u_j \\ v_j \end{array}\right]_- &= -c\Bigg\{e^{\frac{\xi}{2}}\left[\begin{array}{c} e^{-\frac{i}{2}\vartheta} \\ -ie^{\frac{i}{2}\vartheta}\end{array}\right] i^j e^{-j\lambda[E]} - ie^{-\frac{\xi}{2}}\left[\begin{array}{c} e^{-\frac{i}{2}\vartheta} \\ ie^{\frac{i}{2}\vartheta}\end{array}\right] i^{-j}e^{j\lambda[E]} \\ &+ e^{\frac{\xi}{2}}\left[\begin{array}{c} ie^{\frac{i}{2}\vartheta} \\ -e^{-\frac{i}{2}\vartheta}\end{array}\right] i^{-j}e^{-j\lambda[E]} + ie^{-\frac{\xi}{2}}\left[\begin{array}{c} ie^{\frac{i}{2}\vartheta} \\ e^{-\frac{i}{2}\vartheta}\end{array}\right] i^{j}e^{j\lambda[E]}\Bigg\}\end{aligned} \tag{3.26}$$

From Eqs.(3.24,3.26), we therefore find that the eigenmodes corresponding to the $\pm$ solutions are respectively given by:

$$\begin{aligned}\Gamma_+ &= \sum_{j=1}^{\ell}\{[u_j]_+^* c_j + [v_j]_+^* c_j^\dagger\} \\ \Gamma_- &= \sum_{j=1}^{\ell}\{[u_j]_-^* c_j + [v_j]_-^* c_j^\dagger\} \end{aligned} \tag{3.27}$$

which shows that, as expected, one recovers the relation:

$$\Gamma_+ = \Gamma_-^\dagger \equiv \Gamma \tag{3.28}$$

By Eqs.(3.27) and truncating the mode expansion of the real space lattice operators by retaining low-energy modes only, we therefore get:

$$\begin{aligned} c_j &\approx [u_j]_+\Gamma + [v_j]_+^*\Gamma^\dagger \\ c_j^\dagger &\approx [v_j]_+\Gamma + [u_j]_+^*\Gamma^\dagger \end{aligned} \tag{3.29}$$

Now, one may rewrite the tunneling contribution to the Hamiltonian in Eq.(4.46) as :

$$H_\tau = -\tau\{[c_1^\dagger d_{\ell_N} + d_1^\dagger c_{\ell_N}]e^{\frac{i}{4}\Phi} + [d_{\ell_N}^\dagger c_1 + c_\ell^\dagger d_1]e^{-\frac{i}{4}\Phi}\} \tag{3.30}$$

where τ is the weak link amplitude.

Using the truncated expansions in Eqs.(3.29) and the explicit form of the wavefunctions evaluated at $j = 1, \ell$, one eventually approximates Eq.(3.30) as:

$$H_\tau = t_L\{\gamma_L[e^{\frac{i}{4}\Phi} d_{\ell_N} - e^{-\frac{i}{4}\Phi} d_{\ell_N}^\dagger]\} + it_R\{\gamma_R[e^{-\frac{i}{4}\Phi} d_1 + e^{\frac{i}{4}\Phi}]d_1^\dagger\} \tag{3.31}$$

with

$$\begin{aligned} \gamma_L &= e^{-i\frac{\pi}{4}}\Gamma + e^{i\frac{\pi}{4}}\Gamma^\dagger \\ \gamma_R &= -i\{e^{-i\frac{\pi}{4}}\Gamma - e^{i\frac{\pi}{4}}\Gamma^\dagger\} \end{aligned} \tag{3.32}$$

and $t_L = t_R = \Upsilon\tau$, with:

$$\begin{aligned} u_{1,+} &= -e^{-i\frac{\pi}{4}}\Upsilon \\ v_{1,+} &= -e^{-i\frac{\pi}{4}}\Upsilon \\ u_{\ell,+} &= -e^{-i\frac{\pi}{4}}\Upsilon \\ v_{\ell,+} &= e^{-i\frac{\pi}{4}}\Upsilon \quad . \end{aligned} \tag{3.33}$$

Finally, to recover the energy bias between the Dirac modes, we add a term of the form:

$$H_\Gamma = 2\epsilon\{2\Gamma^\dagger\Gamma - 1\} = -2\epsilon i\gamma_L\gamma_R \tag{3.34}$$

In general, t_L, t_R are smooth functions of μ. The dependence of ϵ on μ can be inferred by, for instance, numerically solving Eq.(3.15), as we did in the main text, to also derive the dependence of ℓ_M on the chemical potential.

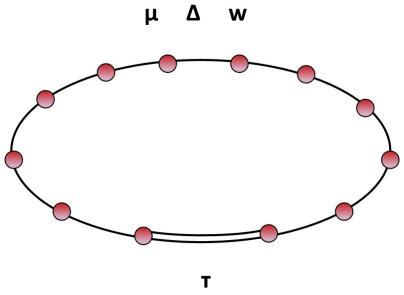

Figure 3.3: Sketch of the one-dimensional p-wave superconducting ring described by H_K in Eq.(3.10) plus $H_\tau[\Phi]$ in Eq.(3.35).

3.2.2 The clean case for a finite-length $p-$wave superconducting ring

Let us consider our p-wave superconducting ring interrupted by a weak normal link and pierced by a magnetic flux Φ, which induces a persistent current $I[\Phi]$ through the ring (as we have already show in the previous chapter - see Fig. 3.3). We first start with the description of what happens in the "clean case", i.e. in absence of disorder.

To formally describe the p-wave superconductor we use again the Kitaev's one-dimensional lattice model Hamiltonian (142). Indeed, despite its apparent simplicity and mathematical tractability, the Kitaev model can be regarded as an effective low-energy description of a quantum wire with a strong spin-orbit coupling and a large enough Zeeman effect, which turns into a one-dimensional p-wave superconductor by proximity to a "standard" s-wave bulk superconductor (98; 99).

The Kitaev lattice Hamiltonian for a one-dimensional p-wave superconductor is given by Eq.(3.10) (142). In Eq.(3.10) the operators c_j ($c_j^\dagger$) ($j = 1, \ldots, \ell$) are single-fermion annihilation (creation) operators defined on site-j of the one-dimensional chain. They satisfy the canonical anticommutation relations $\{c_j, c_{j'}^\dagger\} = \delta_{j,j'}$, all the other anticommutators being equal to 0. Here, w and Δ are respectively the normal single-electron hopping amplitude and the p-wave superconducting pairing, while μ is the chemical potential. For the sake of simplicity, without any loss of generality, we further simplify H_K by choosing $w = \Delta$ (which does not qualitatively affect the spectrum and the eigenfunctions with respect to the general case) and $\mu \geq 0$ (the complementary situation $\mu < 0$ can be easily recovered by symmetry). Besides its mathematical simplifity, it is also worth noticing that the Hamiltonian in Eq.(3.10) with $w = \Delta$ takes a precise physical meaning, as it be obtained from the Hamiltonian open quantum Ising chain via Jordan-Wigner transformation (100).

In Appendix B, we review the main properties of H_K for $w = \Delta$. In particular, we highlight the appearance of zero-energy Majorana modes localized at the endpoints of the chain (142). The Majorana modes can then be combined into a zero-energy Dirac mode, which implies a twofold spectral degeneracy of H_K, with degenerate eigenstates differing from each other by the total fermion parity corresponding to the zero-energy

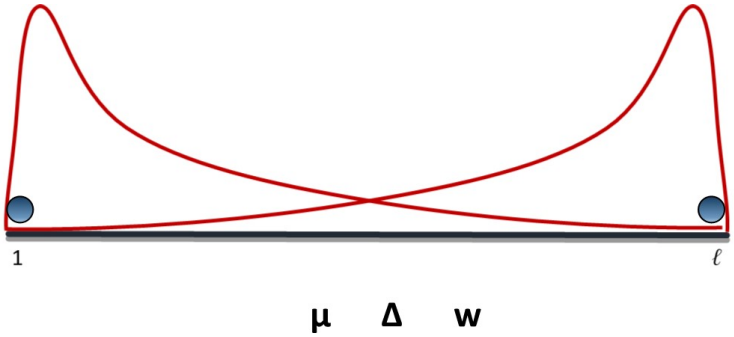

Figure 3.4: Sketch of the hybridization of Majorana Modes at the end point of a finite-lenght Kitaev chain in the topological phase.

mode being populated, or empty. For a finite-length chain (that is, with ℓ of the same order as the superconducting coherence length of the p-wave superconductor, ξ_0), the Majorana modes are hybridized by means of an overlap matrix element that is $\sim e^{-\frac{\ell}{\xi}}$. In this case, strictly speaking, Majorana modes are not anymore true eigenstates of H_K. Instead, one may rather speak ot two putative Majorana modes that hybridize into a finite-energy Dirac mode, with corresponding disappearance of the fermion-parity related degeneracy (Fig.3.4).

In Appendix B we show that, Majorana modes as well as putative Majorana modes only emerge within the phase in parameter space characterized by $\frac{2w}{\mu} > 1$. Strictly speaking, one may dub it "topological" only when Majorana modes lie exactly at zero energy. In general, we rather speak of a putative topological phase, with corresponding putative Majorana modes hybridized into nonzero energy Dirac modes. Instead, neither Majorana modes, or putative Majorana modes, appear in the spectrum for $\frac{2w}{\mu} < 1$. To trade the open Kitaev chain for a one-dimensional p-wave ring, we add to H_K a normal weak link hopping term H_τ. Defining τ to be the normal hopping amplitude and taking into account that the applied flux Φ can be fully loaded on the weak link by means of a simple canonical transformation of the fermionic operators, the weak link Hamiltonian H_τ can be presented as (101)

$$H_\tau[\Phi] = -\tau\{e^{\frac{i}{2}\Phi}c_1^\dagger c_\ell + e^{-\frac{i}{2}\Phi}c_\ell^\dagger c_1\} \tag{3.35}$$

In the following, we will use the full Hamiltonian $H[\Phi] = H_K + H_\tau[\Phi]$ to compute the density of states and the persistent current $I[\Phi]$. In a ring made with a conventional s-wave superconductor, as well as in a ring made with a p-wave superconductor in the nontopological phase, $I[\Phi]$ is tipically a periodic function of Φ with period 2π. At variance, when the p-wave superconductor is within its topological phase, if fermion parity is conserved, the presence of Majorana modes at the endpoints of the superconductor (and, therefore, at the two sides of the weak link) typically makes $I[\Phi]$ periodic with period equal to 4π, provided there is a negligible overlap between the Majorana mode wavefunctions (102); note that, for a finite size ring one should carefully spell out

whether the 4π-periodicity is really due to fermion parity conservation in the presence of Majorana modes, or is a simple effect of the crossover from a superconducting to a mesoscopic ring as $\ell \leq \xi_0$ (140). In general, in a one-dimensional p-wave superconducting ring, one expects a coexistence of a 2π- and of a 4π-harmonics, due to the existence of two possible "channels" for the Majorana modes to hybridize into a Dirac mode: through the finite-length p-wave superconducting chain, as well as via the weak link. Both mechanisms are expected to determine a zero-mode level splitting but the relative sign of the corresponding contribution to the splitting energy can be tuned by acting on Φ (see Appendix C for a detailed discussion of this point), thus inducing competition between the two of them. The presence of the two harmonics and the value of their relative weight can be readily understood from our equation for the energy eigenvalues of the putative Majorana fermnions and from the exact condition for recovering a putative zero-energy level crossing at pertinent values of Φ, Appendix C. Indeed, from Eq.(C.21) one expects that $E_{\rm GS}[\Phi]$ and, correspondingly, $I[\Phi]$ are 4π-periodic functions of Φ, as the applied flux only enters the equation for the energy eigenvalues. As this picture strongly relies upon assuming fermion parity conservation, which is hard to recover in a quasistatic dc current measurement, in Ref.(159) it was noted that, since fermion parity changing processes are expected to take place via relaxation processes that happen just at the putative Majorana fermion level crossing, one may just get rid of level crossings by pertinently tuning the system parameters. Formally, we rigorousely argue it in Appendix C, where we prove that putative Majorana fermion level crossing takes place at $\Phi = \Phi_*$, with Φ_* satisfying the equation:

$$\frac{2w\tau}{\mu^2 - \tau^2} \cos\left(\frac{\Phi}{2}\right) = e^{-(\ell-2)\delta_0} \Rightarrow \cos\left(\frac{\Phi}{2}\right) = \frac{\mu^2 - \tau^2}{2w\tau} e^{-(\ell-2)\delta_0} \tag{3.36}$$

with δ_0 defined as:

$$\delta_0 = 2\sinh^{-1}\left\{\sqrt{\frac{\Delta_w^2}{8w\mu}}\right\} \tag{3.37}$$

From Eq.(3.36) we see that a putative Majorana fermion level crossing happens whenever the energy gap associated to the Majorana mode-hybridization through the finite superconducting chain (that is, the term $\propto e^{-\ell\delta_0}$) becomes equal, though opposite in sign, to the energy gap associated to Majorana modes-hybridization through the weak link (which is $\propto \tau$). Clearly, as the latter contribution is modulated by $\cos\left(\frac{\Phi}{2}\right)$, the level crossing can only happen provided the condition $\left|\frac{\mu^2-\tau^2}{2w\tau} e^{-(\ell-2)\delta_0}\right| \leq 1$ is met, that is, either the chain must be long enough (as $\delta_0 \sim \xi_0^{-1}$), or the coupling τ must be strong enough, or both. Thus, to avoid putative Majorana fermion level crossing one has to make it impossible to satisfy Eq.(3.36) at any value of Φ. This strategy was actually pursued in Ref.(159) by assuming $\tau/w \ll 1$ and, at the same time, by considering the ring close to the topological phase transition, at which $\xi_0 \to \infty$ (142) and, accordingly, the contribution to the putative Majorana modes energy levels arising from

the hybridization through the superconductor is always larger than the one due to the hybridization through the weak link. This implies consistent spectral weight for the 4π-harmonics, which appears as a modulation of the 2π-periodicity in $I[\Phi]$, as a result of the competition between the "Kondo-like" Kondo hybridization between the putative Majorana modes mediated by the weak link (86), and the "RKKY-like" interaction mediated by the finite chain length. At variance, when going across the phase transition, the putative Majorana modes disappear, thus determining a full disappearance of the 4π-harmonics and a purely 2π periodic persistent current.

Now we show the evolution of putative Majorana modes energy $\pm\epsilon_0[\Phi]$ as a function of the flux Φ, in order to show the level crossing when the system lies in the topological phase and, as a difference, the spectrum of an s-wave ring (see Appendix A for more details about the properties of this system). In Fig.3.5**a**), we plot $\pm\epsilon_0[\Phi]$ for $\frac{\mu}{2w} = 0$, $\frac{\tau}{2w} = 0.15$, and for $\ell = 40$. $\mu = 0$ corresponds to a level crossing exactly located at $\Phi = \pi$, as evidenced in Fig.3.5**a**). By comparison, in Fig.3.5**b**) we draw a similar diagram constructed for an s-wave superconducting ring described by the (spinful) Hamiltonian $H_s = H_{s-wave} + H_{s-\tau}$, with

$$H_{s-wave} = -w\sum_{\sigma}\sum_{j=1}^{\ell-1}\{c^{\dagger}_{j,\sigma}c_{j+1,\sigma}+c^{\dagger}_{j+1,\sigma}c_{j,\sigma}\}-\mu\sum_{\sigma}\sum_{j=1}^{\ell}c^{\dagger}_{j,\sigma}c_{j,\sigma}+\Delta\sum_{j=1}^{\ell}\{c_{j,\uparrow}c_{j,\downarrow}+c^{\dagger}_{j,\downarrow}c^{\dagger}_{j,\uparrow}\} \tag{3.38}$$

and the weak link Hamiltonian given by

$$H_{s-\tau} = -\tau\sum_{\sigma}\{e^{\frac{i}{2}\Phi}c^{\dagger}_{1,\sigma}c_{\ell,\sigma} + e^{-\frac{i}{2}\Phi}c^{\dagger}_{\ell,\sigma}c_{1,\sigma}\} \tag{3.39}$$

Specifically, in Fig.3.5**b**) we set $\Delta = w$ and $\frac{\tau}{2w} = 0.15$. We again see a level modulation with Φ but now the levels emerge near by the gap edge and keep well separated from each other at any values of the applied flux.

Differently from Ref.(159), here we do assume putative Majorana fermion level crossing at a pertinent value of Φ and, at the same time, we assume absence of fermion parity conservation, which makes $I[\Phi]$ to be a 2π-periodic function of Φ. According to Eq.(3.36), we have to assume that $\left|\frac{\mu^2-\tau^2}{2w\tau}e^{-(\ell-2)\delta_0}\right| \leq 1$. Indeed, this does not require any challenging fine-tuning of the system parameters: for instance, it is enough to make a large enough ring, so to make sure that $\ell/\xi_0 \gg 1$. Once this condition is met, either there are subgap putative Majorana modes states, and their energies cross at $\Phi = \Phi_*$, or there are no putative Majorana modes states at all. Our second assumption, that is, the absence of fermion parity conservation, is quite a natural consequence of having a quasistatic processes, as noted above, as the system is likely to always lie within its thermodynamic groundstate, even when going across putative Majorana fermion level crossing. Then, while $E_{\rm GS}[\Phi]$ is continuous across putative Majorana fermion level crossings, its first derivative with respect to Φ, $I[\Phi]$, is not. Therefore, at each level crossing, we expect a discontinuous jump in $I[\Phi]$, due to the different slope of the putative Majorana mode energies $\pm\epsilon_0[\Phi]$ when approaching Φ_* from the left and from the

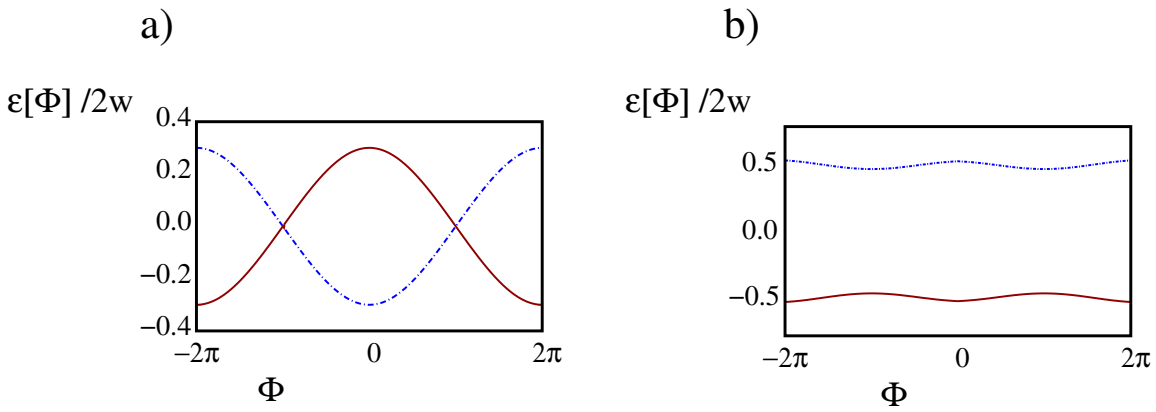

$\Delta = w$ and $\frac{\tau}{2w} = 0.15$ (104).

Figure 3.5: Subgap energy levels as a function of the applied magnetic flux Φ for: **a**): The p-wave superconducting ring with a weak link described by H_K in Eq.(3.10) plus H_τ in Eq.(3.35) with $\frac{\tau}{2w} = 0.15$;
b) The s-wave superconducting ring with a weak link described by H_{s-wave} in Eq.(3.38) plus $H_{s-\tau}$ in Eq.(3.39) with
$\Delta = w$ and $\frac{\tau}{2w} = 0.15$ (104).

right. To illustrate this feature, in Fig.3.6, we plot $I[\Phi]$ *vs.* Φ through the ring with $\frac{\tau}{2w} = 0.15$, $\Delta = w$, $\ell = 40$, and $\frac{\mu}{2w} = 0$ (panel **a**)), and $\frac{\mu}{2w} = 0.75$ (panel **b**). In both cases, we see the expected jump in the current. Remarkably, while the discontinuity in $I[\Phi]$ in Fig.3.6**a**) takes place exactly at $\Phi_* = \pm\pi$, the discontinuity points in Fig.3.6**b**) are slightly displaced from $\pm\pi$, according to the result of Appendix C). Note that in both cases the condition for having subgap putative Majorana modes is satisfied, as it must be. For comparison, in Fig.3.7, we plot $I[\Phi]$ *vs.* Φ, for a s-wave superconducting ring with $\ell = 40$, $\Delta = 0.5(2w)$, $\tau = 0.15(2w)$, and $\mu = 0$ (panel **a**)), and for a 1pSR with $\ell = 40$, $\Delta = w$, $\tau = 0.15(2w)$, and $\mu = 1.25(2w)$ (panel **b**): this last choice of parameters implies no subgap putative Majorana modes). As a result, in both cases $I[\Phi]$ is a continuous function of Φ, with no discontinuities within the whole interval $[-2\pi, 2\pi]$.

An important remark about the discontinuity in $I[\Phi]$ is that in Figs.(3.6,3.7) we have plotted the exact current $I[\Phi]$ at $T = 0$ using both parameters that make us fall into the topological phase, or not, computed from Eq.(3.9) by summing over all the quasiparticle levels with $\epsilon_n < 0$. Nevertheless, the discontinuity is clearly determined only by the change in the slope of the putative Majorana modes energy at the level crossing. Indeed, all the levels with energy $|\epsilon_n| > \Delta_w$, together with their derivatives, are continuous functions of Φ, so that they contribute $I[\Phi]$ by a component that is a smooth function of Φ. To highlight this point, in Fig.3.8 we plot the energy levels *vs.* Φ in a one-dimensional p-wave ring with $\ell = 8$, $\Delta = w$, a weak link with $\tau = 0.25(2w)$, $\mu = 0.75(2w)$ (panel **a**)), and $\mu = 1.25(2w)$ (panel **b**)). According to the above discussion, in the level plot in Fig.3.8**a**), we see a set of non-crossing levels, whose position smoothly changes with

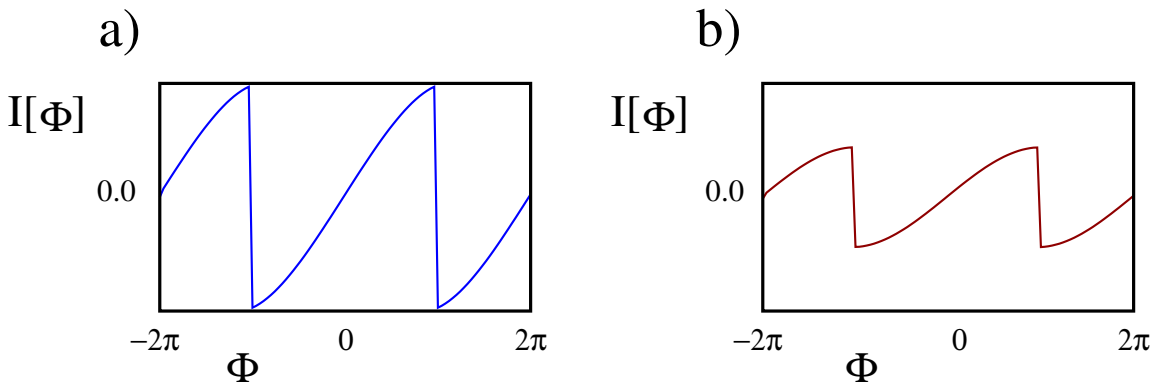

Figure 3.6: Persistent current $I[\Phi]$ (arbitrary units) *vs.* Φ in a p-wave superconducting ring with $\ell = 40$, $\Delta = w$, a weak link of strength $\tau = 0.15(2w)$, and with: **a**): Chemical potential $\mu = 0$; **b**) Chemical potential $\mu = 0.75(2w)$ (104).

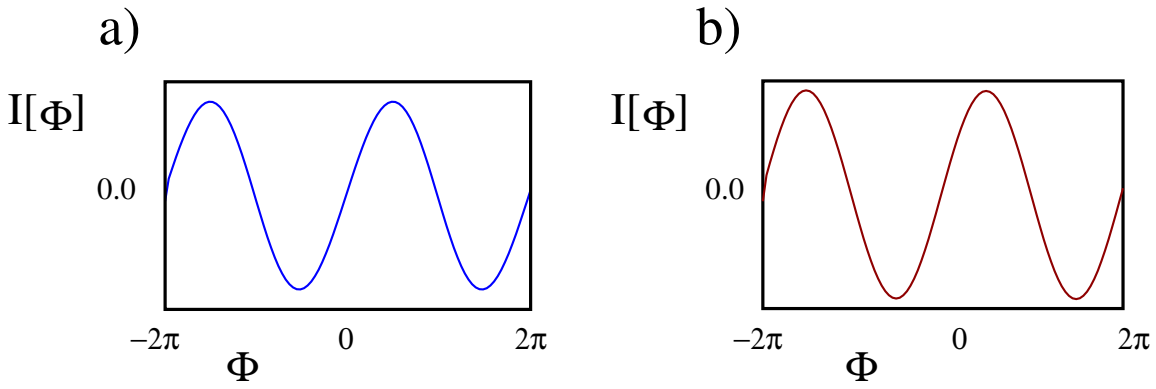

Figure 3.7: **a**) Persistent current $I[\Phi]$ (arbitrary units) *vs.* Φ in an s-wave superconducting ring with $\ell = 40$, $\Delta = 0.5(2w)$, a weak link of strength $\tau = 0.15(2w)$, and $\mu = 0$;
b) Persistent current $I[\Phi]$ (arbitrary units) *vs.* Φ in a p-wave superconducting ring with $\ell = 40$, $\Delta = w$, a weak link of strength $\tau = 0.15(2w)$, and $\mu = 1.25(2w)$ (104).

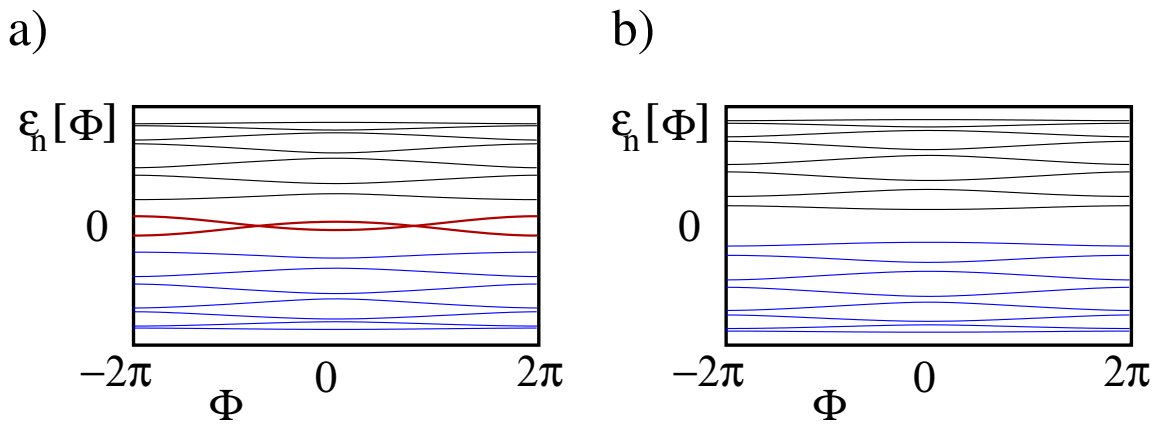

Figure 3.8: **a**) Single-quasiparticle energy levels $\epsilon_n[\Phi]$ in a p-wave superconducting ring with $\ell = 8$, $\Delta = w$, a weak link of strength $\tau = 0.25(2w)$, and $\mu = 0.75(2w)$. The subgap putative Majorana modes appearing close to zero-energy are highlighted in red color; **b**) Single-quasiparticle energy levels $\epsilon_n[\Phi]$ in a p-wave superconducting ring with $\ell = 8$, $\Delta = w$, a weak link of strength $\tau = 0.25(2w)$, and $\mu = 1.25(2w)$. Consistently with the discussion in the main text, no putative Majorana mode-levels appear, in this case (104).

Φ, together with the two levels corresponding to the putative Majorana modes nearby the energy zero, crossing each other at $\pm\Phi_* \approx \pm\pi$. At $T = 0$, all the negative-energy quasiparticle levels contribute $I[\Phi]$, by means of terms smoothly depending on Φ for the levels far from the Fermi level (highlighted in blue in Fig.3.8**a**)), by means of a term discontinuous at $\Phi = \pm\Phi_*$ for the putative Majorana modes-levels (highlighted in red). At variance, the plot in Fig.3.8**b**) shows no subgap putative Majorana modes-levels. In this case, all the negative-energy quasiparticle levels contribute $I[\Phi]$ by means of smooth contributions and, as we found by direct calculation, the current is a continuous function of Φ, $\forall\Phi \in [-2\pi, 2\pi]$.
The discontinuity of $I[\Phi]$ at $\Phi = \Phi_*$ is a readily detectable feature that, under minimal requirements on the system parameters, can be effectively used to mark the existence of putative Majorana modes level crossing by just measuring $I[\Phi]$ in a static experiment and looking at the specific dependence of the current on the applied flux. The remarkable feature of our approach is that, as we are going to discuss in the following, it can be straightforwardly extended to study to which extent a putative Majorana modes level crossing survives in the presence of disorder. Indeed, in analogy to the topological phase for an infinite open chain, we may define a "putative topological phase" (PTP), characterized by a putative Majorana modes level crossing at $\Phi = \Phi_*$. Indeed, at $\Phi = \Phi_*$ we recover zero-energy Majorana modes at the ring, exactly like what happens in an infinite Kitaev chain in its topological phase. In the spirit of our discussion, the observable signature of the putative topological phase in a finite ring is just given by a discontinuity in $I[\Phi]$ at $\Phi = \Phi_*$. As we are going to discuss in the following, our

approach can readly be efficiently implemented to characterize the putative topological phase also in the case of a disordered one-dimensional p-wave ring.

3.3 The disordered case for a finite-length $p-$wave superconducting ring

As we discuss in the previous subsection, for a long enough one-dimensional p-wave ring and (or) for a strong enough coupling τ at the weak link, there always exists a special value of the magnetic flux $\Phi = \Phi_*$ at which the putative Majorana modes energy is exactly equal to 0. So, by setting the magnetic flux at $\Phi = \Phi_*$, we recover the zero-energy Majorana modes γ_1, γ_2 (as we show in Appendix C).

The applications of the Majorana modes, as we have already discussed in the introduction of this Chapter, can be manifold. However, the experimental environments is often not possible to describe it through the "clean case", because it does not take into account the fact that it can be realized with impurities of all sorts or structural defects. But even if we could make an absolutely perfect ring, we should consider the effects of disorder. If we imagine, indeed, to insert our perfect superconducting ring in a broader context, it will be easy for us to understand how, even if minimally interacting with the rest of the apparatus, it can be affected by noise-related effects. In this subsection, we discuss the robustness of the putative Majorana fermion level crossing against disorder in the one-dimesional p-wave ring. It is by now estabilished not only that the topological phase survives a moderate amount of disorder in a disordered quantum wire in the presence of a strong spin-orbit coupling and at a large enough Zeeman effect (107; 108; 109), but also that a limited amount of disorder stabilizes the topological phase of an open, infinite Kitaev chain (110; 111). Moreover, it was also stated that moderate disorder does not substantially affect the 4π-periodic component of $I[\Phi]$ in a fermion parity-conserving p-wave superconducting ring with a weak link (159). Here, instead, if we have a fermion parity non-conserving system, we study how much the putative Majorana modes level crossing are robust against disorder in the ring. Specifically, we perform a detailed analysis of the density of states (DOS) to analize and underline the effects of the Griffiths' singularities and of the dependence of the energy levels on Φ, with particular emphasis onto the putative Majorana modes in the presence of disorder. As outlined in the following, we provide numerical evidence that, at a given disorder strength, either subgap putative Majorana modes energy levels are still present, and they exhibit a level crossing at a pertinent value of Φ, or they are fully washed out by disorder. This leads us to the remakable conclusion that, as long as putative Majorana modes are not washed out by disorder, looking at the discontinuities in $I[\Phi]$ is still an effective way to probe their existence, exactly as in the absence of disroder.

To model the disorder in our superconducting ring, we modify the clean system Hamiltonian by introducing a random component to the on-site potential, so that, at a fixed disorder realization, the total Hamiltonian $H = H_K + H_\tau[\Phi]$ is modified as:

$$H_K + H_\tau[\Phi] \longrightarrow H_{\{V\}}[\Phi] \equiv H_K + H_\tau[\Phi] - \sum_{j=1}^{\ell} V_j c_j^\dagger c_j \tag{3.40}$$

In general, the $\{V_j\}$ must be regarded as random variables, described by a probability distribution $P[\{V_j\}] = \prod_{j=1}^{\ell} p(V_j)$, with $p(V)$ being a probability distribution for V with average $\bar{V} = \int dV\, V p(V) = 0$, and with variance $\sigma_V^2 = \int dV\, V^2 p(V)$. In addition, the V_j at each site have to be regarded as independent random variables, so that we have:

$$\begin{aligned} \overline{V_j} &= \int \prod_{j=1}^{\ell} dV_j\, P[\{V_j\}] V_j = 0 \\ \overline{V_i V_j} &= \int \prod_{j=1}^{\ell} dV_j\, P[\{V_j\}] V_i V_j = \sigma_V^2 \delta_{i,j} \end{aligned} \tag{3.41}$$

where $\overline{O[\{V\}]}$ denotes the ensemble average of a generic functional of $\{V\}$ with respect to the probability distribution $P[\{V\}]$. As the actual functional form of $p(V)$ is not expected to really matter when ensemble-averaging over a large enough number of realizations of disorder, we choose to use a white noise probability distribution for the impurity potential, that is, we set:

$$p(V) \;=\; \begin{cases} \frac{1}{2\sqrt{3}W} \;\text{, for } -\sqrt{3}W \leq V \leq \sqrt{3}W \\ 0 \;\text{, otherwise} \end{cases} \tag{3.42}$$

which corresponds to setting $\sigma_V^2 = W^2$. We now consider how disorder modifies the single-particle density of states of the ring. In general, for a finite-size system, one expects that the effects of disorder strongly depend on the ratio between the system size, in this case ℓ, and the disorder-associated mean free path λ. Indeed, a "weak" disorder, with $\lambda > \ell$, is expected to merely quantitatively affect the density of states, by, for instance, renormalizing the single quasiparticle gap, the bandwidth. At variance, in view of the analytical results obtained for an open chain in Ref.(112) within self-consistent Born approximation, later on numerically confirmed in Ref.(113), we expect that a moderate disorder just slightly broadens the subgap peaks corresponding to the putative Majorana modes energy levels and provides a possible slight renormalization of Φ_*, without spoiling the existence of a level crossing at a pertinent value of Φ. To check our guess, we numerically computed the exact single quasiparticle density of states for the Hamiltonian in Eq.(3.40) at fixed $\{V\}$ with the V_j randomly extracted with probability density as in Eq.(3.42) at fixed W (i.e., at fixed σ_V) for a one-dimesional p-wave ring whose parameters we list below. Therefore, to pertinently account for the disorder, we numerically ensemble-average the result over 300 realization of the disorder. Specifically, we chose the system parameters so that $w = \Delta$, $\mu/(2w) = 0.15$

and $\tau/(2w) = 0.25$. At these values for the system parameters, the derivation of Appendix C predicts in the absence of disorder subgap putative Majorana modes with a level crossing at $\Phi_* \sim \pi$. This is confirmed by the density of states we plot in Fig.3.9**a**) and in Fig.3.9**c)**, which is derived by respectively setting $\Phi = 0$ and $\Phi = \pi$ and with a tiny amount of disorder added to the clean system ($\sigma_V/w = 0.05$), for the only purpose of regularizing the divergences encountered when E equals one of the Hamiltonian eigenvalues. In Fig.3.9**a**) we see the two subgap peaks corresponding to the putative Majorana modes, symmetrically located with respect to the zero-energy point, which, in Fig.3.9**c)** merge into a taller peak at $E = 0$, a signature of the level crossing at $\Phi \sim \pi$. At variance, in Fig.3.9**b**) and in Fig.3.9**d)**, we plot the DOS with $\sigma_V/w = 0.3$ and all the other parameters as in the previous case, respectively at $\Phi = 0$ and at $\Phi = \pi$. At a given value of σ_V, one may estimate λ as $\lambda \sim (2w/\sigma_V)^2$ (159), which implies that, for $\sigma_V = 0.3$, one still has $\lambda > \ell$. Therefore, we see that, as expected from the discussion given in Ref.(112; 113) , the main effect of increased disorder are the emergence of a finite width for the putative Majorana modes and a slight renormalization of the effective superconducting gap.
A complementary situation sets in at strong disorder, that is, for $\lambda \ll \ell$. In this limit, the energy levels of the system become distributed according to the appropriate symmetry class of random matrices (114; 115). In particular, since the model Hamiltonian for the ring breaks both spin rotational invariance and time-reversal symmetry, it falls into symmetry class D of Altland-Zirnbauer classification (115). The level statistics for class-D model Hamiltonians is described by the probability distribution of the $GE_u(\ell)$ esemble and is given by (116; 115; 114):

$$\mathcal{P}[\{\epsilon_j\}] \prod_j d\epsilon_j \propto \prod_{i<j} |\epsilon_i^2 - \epsilon_j^2|^\beta \prod_k [|\epsilon_k|^\alpha \, e^{-\frac{\epsilon_k^2}{\sigma_V^2}} \, d\epsilon_k] \tag{3.43}$$

with $\beta = 2$ and $\alpha = 0$ and the product taken over positive-energy levels only. On extracting the single-particle density of states $\rho(\epsilon)$ from Eq.(3.43), we get, as $\epsilon \to 0$, $\rho(\epsilon) \propto |\epsilon|^\alpha$ (115).

3.3.1 Griffiths effects in the topological disordered ring

For class-D symmetry systems, as we have already seen, we expect a low-energy uniform density of states, with no evidence of low-lying putative Majorana modes. On increasing its strength, the disorder washes out putative Majorana modes (117): assuming that at zero disorder the system lies within its topological phase, one finds that, for weak disorder, fluctuations in the random potential may open "nontopological islands" within the topological background, of typical size $\ell_{\rm NT} \ll \ell$. At each interface between topological and nontopological regions, Majorana modes emerge, which suddenly hybridize into "high-energy Dirac modes", at typical energy scales $\epsilon_{NT} \sim e^{-\frac{\lambda}{\xi_0}}$, lying below the gap but still higher than the typical energy associated to the "true" putative Majorana modes.

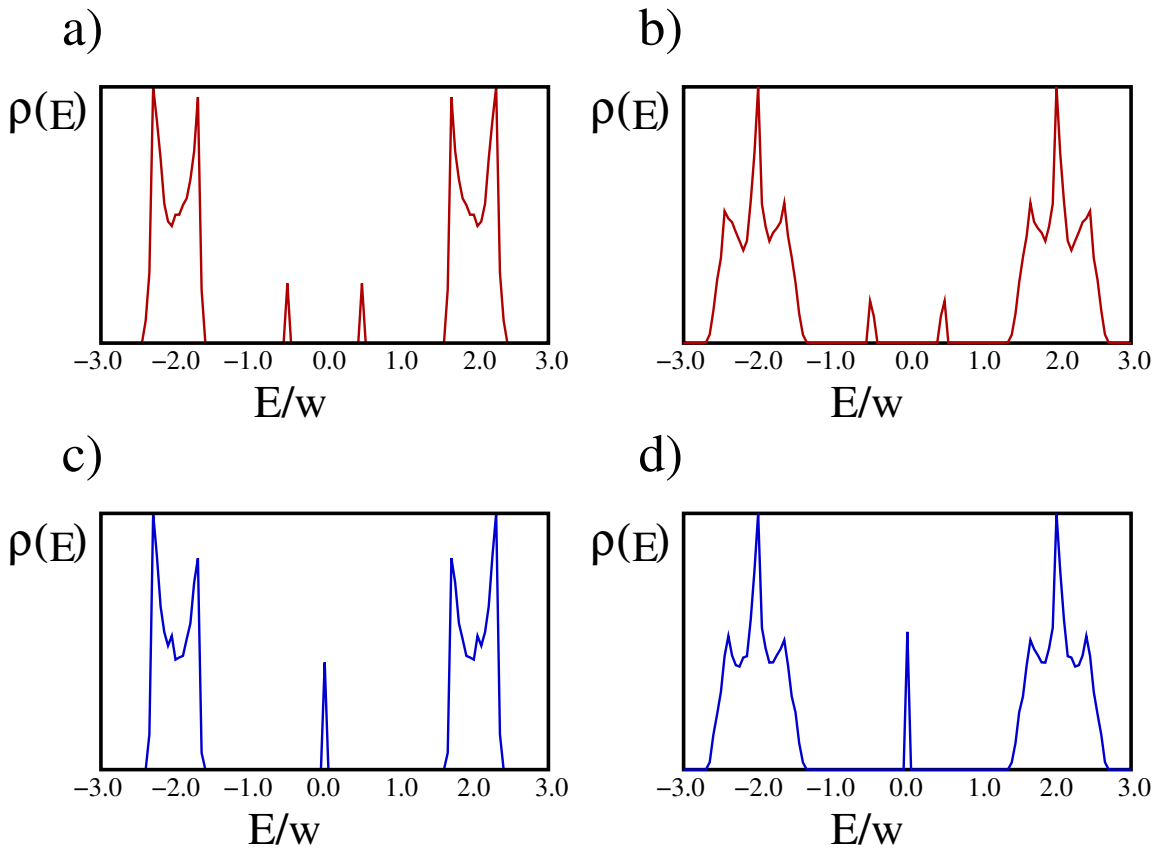

Figure 3.9: Single-quasiparticle density of states $\rho(E)$ *vs.* E for a ring with $w = \Delta$, $\mu/(2w) = 0.15$ and $\tau/(2w) = 0.25$, at a given value of the flux Φ and of σ_V. The remaining parameters used to generate the plots in the various panels have been set as outlined below (see main text for a detailed discussion of the results): **a**) $\Phi = 0$, $\sigma_V/w = 0.05$; **b**) $\Phi = 0$, $\sigma_V/w = 0.3$; **c)** $\Phi = \pi$, $\sigma_V/w = 0.05$; **d)** $\Phi = \pi$, $\sigma_V/w = 0.3$ (104).

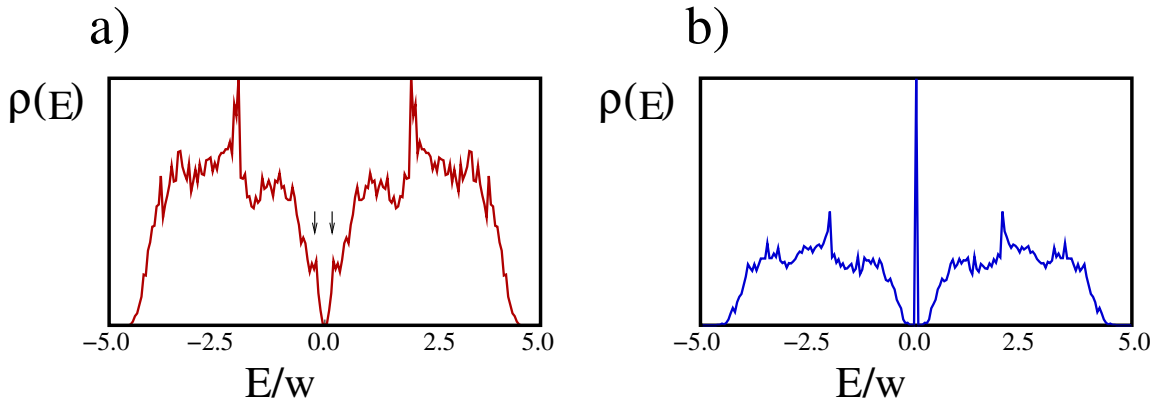

Figure 3.10: Single-quasiparticle density of states $\rho(E)$ *vs.* E for a ring with $w = \Delta$, $\mu/(2w) = 0.15$ and $\tau/(2w) = 0.25$, at a given value of the flux Φ and of σ_V. The remaining parameters used to generate the plots in the various panels have been set as outlined below (see main text for a detailed discussion of the results): **a**) $\Phi = 0$, $\sigma_V/w = 1.5$ (the small black arrows highlight the peaks corresponding to the putative Majorana modes energy levels); **b**) $\Phi = \pi$, $\sigma_V/w = 1.5$ (104).

On one hand, this implies the ploriferation of subgap, disorder induced states. On the other hand, low-energies putative Majorana modes are still protected by the very fact that their energies are quite lower than the energies associated to disorder-induced states, and such is the corresponding level crossing at Φ_*. Summarizing, as σ_V increases, one legitimately expects that disorder-induced energy levels fill in the subgap region but also that level repulsion between states with different energy, encoded in $\mathcal{P}[\{\epsilon_j\}]$ in Eq.(3.43), acts to "protect" the low-lying putative Majorana modes. This is clearly evidenced by the density of states plots we provide in Fig.3.10. In particular, in Fig.3.10**a**), we plot $\rho(E)$ *vs.* E for the same values of the system parameters we used to generate Fig.3.9, with $\Phi = 0$ and with $\sigma_V/w = 1.5$, while to draw Fig.3.10**b**) we have set $\Phi = \pi$. At such a value of σ_V we estimate that $\lambda/\ell \sim 0.1$. Accordingly, in both Fig.3.10**a**) and Fig.3.10**b**), we see that disorder-induced levels have largely filled in the energy gap. Moreover, in Fig.3.10**a**) the persistence of the two peaks corresponding to the putative Majorana modes-energy levels is evidenced by the dip in the density of states at $E = 0$, due to the finite gap between putative Majorana modes-levels which cannot be filled in by disorder-induced states. At variance, Fig.3.10**b**) we see the persistence of a central sharp peak, corresponding to degenerate putative Majorana modes-energy levels that "pile up" on top of each other. The persistence of this central peak evidences the remarkable result that the putative Majorana fermion level crossing at $\Phi = \Phi_*$ is not spoiled by disorder, even at σ_V as large as $1.5w$.
It is worth stressing, at this point, that, despite the apparent similarity of the plot in Fig.3.10**b**) with the density of states derived at not-too-strong disorder for a symmetry class-D Hamiltonian with an odd number $\mathcal{N}$ of rows and columns (118; 119; 120), the origin of the peak at $E = 0$ in the two cases is deeply different. In Ref.(120), the peak

at $E = 0$ is a simple consequence of $\mathcal{N}$ being odd, which leads to a "natural" protection mechanism against disorder. In our case, it arises at an "accidental" degeneracy between putative Majorana modes, reached upon tuning Φ at the degenerate point $\Phi = \Phi_*$. Therefore, in our case there is no "a priori" reason to expect a protection of the peak against disorder.

3.3.2 Consequences on the physics of Majorana modes

To investigate the fate of putative Majorana modes and of putative Majorana fermion level crossing at strong disorder, in Fig.3.10 we show $\rho(E)$ *vs.* E for $w = \Delta$, for $\mu/(2w) = 0.15$ and $\tau/(2w) = 0.25$, and for $\sigma_V/w = 4.0$. We note a number of remarkable features, that are directly related to the onset of the probability distribution in Eq.(3.43) as a description of the energy level statistics for the system (115). First of all, we see that there is no detectable difference between the plots at $\Phi = 0$ and at $\Phi = \pi$. Indeed, the insensitivity of the DOS to the applied phase can be regarded as a specific manifestation of the insensitivity to the boundary conditions (such as the one imposed by the applied flux Φ on the single-quasiparticle wavefunction) of the energy levels corresponding to localized states (121; 122). Therefore, this result leads us to the conclusion that all the states filling in the gap at strong disorder are disorder induced states, while strongly Φ-sensitive putative Majorana modes have been completely washed out. To further ground our conclusion, in Fig.3.12**a**), we plot the first quasiparticle energy levels $\epsilon_n[\Phi]$ *vs.* Φ at $\sigma_V/w = 2.2$ (see the corresponding caption for details about the numerical values of the other parameters). We cleary see a set of disorder-induced states (drawn in red in the figure) which exhibit a weak dependence on Φ and are situated symmetrically with respect the 0-energy level, consistently with the survival of particle-hole symmetry against disorder. The states closest to the Fermi level (depicted in blue in the figure) are, instead, to be clearly identified with putative Majorana modes. They take a strong dependence on Φ and cross with each other at pertinent values of Φ. At variance, in Fig.3.12**b**), we draw a similar plot, but realized for a single disorder realization with $\sigma_V/w = 4.2$. The much larger amount of disorder has now determined the full disappearance of putative Majorana modes (123): there are no blue states, but only red impurity states, basically independent of Φ (a clear signal of strong localization of these states).
The remarkable peak centered at $\epsilon = 0$ in the plots at strong disorder in Fig.3.10 corresponds to Griffiths' singular behavior in the density of states cutoff at the finite level spacing $\delta_0 \sim 2\pi w/\ell$ (120). Indeed, on increasing σ_V, the disorder washes out the putative Majorana modes via the Griffiths effect (the proliferation of topological-non topological islands in the system) taking place in the finite wire (117; 113). When the nontopological regions start to proliferate, the increasing probability of hybridization between putative Majorana modes and zero-modes located at the interfaces between topological and nontopological regions eventually washes out the putative Majorana modes themselves, together with the degenerate point at $\Phi = \Phi_*$, driving the system outside of the putative topological phase (117; 113).

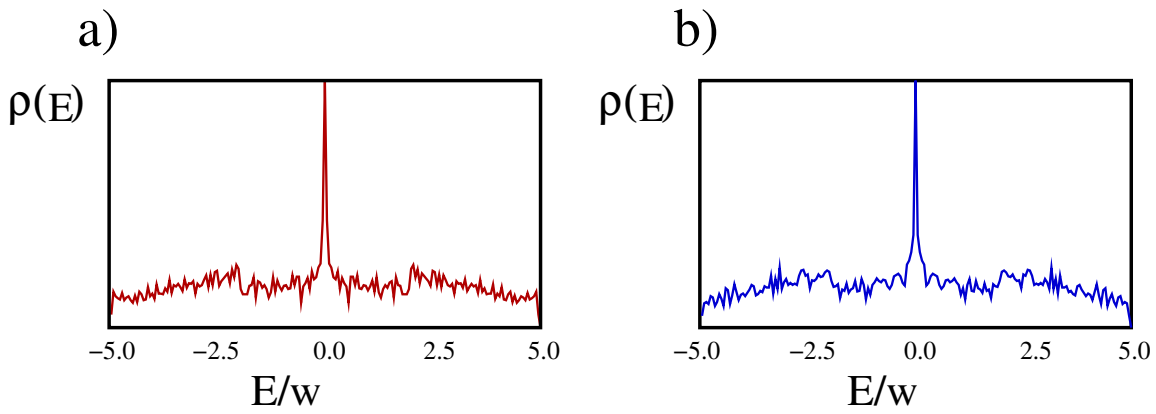

Figure 3.11: Single-quasiparticle density of states $\rho(E)$ *vs.* E for a ring with $w = \Delta$, $\mu/(2w) = 0.15$ and $\tau/(2w) = 0.25$, at a given value of the flux Φ and of σ_V. The remaining parameters used to generate the plots in the various panels have been set as outlined below (see main text for a detailed discussion of the results): **a**) $\Phi = 0$, $\sigma_V/w = 4.0$;
b) $\Phi = \pi$, $\sigma_V/w = 4,0$ (104).

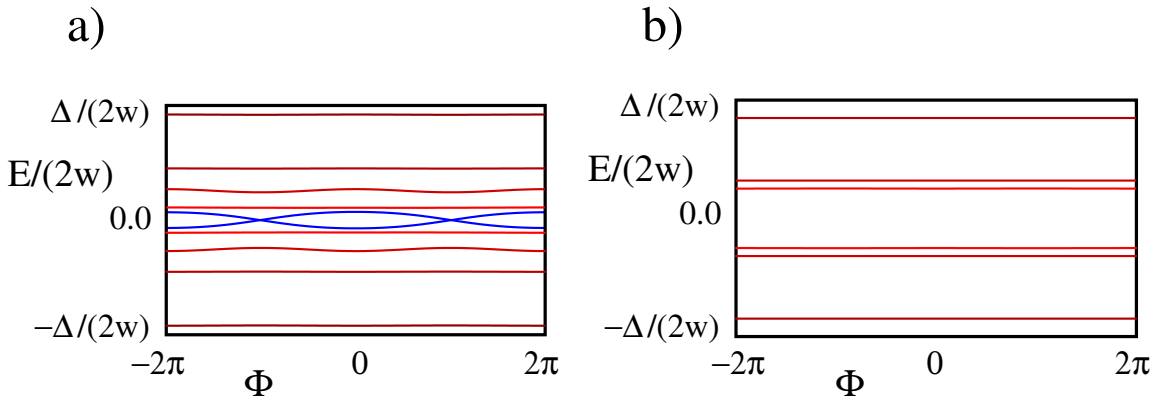

Figure 3.12: **a**) Sub-gap energy levels $\epsilon_n[\Phi]$ computed for one realization of the disorder potential in a p-wave superconducting ring with $\ell = 40$, $\Delta = w$, a weak link of strength $\tau/(2w) = 0.25$, $\mu/(2w) = 0.75$, and $\sigma_V/w = 2.2$. The subgap putative Majorana modes appearing close to zero-energy are highlighted in blue color;
b) Sub-gap energy levels $\epsilon_n[\Phi]$ computed for one realization of the disorder potential in a p-wave superconducting ring with $\ell = 40$, $\Delta = w$, a weak link of strength $\tau/(2w) = 0.25$, $\mu/(2w) = 0.75$, and $\sigma_V/w = 4.2$. No subgap putative Majorana modes appear in this case (104).

In the subsection dedicated to the "clean case", we have shown that, in the absence of disorder, if the one-dimensional superconducting ring lies at any time within its thermodynamic groundstate, a level crossing at $\Phi = \Phi_*$ between putative Majorana fermion energies is uniquely associated to discontinuities $I[\Phi]$ when going across Φ_*. Now, we want to show how this correspondance readily generalizes to a disordered one-dimensional superconducting ring, which eventually allows us to use the individuation of the discontinuities in $I[\Phi]$ as an effective mean to map out the whole putative topological phase in the disorder strength-chemical potential plane.

In the presence of disorder, physical quantities must first be computed at fixed disorder by using the Hamiltonian $H_{\{V\}}[\Phi]$ in Eq.(3.40). Then, the final result must be ensemble-averaged over all possible realizations of disorder. Numerically diagonalizing $H_{\{V\}}$ for different $\{V\}$ leads to slightly different energy levels for the putative Majorana modes. Thus, in order to repeat the analysis of the clean case for a disordered one-dimensional superconducting ring, we must rather refer to the ensemble averaged density of states at fixed σ_V as a function of Φ, $\rho(E)$. To do so, we numerically construct $\rho(E)$, by collecting the eigenvalues generated via an exact Hamiltonian diagonalization procedure into bins defined in the E-Φ plane and eventually averaging over the disorder, thus generating three-dimensional plots of $\rho(E)$ as a function of both E and of Φ for E ranging throughout the interval $[-E_C, E_C]$, with the half-bandwidth $E_C = 2w + \mu$ and $\Phi \in [-2\pi, 2\pi]$. Specifically, we ensemble averaged over a uniformly-distributed disorder, with $p(V)$ given in Eq.(3.42) and $\sigma_V/w = 0.2$ (Fig.3.13**a**), $\sigma_V/w = 0.8$ (Fig.3.13**b**). In Fig.3.13, despite the presence of disorder, we clearly see the subgap putative Majorana modes, which are characterized by their strong dependence on Φ (to be contrasted with the observations that all the other levels displayed in the figure are basically independent of Φ) and, more importantly, that there are evident level crossings, evidenced by the sharp peaks - a consequence of the two putative Majorana modes density pile-up at those points-. The level crossings are not washed out by disorder, which implies that, in a sense that we are going to clarify in the following, there is still a sort of discontinuity in $I[\Phi]$ at $\Phi = \Phi_*$. Another important observation is that, though, on increasing the disorder, part of the spectral weight is transferred from putative Majorana modes to disorder-induced Griffiths states that fill in the gap (as can be clearly seen by comparing Fig.3.13**a**) and Fig.3.13**b**) with each other), the level crossings survive and clearly evidenced by the peaks in Fig.3.13**b**).
By contrast, in Fig.3.14, we plot $\rho(E)$ with the same parameters as we chose in Fig.3.13, but with $\sigma_V/w = 6.0$. We see that the spectral is largely broadened throughout the interval $[-E_C, E_C]$, there is no dependence of the energies on Φ and, at the same time, the subgap putative Majorana modes have disappeared. This confirms that a strong enough disorder is actually effective in washing out the subgap putative Majorana modes.
To generalize to a disordered one-dimensional superconducting ring the correspondence between putative Majorana fermion level crossings and discontinuities in $I[\Phi]$, we start by dividing the region of interest in the $\sigma_V - \mu$ planes into square bins and by defining at the center of each bin a function $F[\sigma_V, \mu]$ which, at the start, is everywhere equal

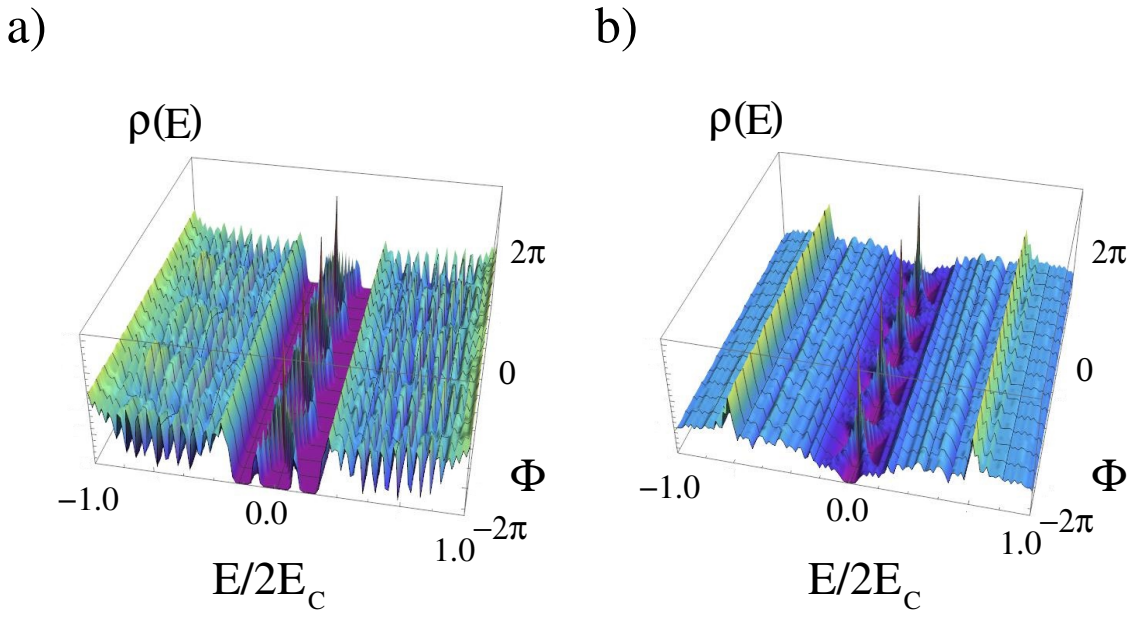

Figure 3.13: **a**) Density of states $\rho(E)$ for a disordered ring described by the Hamiltonian in Eq.(3.40) with $\Delta = w$, $\mu/(2w) = 1.2$, $\tau/(2w) = 0.25$, $\ell = 40$, obtained by ensemble-averaging over 100 realization of the disorder with $\sigma_V/w = 0.2$. The subgap putative Majorana modes close to the Fermi level are clearly displayed;
b) Density of states $\rho(E)$ for a disordered ring described by the Hamiltonian in Eq.(3.40) with $\Delta = w$, $\mu/(2w) = 1.2$, $\tau/(2w) = 0.25$, $\ell = 40$, obtained by ensemble-averaging over 100 realization of the disorder with $\sigma_V/w = 0.8$. The subgap putative Majorana modes are less resolved, but there are clear peaks at the level crossings, due to the pile-up of the density of states of the two putative Majorana modes (104).

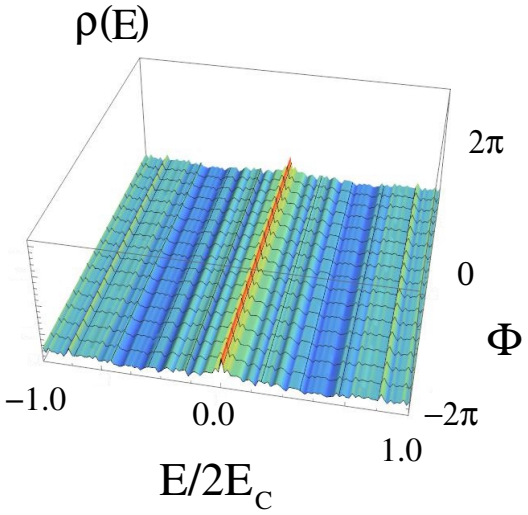

Figure 3.14: Density of states $\rho(E)$ for a disordered ring described by the Hamiltonian in Eq.(3.40) with $\Delta = w$, $\mu/(2w) = 1.2$, $\tau/(2w) = 0.25$, $\ell = 40$, obtained by ensemble-averaging over 100 realization of the disorder with $\sigma_V/w = 6.0$. The spectral density is broadened throughout the interval $[-E_C, E_C]$, there is a negligible dependence on Φ, and the subgap putative Majorana modes have disappeared (104).

to 0. Then, at each bin $(\sigma_{V,i}, \mu_j)$, we extract a realization $\{V\}$ of the disorder $\{V\}$ with probability having $\sigma_V = \sigma_{V,i}$ and exactly diagonalize the Hamiltonian $H_{\{V\};\mu_j}[\Phi]$, which is given by Eq.(3.40) with $\mu = \mu_j$. Then, we use the result to compute the corresponding persistent current, $I_{\{V\}}[\Phi]$. Therefore, we check whether $I_{\{V\}}[\Phi]$ exhibits a discontinuity at a value $\Phi = \Phi_* \sim \pi$, or not. If yes, we increment $F[\sigma_{V,i}, \mu_j]$ by 1, otherwise, we leave it unchanged. After summing, at each bin, over $\mathcal{N} = 300$ random realizations of the disorder, we normalize $F[\sigma_{V,i}, \mu_j]$ to $f[\sigma_{V,i}, \mu_j]$ by simply dividing $F[\sigma_{V,i}, \mu_j]$ by $\mathcal{N}$, so that $0 \leq f[\sigma_{V,i}, \mu_j] \leq 1$, $\forall i, j$. We draw our result in Fig.3.15, where we show a color-scale plot of $f[\sigma_V, \mu]$ computed for a ring with $\ell = 60$, $w = \Delta$, and $\tau/(2w) = 0.25$. In detail, we constructed the plot by increasing both σ_V/w and μ/w by step of 0.05 and by accordingly defining yjr bins in the $\sigma_V - \mu$-plane. As stated above, at each bin, we ensemble-averaged over 300 disorder realization. The region marked in full red corresponds to $f = 1$, that is, to a current which is singular at Φ_* for any realization of the disorder. Conversely, the white portion of the graph corresponds to $f = 0$, that is, to a current that is a continuous function of Φ for any realization of the disorder (see Fig.3.15 for a graphic summary of the color code). Clearly, points in the red region are characterized by putative Majorana modes that undergo a level crossing at $\Phi = \Phi_*$, that is, we may identify the red region with the putative topological phase in the presence of disorder. By converse, points in the white region are characterized by the absence of putative Majorana modes. The shaded region, where the color varies from red to white, defines the transition region at which the putative topological phase disappears and the putative Majorana modes are washed

out of the spectrum. By analogy, we would expect a sharp transition line, such as the one separaring the topological from the nontopological phases of the infinite Kitaev chain, drawn in Refs.(110; 111) by using transfer matrix method. Nevertheless, we do obtain a broad transition region, rather than a sharp phase boundary, because, or each disorder realization we exactly diagonalize a well-defined Hamiltonian, which either presents putative Majorana modes with a finite-Φ level crossing, or not. Near the phase tranistion, when averaging over $\mathcal{N}$ different realization of the disorder, there can be a nonzero probability that some realizations wash out putative Majorana modes at values of the system parameters where putative Majorana modes are present in the large majority of cases or, conversely, that putative Majorana modes appear at points in parameter space where they are absent in the large majority of cases. To be more precise, when the system lies within the putative topological phase, strong fluctuations in the mean value of the impurity potential on a single realization of disorder may drive it outside of the putative topological phase, and vice versa.

As a result, close to the point of disappearance of the putative topological phase, we expect that, on ensemble averaging over disorder, the percentage of single disorder realizations respectively leading to a discontinuous, or to a continuous, current will be both different from zero (incidentally, we note that this is quite a common feature of finite system undergoing a Griffith phase transition (113)). At variance, far from the transition there is no ambiguity in that either $I[\Phi]$ is discontinuous, or continuous for any realization of disorder, just as we can see from the plot of $f[\sigma_V, \mu]$ in Fig.3.15. Eventually, to map out the (broad) phase boundary of the putative topological phase in the disorder strength-chemical potential plane, we start from within the putative topological phase at zero disorder strength. Then, we move along the horizontal axis at fixed μ by probing the existence of the discontinuity in $I[\Phi]$ at increasing σ_V: for $0 \leq \mu/w < 2$ and for $\sigma_V = 0$, we typically obtain $f[0, \mu] = 1$. Consistently with the above discussion, at some μ-dependent "lower critical" value of σ_V, $\sigma_{\mu;l}$, we start to obtain $f[\sigma_{V;l}, \mu] < 1$. This signals the start of the transition region when going across which the putative topological phase disappears. On further increasing σ_V, we typically reach an "upper critical" value, $\sigma_{\mu;u}$, such that $f[\sigma_V; \mu] = 0$ for $\sigma_V > \sigma_{\mu;u}$. Therefore, $\sigma_{\mu;l}$ and $\sigma_{\mu;r}$ determine the transition region at a given μ as the set of points (σ_V, μ) such that $\sigma_{\mu;l} < \sigma_V < \sigma_{\mu;u}$. Repeating the procedure along constant-μ lines, we mapped out the full color scale plot of $f[\sigma_V, \mu]$ in Fig.3.15.

Besides the broadening related to the Griffith mechanism, Fig.3.15 shows a remarkable analogy with the phase diagram for a long Kitaev chain with open boundary conditions reported in Fig.1 of Ref.(110). In particular, the two diagrams share the remarkable feature of a reentrant topological phase at not-too-large values of σ_V, that is, a small amount of disorder appears to favor, rather than suppressing, the topological phase. In our specific finite-size ring, we interpret the reentrant phase as an effect of the disorder-induced renormalization of the chemical potential which, at nonzero σ_V, pushes the phase transition to values of μ higher than the zero-disorder critical value $\mu_c = 2w$, or lower than $-\mu_c = -2w$. As discussed above, the finite width of the transition region has to be regarded as a consequence of the Griffiths mechanism in a finite

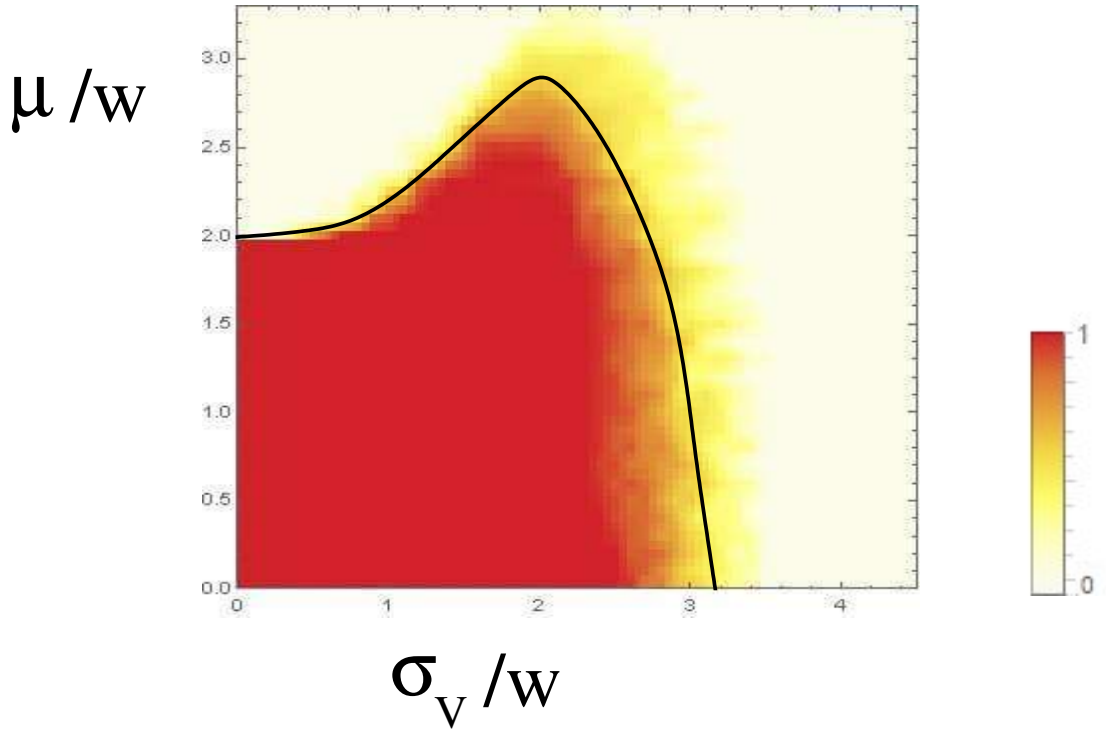

Figure 3.15: Color-scale plot of $f[\sigma_V, \mu]$ in the $\sigma_V - \mu$ plane. The color code is summarized at the right-hand side of the plot. The shaded region, where the color varies from red to white , defines the transition region at which the putative topological phase disappears and the putative Majorana modes are washed out of the spectrum (104). The red line is a sketch of the variation of the center of mass of the transition region as a function of μ: in the $\ell \to \infty$ limit and after averaging over a large number of realizations of disorder, it is expected to coincide with the solid black line of Fig.1 of Ref.(110).

system (113): in the $\ell \to \infty$ limit and after averaging over a large number of realizations of disorder, the transition region is nevertheless expected to shrink to a sharp phase boundary, coinciding with the solid black line of Fig.1 of Ref.(110).

Chapter 4

Transfer matrix approach to investigate signatures of Majorana Modes in the persistent current of a $p-$wave superconducting hybrid ring

In the previous chapter we have investigated and analyzed the presence of Majorana modes in a $p-$wave superconducting hybrid ring. We have seen how through the jumps of the persistent current $I[\Phi]$, in the absence of fermionic parity conservation, it is possible to obtain a signature of the presence of Majorana Modes in the system and how these can be measured in a completely non-invasive way (105). Again, we have seen, through analytic techniques and numerical processing, how robust they are against the effects of disorder induced into the system. The discussion ended with the building of a phase diagram in which the presence or the absence of the topological phase in the system was highlighted with the variation of the chemical potential μ and the intensity of disorder σ. We stress that in the previous discussion we used a numerical approach and we calculated the persistent current of the system by simply exactly diagonalizing the Hamiltonian of the system.

Apparently, it is therefore important to be able to compute $I[\Phi]$ in a given NSHR in the cases of interest. Nevertheless, even after a number of simplifications like considering a ballistic system (which allows for resorting to a noninteracting electronic model Hamiltonian for the normal region), using a non self-consistent model for the superconducting region, such as BTK model for a s-wave superconductor in the continuum formulation (151), or its corresponding lattice version for a s-wave (152), or for a p-wave superconductor (142), computing $I[\Phi]$ is typically still quite a challenging task. Indeed, the "standard" approach to the problem consists in computing the current as

$$I[\Phi] = e\partial_{\Phi}\mathcal{F}[\Phi;T] \tag{4.1}$$

with $\mathcal{F}[\Phi;T]$ being the system's free energy at applied flux Φ and temperature T. At $T=0$ Eq.(4.1) yields:

$$I[\Phi] = e\partial_\Phi E_{\rm GS}[\Phi] = e\partial_\Phi \sum_n E_n \tag{4.2}$$

where the sum is taken over energies of the occupied single-quasiparticle states. To compute these energies, one has to solve the secular equation for the energy eigenvalues at nonzero Φ with periodic boundary conditions over the whole ring. In general, the resulting set of equations looks quite formidable and hard to deal with, which requires resorting to various approximations, such as retaining only the low-energy part of the spectrum (141), or employing various approximations for the single-quasiparticle energies as a function of Φ in various regions of the spectrum (140).

In this chapter we present a technique that, under very general assumptions such as the ones listed above, allows for exactly expressing $I[\Phi]$ as a single integral of a pertinently construced function of the system's parameters. At $T=0$, our approach is based on first writing Eqs.(4.2) in terms of a single integral over an appropriate path in the complex energy plane, and on eventually deforming the integration path to the imaginary axis. In this respect, our approach can be regarded as an adapted version of the technique developed in (153; 154; 155) to compute the dc Josephson current across an SNS-junction. Besides providing an exact formula allowing to easily compute $I[\Phi]$ by numerically integrating a known function at fixed Φ, in the large-ring limit, our technique is also suitable for a systematic expansion in inverse powers of the system's length, which is the counterpart for a NSHR of the expansion in inverse powers of the length of a long SNS junction discussed in (155) for a singe-channel system and generalized in (156) to the multi-channel case. In this limit the formula for $I[\Phi]$ is greatly simplified, which does even allow for working out analytic closed-form formulas for the current in a number of cases of interest.

It is, however, worth stressing that, at least in the formulation we provide in this chapter, our approach does not account for a number of features that can be in principle important in NSHRs, such as quantum phase slips (157), electronic interaction effects (136), disorder (133; 134), etc.

The chapter is structured as follows:

- In Section 4.1 we introduce the analytic computation of the persistent current for a normal mesoscopic ring based on the solution of the Heisenberg equation; here we will introduce a model Hamiltonian for this system and compute the current for a normal homogeneous ring and we will emphasize the difficulties related to the generalization to more complicated cases.

- In Section 4.2 we introduce our model system, the concept of transfer matrix and the integration technique on the complex plane, showing how the calculation of the system resolvent can be traced, at zero temperature, to the calculation of the residues of an integral suitably constructed using the transfer matrix of the system.

- In Section 4.3 we show step by step how to calculate the persistent current by using the technique explained in the previous section, and how to exploit the transfer matrix factorization properties for this purpose. Moreover, here we show the signatures of the persistent current in the presence of topological phase.
- In Section 4.4 we analyze the large-ring limit, showing how it is possible, in some cases, using this kind of approximation to facilitate the calculation of the current. Moreover, here we will discuss our technique in the case of non-zero temperature.

4.1 Standard approach to the persistent current in normal mesoscopic rings

Although small mesoscopic systems have been under intensive study for quite a long time, they have usually been analyzed by making contacts with metallic leads. As a result, one has to apply a finite voltage bias, in order to recover a nonzero current across the system. The experiments by Lévy et al. (1990) (90) and by Chandrasekhar et al. (1991) (91) were carried out in such a way that the metallic rings remained isolated. A slowly varying magnetic field was applied and a magnetic response was measured. In this situation it became possible to observe persistent currents in quite dirty samples in which the elastic mean free path l was much shorter than the circumference L of the ring: in this case, we talk about a mesoscopic systems in a ballistic regime. In particular, the scale of such systems lies between the size of a a molecule and the micrometres (μm). The lower limit can also be defined as being the size of individual atoms, then at the micrometer level are bulk materials. As is the case for macroscopic physics, mescoscopic objects contain a large number of atoms. The relevance of mesoscpic system is related to the quantum interference that proved to be so crucial to the localizzation problem. Although the conductors may contain internal defects, disorder does not destroy the coherence of the wave functions and quantum effects can become very important, leading to completely new physical phenomena: for example, at the macroscopic level the conductance of a wire increases continuously with its diameter. Another particular behaviour of mesoscopic systems is the presence of a persistent current in normal rings. Indeed, materials that have a resistance can not have a current that persists in time; however the electron mean free path in a metal is of the same order of the length of the mescoscopic ring. This allows to consider a normal ring as if we had no resistance.

Then, the persistent current is a phenomenon that appears also in normal materials as long as we are in the mesoscopic scale.

At first we must introduce the lattice-model formalism, so as to contextualize our work. We start to define an electrons chain of finite length ℓ described by the hamiltonian:

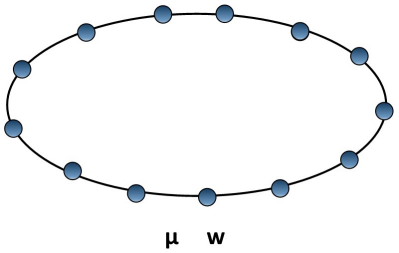

Figure 4.1: Sketch of a normal one-dimensional ring

$$H = -\sum_{j=1}^{\ell} w_j \left(c_j^\dagger c_{j+1} + c_{j+1}^\dagger c_j \right) - \sum_{j=1}^{\ell} \mu_j \left(c_j^\dagger c_j - \frac{1}{2} \right) \tag{4.3}$$

where w_j is the hopping amplitude, μ_j is the chemical potential and c_j and $c_j^\dagger$ are respectively creation and annihilation operators on the j-site. Starting by this hamiltonian, we can make a ring (Fig.4.1) by introducing periodic boundary conditions to the wave function equations and consider the presence of the magnetic flux through the Aharonov-Bohm phase by studying the new hamiltonian:

$$H = -\sum_{j=1}^{\ell} w \left(e^{-i\varphi} c_j^\dagger c_{j+1} + e^{i\varphi} c_{j+1}^\dagger c_j \right) - \sum_{j=1}^{\ell} \mu_j c_j^\dagger c_j \tag{4.4}$$

where φ is the magnetic flux.

In the following subsections we will describe the persistent current in a mesoscopic normal ring, linking the trend of the persistent current to a particular shape of the ground state energy level and introducing the study of large-ℓ rings, comparing the obtained results.

In order to describe a quantum ring, as we said before, we introduce the periodic boundary condition to the wave functions:

$$u_{\ell+1} = u_1 \tag{4.5}$$

which physically is like saying that the chain is closed on itself.

To find an expression for the persistent current, we need to achieve the ground energy value, to improve the formalism of Eq.(3.6). To do this, we can solve the eigenvalues equation for an electron defining an appropriate eigenmode Γ_E with a related energy E, so that:

$$\Gamma_E = \sum_{j=1}^{\ell} u_j^* c_j \tag{4.6}$$

In order to solve the eigenvalues equation in a discrete system, we improve a lattice time-independent Shrödinger equation, calculating the commutation relation between the hamiltonian in Eq.(4.4) and the eigenmode Γ_E:

$$
\begin{aligned}
E\Gamma_E &= [H, \Gamma_E] \\
E\sum_{j=1}^{\ell} u_j^* c_j &= \left[-\sum_{j=1}^{\ell} w \left(e^{-i\varphi} c_j^\dagger c_{j+1} + e^{i\varphi} c_{j+1}^\dagger c_j \right) - \sum_{j=1}^{\ell} \mu c_j^\dagger c_j, \sum_{j'=1}^{\ell} u_{j'}^* c_{j'} \right] \\
E\sum_{j=1}^{\ell} u_j^* c_j &= -\sum_{j=1}^{\ell} \left(w e^{-i\varphi} u_j^* c_{j+1} + w e^{i\varphi} u_{j+1}^* c_j \right) - \sum_{j=1}^{\ell} \mu u_j^* c_j
\end{aligned} \tag{4.7}
$$

Doing this, we obtain the equation:

$$
Eu_j = -w \left(e^{i\varphi} u_{j-1} + e^{-i\varphi} u_{j+1} \right) - \sum_{j=1}^{\ell} \mu u_j \tag{4.8}
$$

using that $w^* = w$ and $\mu^* = \mu$ and supplemented with the boundary condition $u_{\ell+1} = u_1$. In order to simplify and complete the calculation, we redefine the eigenstates performing the canonical transformation:

$$
u_j \to e^{ij\varphi} u_j
$$

in Eq.(4.8), paying attention to the value of the j-site, gaining:

$$
Eu_j e^{ij\varphi} = -w \left(e^{i\varphi} e^{i(j-1)\varphi} u_{j-1} + e^{-i\varphi} e^{i(j+1)\varphi} u_{j+1} \right) - \sum_{j=1}^{\ell} \mu u_j e^{ij\varphi} \tag{4.9}
$$

that becomes:

$$
Eu_j = -w \left(u_{j-1} + u_{j+1} \right) - \sum_{j=1}^{\ell} \mu u_j \tag{4.10}
$$

supplemented now with the boundary condition

$$
u_{\ell+1} = u_1 e^{i\ell\varphi} \tag{4.11}
$$

Note that the phase-factor $e^{\pm i\varphi}$ is absorbed by the boundary conditions just expressed. Now, inasmuch as the energy in the momentum space is equal to the energy in the coordinate space, we can switch the eigenvectors u_j, that has a dependence by the site j, in u_k, that depend now by momentum k, in: $u_j = e^{ijk} u_k$. We obtain:

$$
Ee^{ijk} u_k = -w \left(u_k e^{i(j-1)k} + u_k e^{i(j+1)k} \right) - \sum_{j=1}^{\ell} \mu e^{ijk} u_k \tag{4.12}
$$

which becomes:

$$Eu_k = -w\left(u_k e^{-ik} + u_k e^{ik}\right) - \sum_{j=1}^{\ell} \mu u_k \tag{4.13}$$

Now, in order to consider not trivial solutions, we have that the energy $E(k)$ takes the form:

$$E(k) = -2w\cos(k) - \mu \tag{4.14}$$

We can take now advantage of the periodicity conditions to find the allowed values of the momentum k:

$$k = k_n = \frac{2\pi n}{\ell} + \varphi \tag{4.15}$$

noting the presence of the quantized flux φ; if we replace this expression in Eq.(4.14), we obtain:

$$E_n(k) = \epsilon_n = -2w\cos(k_n) - \mu \tag{4.16}$$

where $n \in N$, that we can write underling the magnetic flux dependence as follows:

$$E_n(\varphi) = \epsilon_n = -2w\cos\left(\frac{2\pi n}{\ell} + \varphi\right) - \mu \tag{4.17}$$

From the spectrum we note that the energy levels of the electrons on the ring are a periodic function which depends from the magnetic flux φ (Fig.1).

Now, we can calculate the persistent current of the n-energy state, doing just a partial derivative:

$$I_n(\varphi) = e\frac{\partial}{\partial\varphi}E_n(\varphi) = \frac{4\pi we}{\ell}\sin\left(\frac{2\pi n}{\ell} + \varphi\right) \tag{4.18}$$

that we can write as

$$I_n(\varphi) = e\frac{\partial}{\partial\varphi}E_n(\varphi) = \tilde{I_n}\sin\left(\frac{2\pi n}{\ell} + \varphi\right) \tag{4.19}$$

where $\tilde{I_n} = \frac{4\pi we}{\ell}$ is called current amplitude.

We have pointed up that the energy, once we fix the ring length ℓ, the chemical potential μ and the hopping amplitude w, is a periodic function of the flux φ. If we consider the occupied levels, we can observe that generally the energy of the electrons on the left increases until it crosses the Fermi energy level (that, in our specific case, in which we scaled the energy with the chemical potential μ, is the abscissa axis), while that of the electrons on the right decreases going down to the Fermi energy level. Indeed, if we call ν the positive integer for which the energy function cross the x axis

and $-\nu$ the negative integer for which the energy function cross the x axis, we can write:

$$\begin{aligned} 0 &= -2w\cos\left(\frac{2\pi\nu}{\ell}+\varphi\right)-\mu \\ 0 &= -2w\cos\left(\frac{2\pi\nu}{\ell}-\varphi\right)-\mu \end{aligned} \tag{4.20}$$

that are equals to each other when $\varphi = 0$, while, when the potential is different from zero, the energy grows in the first equation and decreases in the second one. However, by increasing the potential, we observe that the translation reaches a level such that the energy function becomes the same but with the opposite sign, and we can note the opposite phenomenon compared to the previous: the right electrons go up to the Fermi energy level and the left ones go down. This invertion (Fig.2) starts when $\varphi = \frac{\pi}{\ell}$, or, better, when $\Phi = \pi$. In particular, we can see it considering the $-\nu + 1$ site, that, during the rise of φ, return on the Fermi level; we have that:

$$\begin{aligned} -2w\cos\left(\frac{2\pi\nu}{\ell}+\varphi\right)-\mu &= -2w\cos\left(\frac{2\pi\nu+1}{\ell}-\varphi\right)-\mu \\ \frac{2\pi\nu}{\ell}+\varphi &= \frac{2\pi\nu+1}{\ell}-\varphi \\ 2\varphi &= \frac{2\pi}{\ell} \end{aligned} \tag{4.21}$$

that means that $\varphi = \frac{\pi}{\ell}$, as observed.

Now, we want to evaluate the ground energy of the system, and then the persistent current. To do this, we can express the ground state energy at $T = 0$K as a sum over n of the single quasi-particle energy levels discussed before. We obtain that:

$$E_G(\varphi) = \sum_n E_n(\varphi) \tag{4.22}$$

where $n \in \{\frac{\ell}{2\pi}\left(-\frac{\pi}{2}-\varphi\right), \frac{\ell}{2\pi}\left(\frac{\pi}{2}-\varphi\right)\}$ is an integer. We can now plot the ground energy $E_G(\varphi)$ as function of φ (Fig.3) obtaining a particular shape of the function that highlights the presence of level crossing.

Moreover, by doing a partial derivative on the ground state energy function, we can calculate the persistent current at $T = 0$K:

$$I(\varphi) = e\frac{\partial}{\partial\varphi}E_G(\varphi) = \sum_n I_n(\varphi) \tag{4.23}$$

that can be plotted vs φ, obtaining a periodic and discontinuous function (Fig. 4.2 b.), due to the cusps that appear in the energy level crossing (Fig. 4.2 a.).

We will see in the next subsection that this particular trend of the persistent-current function appears also in more complex systems.

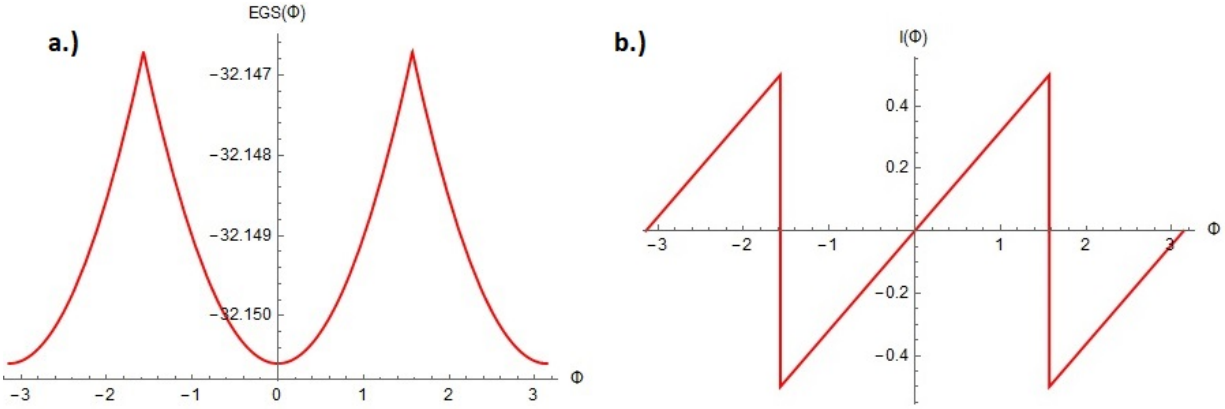

Figure 4.2: a.) Ground-state energy $EGS(\Phi)$ for an homogeneous normal mesoscopic ring as a function of Φ; b.) Persistent current $I(\Phi)$ for an homogeneous normal mesoscopic ring as a function of Φ.

This approach underlines the relation between the levels dynamic and the particular shape of the persistent current, in particular we have shown how the phase factor introduced in the hopping amplitude becomes crucial on the determination of the ground energy state. This result was proposed by Maiti (89) and experimentally proofs in different works (90; 91; 92).

However this approach result inadequate to describe more complex systems because of the difficulty related to the Schrödinger equation solution. For this reason, we will introduce in the next subsection another formalism, with which is easier obtain $I(\varphi)$ for non-homogeneous systems and superconducting devices.

4.2 The transfer matrix and the complex-plane integral for non-homogeneous SN rings

In this section we focus our attention to the definition, the computation and the applicatin of the transfer matrix in order to build an integral formula for the calculation of the persistent current in non-homogeneous superconducting-normal rings.

Let us start with the definition of the transfer matrix. Suppose we have a junction between two wires. The scattering matrix binds the wave functions that enter the junction to those that come out; instead the transfer matrix, which we will indicate with $\mathcal{M}$, binds the wavefunctions to the right of the junction to those to the left. More precisely, if we indicate with $\{a_L,\ a_R\}$ the incoming wave functions, where L stay for "left" and R stay for "right" , and with $\{b_L,\ b_R\}$ the outcoming wavefunctions, we already know that we can define the scattering matrix S as:

$$\begin{bmatrix} b_L \\ b_R \end{bmatrix} = S \begin{bmatrix} a_L \\ a_R \end{bmatrix} \tag{4.24}$$

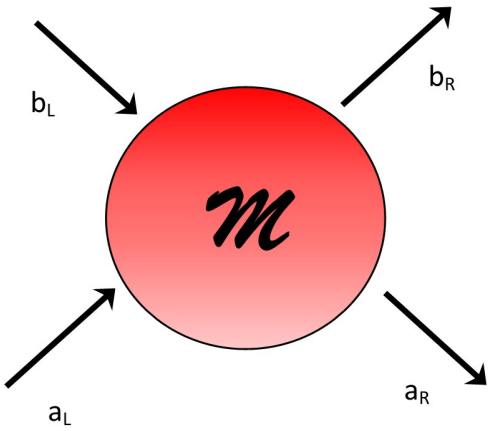

Figure 4.3: Sketch of the transfer matrix $\mathcal{M}$.

while, the transfer matrix $\mathcal{M}$ connects the wavefunctions on the left of the barrier with the right ones (see Fig. 4.3); we can define it as:

$$\begin{bmatrix} b_R \\ a_R \end{bmatrix} = \mathcal{M} \begin{bmatrix} b_L \\ a_L \end{bmatrix} \tag{4.25}$$

The transfer matrix of a non-homogeneous ring, for example, can be expressed as a product of relative transfer matrices to the individual blocks that make up the system. To prove this, we suppose to have a chain with two junctions and an electron that moves along it. Assume that the scattering occurs from the left to the right and that each junction can be considered as a potential barrier on which the electron scatters entering to the left and exiting from the right. After the first scattering, the incoming wave to the left is a wave coming out to the right from the previous junction; in particular we have that $b_R \to a_L$ and $a_R \to b_L$; we conclude that the transfer matrix of these two scatterings, which transfer the electron from the left to the right of each junction, compose the transfer matrix total system. This property is valid for any number finished joints. This property will be used below to write the transfer matrix of a moving electron along a non-homogeneous rings.

As a consequence of the conservation of the number of particles, the scattering matrix is unitary, while, in general, the transfer matrix does not satisfy this request.

It is possible to correlate the scattering matrix to the transfer matrix. This allows us to give physical meaning to the matrix elements that make $\mathcal{M}$. We then write the scattering matrix in terms of transmission and reflection coefficients:

$$S = \begin{bmatrix} \hat{R} & \hat{T}' \\ \hat{T} & \hat{R}' \end{bmatrix} \tag{4.26}$$

and the transfer matrix as:

$$\mathcal{M} = \begin{bmatrix} \hat{m}_1 & \hat{m}_2 \\ \hat{m}_3 & \hat{m}_4 \end{bmatrix} \tag{4.27}$$

Writing the system of equations for a_R, a_L, b_R and b_L in terms of S and $\mathcal{M}$, we have that:

$$\begin{bmatrix} b_L \\ b_R \end{bmatrix} = \begin{bmatrix} \hat{R} & \hat{T\,'} \\ \hat{T} & \hat{R}\,' \end{bmatrix} \begin{bmatrix} a_L \\ a_R \end{bmatrix} \tag{4.28}$$

and that:

$$\begin{bmatrix} b_R \\ a_R \end{bmatrix} = \begin{bmatrix} \hat{m}_1 & \hat{m}_2 \\ \hat{m}_3 & \hat{m}_4 \end{bmatrix} \begin{bmatrix} b_L \\ a_L \end{bmatrix} \tag{4.29}$$

We write the equations (4.28) in terms of b_L e b_R:

$$b_L = \hat{R}a_L + \hat{T\,'}a_R \tag{4.30}$$
$$b_R = \hat{T}a_L + \hat{R}\,'a_R \tag{4.31}$$

and the equations (4.29) in terms of b_R and a_R:

$$b_R = \hat{m}_1 b_L + \hat{m}_2 a_L \tag{4.32}$$
$$a_R = \hat{m}_3 b_L + \hat{m}_4 a_L \tag{4.33}$$

By solving the system in terms of the coefficients of the transfer matrix, we get that:

$$\begin{aligned} \hat{m}_1 &= \hat{T} - \hat{R}'\hat{T}\,'^{-1}\hat{R} = \left(\hat{T}^{\dagger}\right)^{-1} \\ \hat{m}_2 &= \hat{R}'\hat{T}\,'^{-1} \\ \hat{m}_3 &= \hat{T}\,'^{-1}\hat{R}' \\ \hat{m}_4 &= \hat{T}\,'^{-1} \end{aligned} \tag{4.34}$$

where $\hat{T}$ and $\hat{T}\,'$ are transmission coefficients, while $\hat{R}$ and $\hat{R}'$ are reflection coefficients of S.

As it has been defined, the transfer matrix can be block-factored, that is, it is possible to consider a non-homogeneous system as a sequence of homogeneous regions separated by interfaces. Indeed, the TM for a one-dimensional system comes out to be simply the ordered product of the matrices corresponding to the homogeneous regions and of the ones corresponding to the interfaces, taken in the appropriate sequence. From this respect, the matrices corresponding to each homogeneous region and to each interface are sort of "building blocks" of the global transfer matrix .

As we shall see, this important property of the transfer matrix will allow us, in the following sections, to focus only on the equations at the interface of the various systems.

4.2.1 The complex-plane integral

Let us take as a general device a one dimensional ring made by two superconducing homogeneous chains (p-wave or s-wave), each one characterized by different parameters.

Our approach to the persistent current through mesoscopic normal/superconducting rings is based on the transfer-matrix (TM) approach, which can be regareded as a pertinently modified version of the technique used in (155; 156) to computing the Josephson current across an SNS hybrid junction. In its essence, it consists in a simple and compact formula to express the groundstate energy of a system at a finite chemical potential. For the sake of the presentation, in order to illustrate its main features, in this section we review the main steps leading to our final formula for the groundstate energy in the case of a normal, mesoscopic ring. Nevertheless, as we discuss in the following, the generalization to NSHRs containing one, or more, superconducting sections is quite a straightforward generalization of the derivation we provide in this section. To treat the p-wave and the s-wave case on the same footing we choose to perform our derivation within a lattice one-dimensional model Hamiltonian, which, in the superconducting region, corresponds to Kitaev's Hamiltonian in the p-wave case (142), and to the lattice one-dimensional Hamiltonian of Ref.(152) in the s-wave case.

To derive the main formula for the groundstate energy, let us consider as a reference model a normal segment consisting of two "asymptotic" regions for $j < j_1$ and for $j > j_2$ and assume that within the asymptotic regions there is no potential scattering and/or interfaces, so that the fermions freely propagate in a chemical potential μ. This corresponds to assuming an asyptotic lattice Hamiltonian of the form $H_{\rm as} = -J\sum_j\{c_j^\dagger c_{j+1}+c_{j+1}^\dagger c_j\}-\mu\sum_j c_j^\dagger c_j$, with c_j being the single-fermion lattice annihilation operator for spinlòess fermions. As a result, the wavefunction at energy E takes the asymptotic form

$$\begin{array}{rcl} u_j & \sim & A_+^< e^{ikj} + A_-^< e^{-ikj} \ , \ (j < j_1) \\ u_j & \sim & A_+^> e^{ikj} + A_-^> e^{-ikj} \ , \ (j > j_2) \end{array} \tag{4.35}$$

with

$$E = -2J\cos(k) - \mu \tag{4.36}$$

Now, by definition the transfer matrix between sites $j_a < j_1$ and $j_b > j_2$, $\mathcal{M}[E; j_a, j_b]$, relates the solution at $j = j_a$ to the solution at $j = j_b$, that is

$$u_{j_b} = \tilde{A}_+ e^{ikj_a} + \tilde{A}_- e^{-ikj_a} \quad , \tag{4.37}$$

with

$$\left[\begin{array}{c} \tilde{A}_+ \\ \tilde{A}_- \end{array} \right] = \mathcal{M}[E; j_a, j_b] \left[\begin{array}{c} A_+^< \\ A_-^< \end{array} \right] \tag{4.38}$$

A ring of length ℓ is defined by imposing periodic boundary conditions (PBCs) on the solution in Eq.(4.35). Going through Eq.(4.37), this is accounted for by means of the secular equation

$$\mathcal{M}[E; j, j+\ell] \begin{bmatrix} A_+^< \\ A_-^< \end{bmatrix} = \begin{bmatrix} A_+^< \\ A_-^< \end{bmatrix} \tag{4.39}$$

Looking for non trivial solutions for Eq.(4.39), we find the secular equation for E:

$$\det\{\mathcal{M}[E;\ell] - \mathbf{I}\} = 0 \tag{4.40}$$

Besides consituting an alternative way of presenting the eigenvalue equation for a single particle on the ring, Eq.(4.40) also provides an efficient way to compute the groundstate energy of the system, $E_{\rm GS}$, defined as the sum of all the negative (if measured with respect to the chemical potential) single-particle energy eigenvalues, that is

$$E_{\rm GS} = \sum_{E<0} E \tag{4.41}$$

Indeed, single-particle energy eigenvalues are just the zeroes of $\det\{\mathcal{M}[E;\ell] - \mathbf{I}\}$ lying at the negative part of the real axis, if one regards $\det\{\mathcal{M}[E;\ell] - \mathbf{I}\}$ as a function of the complex variable E. To sum over all of them, we adapt the approach of Refs.(155; 156), namely, we first of all note that the energy eigenvalues are the poles of the function $\Psi[E;\ell]$, defined as

$$\Psi[E;\ell] = \frac{\partial_E \det\{\mathcal{M}[E;\ell] - \mathbf{I}\}}{\det\{\mathcal{M}[E;\ell] - \mathbf{I}\}} = \partial_E \ln\det\{\mathcal{M}[E;\ell] - \mathbf{I}\} \tag{4.42}$$

We therefore introduce the integration path Γ depicted in Fig.4.4 and conpute $E_{\rm GS}$ as

$$E_{\rm GS} = \frac{1}{2\pi i} \oint_\Gamma dE\, E\Psi[E;\ell] = -\frac{1}{2\pi i} \oint_\Gamma dE\, \ln\det\{\mathcal{M}[E;\ell] - \mathbf{I}\} \tag{4.43}$$

Now, we deform the integration path as illustrated in Fig.4.4, so to eventually compute the integral over the imaginary axis as

$$E_{\rm GS} = -\frac{1}{2\pi} \int_{-\infty}^{\infty} d\omega\, \ln\det\{\mathcal{M}[i\omega;\ell] - \mathbf{I}\} \tag{4.44}$$

Eq.(4.44) is the hearth of our work: when used to compute the groundstate energy for a ring pierced by a magnetic flux Φ, once derived with respect to Φ it gives the (zero-temperature) persistent current as

$$I[\Phi] = e\partial_\Phi E_{\rm GS}[\Phi] = -\frac{e}{2\pi} \int_{-\infty}^{\infty} d\omega\, \partial_\Phi \ln\det\{\mathcal{M}[i\omega;\ell;\Phi] - \mathbf{I}\} \tag{4.45}$$

In the following we will use Eq.(4.45) to compute the persistent current in the various systems we discuss in this work. $I[\Phi]$ is expected to be a periodic function of Φ: as a

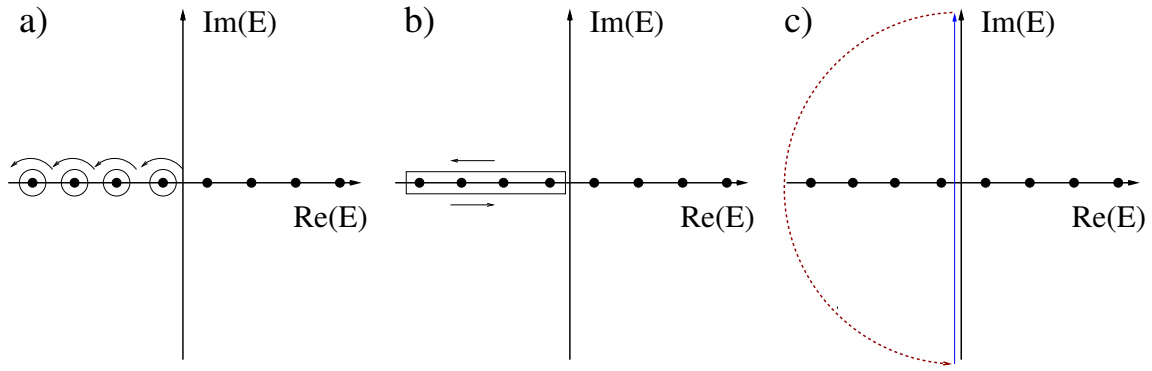

Figure 4.4: Sequence of deformations in the integration path Γ eventually allowing to express $I[\Phi]$ as an integral over the imaginary axis:
a) The path Γ obtained as the union of small circles, each one surrounding one, and only one, negative (with respect to the Fermi level) energy eigenvalue;
b) The integral over Γ can be deformed to an integral over just one closed path, surrounding all the negative energy eigenvalues;
c) The integral over the red-dashed arc is assumed to be equal to 0 in the infinite-radius limit. Only the integral over the imaginary axis (to which the solid-blue line can be continously deformed) is left. (105)

general remark , let us point out that, in the following, we shall measure the flux Φ in units of $\hbar/(2e)$), so that a period Φ_0^* corresponds to a 2π-periodicity, while a period Φ_0 corresponds to a 4π-periodicity.

Now, we just have to introduce the various models that we want to study and calculate, for each of them, the persistent current. To model a hybrid one-dimensional ring, we resort to a lattice model Hamiltonian with position-dependent parameters. Using a lattice model Hamiltonian allows, on one hand, to easily introduce p-wave pairing both in real space and in momentum space, on the other hand, it provides a natural mean to reglarize divergences which would arise in the continuum model when summing over the energies of the occupied levels to compute $E_{\mathrm{GS}}[\Phi]$ (and, therefore, $I[\Phi]$). To highlight special features of p-wave NSHRs, in the following, when possible, we systematically compare the results obtained in p-wave systems to the ones obtained in s-wave systems. Therefore, in this section we present and discuss in detail the lattice model Hamiltonian modelling both cases, eventually deriving the transfer matrix which we shall eventually use in the following to compute the persistent currents.

4.2.2 The p-wave-normal case

In the p-wave case, referring to the one-dimensional Kitaev Hamiltonian (142) for a spinless p-wave superconductor, calling 1 and 2 the two regions, we assume that the normal hopping amplitude, the pairing gap and the chemical potential are respectively given by w_1, Δ_1, μ_1 and by w_2, Δ_2, μ_2. Moreover, we assume that regions 1 and 2 are

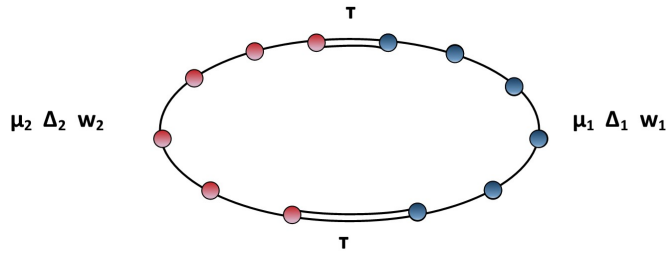

Figure 4.5: Sketch of the system described by the model Hamiltonian in Eq.(4.46).

coupled at their endpoints via a normal hopping term, with hopping amplitude τ (see Fig.4.5). In a ring configuration, we also assume that a magnetic flux Φ pierces the ring. By means of an appropriate canonical redefinition of the lattice fermion operators, it is possible to account for the applied magnetic flux in terms of a phase factor $e^{\pm i\frac{\Phi}{4}}$, symmetrically "loaded" on the two hopping term between the two regions. As a result, we eventually present the model Hamiltonian as:

$$\begin{aligned} H &= -w_1 \sum_{j=1}^{\ell_1-1}\{c_j^\dagger c_{j+1} + c_{j+1}^\dagger c_j\} - \mu_1 \sum_{j=1}^{\ell_1} c_j^\dagger c_j + \Delta_1 \sum_{j=1}^{\ell_1-1}\{c_j c_{j+1} + c_{j+1}^\dagger c_j^\dagger\} \\ &- w_2 \sum_{j=1}^{\ell_2-1}\{d_j^\dagger d_{j+1} + d_{j+1}^\dagger d_j\} - \mu_2 \sum_{j=1}^{\ell_2} d_j^\dagger d_j + \Delta_2 \sum_{j=1}^{\ell_2-1}\{d_j d_{j+1} + d_{j+1}^\dagger d_j^\dagger\} \\ &- \tau\{[c_1^\dagger d_{\ell_2} + d_1^\dagger c_{\ell_1}]e^{\frac{i}{4}\Phi} + [d_{\ell_2}^\dagger c_1 + c_{\ell_1}^\dagger d_1]e^{-\frac{i}{4}\Phi}\} \end{aligned} \tag{4.46}$$

In Eq.(4.46) we have set the lengths of the two arms of the ring respectively at ℓ_1 and at ℓ_2 and used $c_j, c_j^\dagger$ to denote the lattice annihilation/creation operators at site j within region 1, and $d_j, d_j^\dagger$ to denote the lattice annihilation/creation operators at site j within region 2, with standard anticommutation relations $\{d_j, d_{j'}^\dagger\} = \{c_j, c_{j'}^\dagger\} = \delta_{j,j'}$, all the other anticommutators being equal to 0. Once the parameters are taken in the appropriate limit, the model Hamiltonian in Eq.(4.46) is suitable to describing a number of systems of physical interest, such as a p-wave superconducting ring interrupted by a weak link (158), a hybrid p-wave-normal metal ring, a half-topological, half-non-topological superconducting ring (159). Moreover, as we discuss in the following, the limit of a long-superconducting section, the superconducting-normal hybrid ring is mapped onto the effective model for a Josephson junction made with topological superconductors [(160; 125)].

In the following, we will be mostly focusing onto the $\Delta_2 \to 0$ limit. To construct the transfer matrix in this case, we start from the Bogoliubov-de Gennes (BdG) equations for the single-quasiparticle wavefunction at a given energy E. To do so, we consider a generic energy eigenmode Γ_E which, in terms of the single-fermion lattice operators on the ring, is given by

$$\Gamma_E = \sum_{j=1}^{\ell_1} \{[u_j^{(1)}]^* c_j + [v_j^{(1)}]^* c_j^\dagger\} + \sum_{j=1}^{\ell_2} \{[u_j^{(2)}]^* d_j + [v_j^{(2)}]^* d_j^\dagger\} \tag{4.47}$$

with $\begin{bmatrix} u_j^{(1)} \\ v_j^{(1)} \end{bmatrix}$ and $\begin{bmatrix} u_j^{(2)} \\ v_j^{(2)} \end{bmatrix}$ being the single-quasiparticle wavefunction in region-1 and in region-2. On imposing the canonical commutation relation

$$[\Gamma_E, H] = E\Gamma_E \tag{4.48}$$

we therefore obtain the BdG equations for the wavefunctions. Within the homogeneous regions, these are given by

$$\begin{aligned} Eu_j^{(1)} &= -w_1\{u_{j+1}^{(1)} + u_{j-1}^{(1)}\} - \mu_1 u_j^{(1)} + \Delta_1\{v_{j+1}^{(1)} - v_{j-1}^{(1)}\} \\ Ev_j^{(1)} &= w_1\{v_{j+1}^{(1)} + v_{j-1}^{(1)}\} + \mu_1 v_j^{(1)} - \Delta_1\{u_{j+1}^{(1)} - u_{j-1}^{(1)}\} \end{aligned} \tag{4.49}$$

for $1 < j < \ell_1$, and

$$\begin{aligned} Eu_j^{(2)} &= -w_2\{u_{j+1}^{(2)} + u_{j-1}^{(2)}\} - \mu_2 u_j^{(2)} + \Delta_2\{v_{j+1}^{(2)} - v_{j-1}^{(2)}\} \\ Ev_j^{(2)} &= w_2\{v_{j+1}^{(2)} + v_{j-1}^{(2)}\} + \mu_2 v_j^{(2)} - \Delta_2\{u_{j+1}^{(2)} - u_{j-1}^{(2)}\} \end{aligned} \tag{4.50}$$

for $1 < j < \ell_2$. At the interfaces between the two regions, instead, the BdG equations yield:

$$\begin{aligned} Eu_1^{(1)} &= -w_1 u_2^{(1)} - \tau e^{-\frac{i}{4}\Phi} u_{\ell_2}^{(2)} - \mu_1 u_1^{(1)} + \Delta_1 v_2^{(1)} \\ Ev_1^{(1)} &= w_1 v_2^{(1)} + \tau e^{\frac{i}{4}\Phi} v_{\ell_2}^{(2)} + \mu_1 v_1^{(1)} - \Delta_1 u_2^{(1)} \\ Eu_{\ell_2}^{(2)} &= -w_2 u_{\ell_2-1}^{(2)} - \tau e^{\frac{i}{4}\Phi} u_1^{(1)} - \mu_2 u_{\ell_2}^{(2)} - \Delta_2 v_{\ell_2-1}^{(2)} \\ Ev_{\ell_2}^{(2)} &= w_2 v_{\ell_2-1}^{(2)} + \tau e^{-\frac{i}{4}\Phi} v_1^{(1)} + \mu_2 v_{\ell_2}^{(2)} + \Delta_2 u_{\ell_2-1}^{(2)} \\ Eu_1^{(2)} &= -w_2 u_2^{(2)} - \tau e^{-\frac{i}{4}\Phi} u_{\ell_1}^{(1)} - \mu_1 u_1^{(2)} + \Delta_2 v_2^{(2)} \\ Ev_1^{(2)} &= w_2 v_2^{(2)} + \tau e^{\frac{i}{4}\Phi} v_{\ell_1}^{(1)} + \mu_1 v_1^{(2)} - \Delta_2 u_2^{(2)} \\ Eu_{\ell_1}^{(1)} &= -w_1 u_{\ell_1-1}^{(1)} - \tau e^{\frac{i}{4}\Phi} u_1^{(2)} - \mu_1 u_{\ell_1}^{(1)} - \Delta_1 v_{\ell_1-1}^{(1)} \\ Ev_{\ell_1}^{(1)} &= w_1 v_{\ell_1-1}^{(1)} + \tau e^{-\frac{i}{4}\Phi} v_1^{(2)} + \mu_1 v_{\ell_1}^{(1)} + \Delta_1 u_{\ell_1-1}^{(1)} \end{aligned} \tag{4.51}$$

According to Eqs.(4.49,4.50), within the homogeneous regions, we write the wavefunctions as superpositions of the solutions of the homogeneous BdG equations, that is, we set

$$\begin{bmatrix} u_j \\ v_j \end{bmatrix} = \begin{bmatrix} u^{(1)} \\ v^{(1)} \end{bmatrix} e^{ik_1 j} \tag{4.52}$$

in region 1, with $1 \leq j \leq \ell_1$, and

$$\left[\begin{array}{c} u_j \\ v_j \end{array} \right] = \left[\begin{array}{c} u^{(2)} \\ v^{(2)} \end{array} \right] e^{ik_2 j} \tag{4.53}$$

in region 2, with $1 \leq j \leq \ell_2$. At a given energy E, the amplitudes $\left[\begin{array}{c} u^{(a)} \\ v^{(a)} \end{array} \right]$ $(a = 1, 2)$ are determined by solving the equations

$$\begin{aligned} 0 &= \{E + 2w_a \cos(k_a) + \mu_a\} u^{(a)} - 2i\Delta_a \sin(k_a) v^{(a)} \\ 0 &= 2i\Delta_a \sin(k_a) u^{(a)} + \{E - 2w_a \cos(k_a) - \mu_a\} v^{(a)} \end{aligned} \tag{4.54}$$

with k_1, k_2 determined by the dispersion relations

$$E^2 = [2w_1 \cos(k_1) + \mu_1]^2 + 4\Delta_1^2 \sin^2(k_1) = [2w_2 \cos(k_2) + \mu_2]^2 + 4\Delta_2^2 \sin^2(k_2) \tag{4.55}$$

Solving Eq.(4.55) at a given energy, we define the particle-like momenta $k_p^{(a)}$ and the hole-like momenta $k_h^{(a)}$, as

$$\begin{aligned} \cos(k_p^{(a)}) &= -\frac{w_a \mu_a}{2(w_a^2 - \Delta_a^2)} - \frac{1}{2}\sqrt{\frac{E^2 - [\Delta_w^{(a)}]^2}{w_a^2 - \Delta_a^2}} \\ \cos(k_h^{(a)}) &= -\frac{w_a \mu_a}{2(w_a^2 - \Delta_a^2)} + \frac{1}{2}\sqrt{\frac{E^2 - [\Delta_w^{(a)}]^2}{w_a^2 - \Delta_a^2}} \end{aligned} \tag{4.56}$$

with

$$\Delta_w^{(a)} = \Delta_a \sqrt{4 - \frac{\mu_a^2}{w_a^2 - \Delta_a^2}} \tag{4.57}$$

Note that Eqs.(4.56) do in principle hold also for $|E| < \Delta_w$, though with complex values for the momenta. At given $k_p^{(a)}, k_h^{(a)}$, one determines the wavefunctions $(u_p^{(a)}, v_p^{(a)})$ and $(u_h^{(a)}, v_h^{(a)})$, defined as solutions of Eqs.(4.54) with k_a respectively equal to k_p and k_h. Taking the most general linear combinations of wavefunctions at the same energy, one finds that a generic wavefunction at energy E within region-a (=1,2) takes the form

$$\left[\begin{array}{c} u_j^{(a)} \\ v_j^{(a)} \end{array} \right] = A_{(p,+)}^{(a)} \left[\begin{array}{c} u_p^{(a)} \\ v_p^{(a)} \end{array} \right] e^{ik_p^{(a)} j} + A_{(p,-)}^{(a)} \left[\begin{array}{c} u_p^{(a)} \\ -v_p^{(a)} \end{array} \right] e^{-ik_p^{(a)} j} + \tag{4.58}$$

$$+ A_{(h,+)}^{(a)} \left[\begin{array}{c} u_h^{(a)} \\ v_h^{(a)} \end{array} \right] e^{-ik_h^{(a)} j} + A_{(h,-)}^{(a)} \left[\begin{array}{c} u_h^{(a)} \\ -v_h^{(a)} \end{array} \right] e^{ik_h^{(a)} j} \tag{4.59}$$

The transfer matrix is fully determined once one recovers the relations between the amplitudes $A^{(a)}_{(p,+)}, A^{(a)}_{(p,-)}, A^{(a)}_{(h,+)}, A^{(a)}_{(h,-)}$ in the two regions. These are determined by the interface conditions obtained from Eqs.(4.51). In a compact notation, these are given by

$$\Sigma_a[\Phi]\cdot[\Upsilon^{(a)}(E)]\cdot\begin{bmatrix} A^{(a)}_{(p,+)} \\ A^{(a)}_{(p,-)} \\ A^{(a)}_{(h,+)} \\ A^{(a)}_{(h,-)} \end{bmatrix} = \Omega_b[\Phi]\cdot[\Upsilon^{(b)}(E)]\cdot\mathbf{T}_b(E;\ell_b)\cdot\begin{bmatrix} A^{(b)}_{(p,+)} \\ A^{(b)}_{(p,-)} \\ A^{(b)}_{(h,+)} \\ A^{(b)}_{(h,-)} \end{bmatrix} \tag{4.60}$$

with $b = 2(1)$ if $a = 1(2)$, and the matrix $\Sigma_a[\Phi]$ defined as

$$\Sigma_a[\Phi] = \begin{bmatrix} \tau e^{\frac{i}{4}\Phi} & 0 & 0 & 0 \\ 0 & \tau e^{-\frac{i}{4}\Phi} & 0 & 0 \\ 0 & 0 & w_a & \Delta_a \\ 0 & 0 & \Delta_a & w_a \end{bmatrix} \quad , \tag{4.61}$$

the matrix $[\Upsilon^{(a)}(E)]$ defined as

$$[\Upsilon^{(a)}(E)] = \begin{bmatrix} e^{ik_p^{(a)}}u_p^{(a)} & e^{-ik_p^{(a)}}u_p^{(a)} & e^{-ik_h^{(a)}}u_h^{(a)} & e^{ik_h^{(a)}}u_h^{(a)} \\ e^{ik_p^{(a)}}v_p^{(a)} & -e^{-ik_p^{(a)}}v_p^{(a)} & -e^{-ik_h^{(a)}}v_h^{(a)} & e^{ik_h^{(a)}}v_h^{(a)} \\ u_p^{(a)} & u_p^{(a)} & u_h^{(a)} & u_h^{(a)} \\ v_p^{(a)} & -v_p^{(a)} & -v_h^{(a)} & v_h^{(a)} \end{bmatrix} \tag{4.62}$$

the matrix $\Omega_a[\Phi]$ given by

$$\Omega_a[\Phi] = \begin{bmatrix} w_a & -\Delta_a & 0 & 0 \\ -\Delta_a & w_a & 0 & 0 \\ 0 & 0 & \tau e^{-\frac{i}{4}\Phi} & 0 \\ 0 & 0 & 0 & \tau e^{\frac{i}{4}\Phi} \end{bmatrix} \tag{4.63}$$

and, finally, the transfer matrix for a homogeneous region of length ℓ being given by

$$\mathbf{T}_a(E;\ell) = \begin{bmatrix} e^{ik_p^{(a)}\ell} & 0 & 0 & 0 \\ 0 & e^{-ik_p^{(a)}\ell} & 0 & 0 \\ 0 & 0 & e^{-ik_h^{(a)}\ell} & 0 \\ 0 & 0 & 0 & e^{ik_h^{(a)}\ell} \end{bmatrix} \tag{4.64}$$

As a result, the transfer matrix for the full ring takes the form

$$\begin{aligned} \mathcal{M}_{p-wave}[E;\Phi;\ell_1;\ell_2] &= [\Upsilon^{(2)}(E)]^{-1}\cdot\Sigma_2^{-1}[\Phi]\cdot\Omega_1[\Phi]\cdot[\Upsilon^{(1)}(E)]\cdot\mathbf{T}_1(E;\ell_1)\cdot \\ &\cdot\ [\Upsilon^{(1)}(E)]^{-1}\Sigma_1^{-1}[\Phi]\cdot\Omega_2[\Phi]\cdot[\Upsilon^{(2)}(E)]\cdot\mathbf{T}_2(E;\ell_2) \end{aligned} \tag{4.65}$$

Eq.(4.65) is the key ingrediend we need to compute the persistent current in the various regimes of interest. We now derive the analog of Eq.(4.65) in the case of a ring made of s-wave superconducting regions.

4.2.3 The s-wave-normal case

In the case of a system made of two s-wave superconducting regions with parameters respectively given by w_1, Δ_1, μ_1 and by w_2, Δ_2, μ_2, and connected to each other with hopping amplitude τ, the corresponding (spinful) Hamiltonian is given by

$$\begin{aligned} H &= -w_1 \sum_\sigma \sum_{j=1}^{\ell_1 - 1} \{c^\dagger_{j,\sigma} c_{j+1,\sigma} + c^\dagger_{j+1,\sigma} c_{j,\sigma}\} - \mu_1 \sum_\sigma \sum_{j=1}^{\ell_1} c^\dagger_{j,\sigma} c_{j,\sigma} + \Delta_1 \sum_{j=1}^{\ell_1} \{c_{j,\uparrow} c_{j,\downarrow} + c^\dagger_{j,\downarrow} c^\dagger_{j,\uparrow}\} \\ &- w_2 \sum_\sigma \sum_{j=1}^{\ell_2 - 1} \{d^\dagger_{j,\sigma} d_{j+1,\sigma} + d^\dagger_{j+1,\sigma} d_{j,\sigma}\} - \mu_2 \sum_\sigma \sum_{j=1}^{\ell_2} d^\dagger_{j,\sigma} d_{j,\sigma} + \Delta_2 \sum_{j=1}^{\ell_2} \{d_{j,\uparrow} d_{j,\downarrow} + d^\dagger_{j,\downarrow} d^\dagger_{j,\uparrow}\} \\ &- \sum_\sigma \tau \{[c^\dagger_{1,\sigma} d_{\ell_2,\sigma} + d^\dagger_{1,\sigma} c_{\ell_1,\sigma}] e^{\frac{i}{4}\Phi} + [d^\dagger_{\ell_2,\sigma} c_{1,\sigma} + c^\dagger_{\ell_1,\sigma} d_{1,\sigma}] e^{-\frac{i}{4}\Phi}\} \end{aligned} \tag{4.66}$$

Going through the same steps as in the p-wave case, we eventually find that the transfer matrix of the ring is now given by

$$\begin{aligned} \mathcal{M}_{s-wave}[E;\Phi;\ell_1;\ell_2] &= [\tilde{\Upsilon}^{(2)}(E)]^{-1} \cdot \tilde{\Sigma}_2^{-1}[\Phi] \cdot \tilde{\Omega}_1[\Phi] \cdot [\tilde{\Upsilon}^{(1)}(E)] \cdot \mathbf{T}_1(E;\ell_1) \cdot \\ &\cdot \quad [\tilde{\Upsilon}^{(1)}(E)]^{-1} \cdot \tilde{\Sigma}_1^{-1}[\Phi] \cdot \tilde{\Omega}_2[\Phi] \cdot [\tilde{\Upsilon}^{(2)}(E)] \cdot \mathbf{T}_2(E;\ell_2) \end{aligned} \tag{4.67}$$

The $\tilde{\Sigma}_a[\Phi], \tilde{\Omega}_a[\Phi]$ matrices in Eq.(4.67) are simply obtained by setting Δ_a to 0 respectively in Eq.(4.61) and in Eq.(4.63). The matrix $[\tilde{\Upsilon}^{(a)}(E)]$ is given by

$$[\tilde{\Upsilon}^{(a)}(E)] = \begin{bmatrix} e^{ik_p^{(a)}} u_p^{(a)} & e^{-ik_p^{(a)}} u_p^{(a)} & e^{-ik_h^{(a)}} u_h^{(a)} & e^{ik_h^{(a)}} u_h^{(a)} \\ e^{ik_p^{(a)}} v_p^{(a)} & e^{-ik_p^{(a)}} v_p^{(a)} & e^{-ik_h^{(a)}} v_h^{(a)} & e^{ik_h^{(a)}} v_h^{(a)} \\ u_p^{(a)} & u_p^{(a)} & u_h^{(a)} & u_h^{(a)} \\ v_p^{(a)} & v_p^{(a)} & v_h^{(a)} & v_h^{(a)} \end{bmatrix} \tag{4.68}$$

with $u^{(a)}, v^{(a)}$ determined as nontrivial solutions of the algebraic system

$$\begin{aligned} 0 &= \{E + 2w_a \cos(k_a) + \mu_a\} u^{(a)} - \Delta_a v^{(a)} \\ 0 &= -\Delta_a u^{(a)} + \{E - 2w_a \cos(k_a) - \mu_a\} v^{(a)} \end{aligned} \tag{4.69}$$

for k_1, k_2 solving the equation:

$$E^2 = [2w_1 \cos(k_1) + \mu_1]^2 + \Delta_1^2 = [2w_2 \cos(k_2) + \mu_2]^2 + \Delta_2^2 \tag{4.70}$$

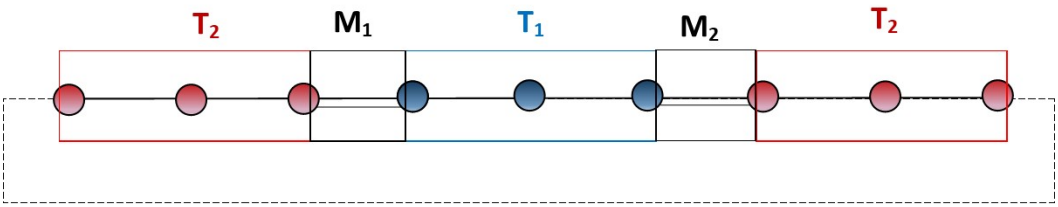

Figure 4.6: Graphical representation of the factorizability of the transfer matrix: for the speficic system depicted in figure, the transfer matrix is given by $\mathcal{M} = \mathbf{T}_2 \cdot M_1 \cdot \mathbf{T}_1 \cdot M_2 \cdot \mathbf{T}_2$ (from right to left).

and $k_p^{(a)}, k_h^{(a)}$ defined by

$$\begin{aligned} \cos[k_p^{(a)}] &= -\frac{\mu_a}{2w_a} - \sqrt{\frac{E^2 - \Delta_a^2}{4w_a^2}} \\ \cos[k_h^{(a)}] &= -\frac{\mu_a}{2w_a} + \sqrt{\frac{E^2 - \Delta_a^2}{4w_a^2}} \end{aligned} \tag{4.71}$$

Besides the differences in the form of the matrices appearing in Eqs.(4.65,4.67), an important point to stress is that both matrices are block-factorizable (see Fig.46 for a graphical representation of the factorizability of the matrix).

4.3 Persistent current and signatures of topological phase transition and Majorana modes

In this section we compute the persistent current in a number of cases of interest. For the sake of the discussion, it is worth comparing the results obtained in p-wave systems with the ones obtained in s-wave systems. Therefore, in the following we perform the calculation in both cases, by using Eq.(4.45), with the transfer matrix computed according to Eq.(4.65) (p-wave case), or to Eq.(4.67) (s-wave case). To keep in touch with the results of Ref.(159), we begin with the calculation of the current in the case of a superconducting ring interrupted by a weak link though, at variance with the discussion of (159), we will not assume fermion parity conservation. As stated above, for comparison, we also compute the current in the case of a ring made with an s-wave superconductor.

4.3.1 Persistent current across a superconducting ring interrupted by a weak link

A p-wave superconducting ring interrupted by a weak link can be physically realized at a semiconducting quantum wire with a sizeable spin-orbit coupling (e.g., an InAs

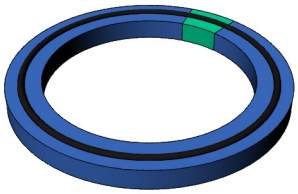

Figure 4.7: Sketch of the superconducting ring interrupted by a weak link as introduced and discussed in (159). A semiconducting ring (depicted as a solid black line) is deposited on top of a bulk superconducting ring, interrupted by a tiny insulating layer (light blu sector). The superconductor induces superconductivity within the semiconducting wire by proximity effect. All the current circulating across the system takes place due to tunneling effect within the semiconducting wire.

wire) deposited onto a bulk superconducting ring pierced by a magnetic flux Φ. The combined effect of spin-orbit coupling, Zeeman spin splitting and proximity-induced superconductivity from the bulk superconductor underneath has been shown to make the wire effectively behave as a one-dimensional superconductor (143; 144). As for what concerns a concrete proposal of an experimental realization of the system we discuss here, we refer to Refs.(159; 150). Specifically, we assume that the weak link is actually realized as a physical interruption of the superconducting ring with, for instance, a tiny insulating layer, which cuts the current within the superconductor, thus allowing the persistent current to only flow across the semiconducting nanowire. Indeed, among other advantages, this geometry allows for recovering as only detectable current the one flowing through the semiconducting wire, which is what we are eventually interested in. In Fig.4.7 we provide a sketch of the system we are considering here, that is, a homogeneous ring interrupted by a weak link. The corresponding model Hamiltonian can be recovered from Eq.(4.46) in p-wave case and from Eq.(A.1) in the s-wave case, by setting to zero the length of one of the two regions. In the former case, it is given by

$$\begin{aligned} H_{p-w} &= -w\sum_{j=1}^{\ell-1}\{c_j^\dagger c_{j+1}+c_{j+1}^\dagger c_j\}-\mu\sum_{j=1}^{\ell}c_j^\dagger c_j+\Delta_1\sum_{j=1}^{\ell-1}\{c_j c_{j+1}+c_{j+1}^\dagger c_j^\dagger\} \\ &- \tau\{c_1^\dagger c_\ell e^{\frac{i}{2}\Phi}+c_\ell^\dagger c_1 e^{-\frac{i}{2}\Phi}\} \end{aligned} \tag{4.72}$$

while in the latter case it can be presented as

$$H_{s-w} = -w\sum_{\sigma}\sum_{j=1}^{\ell-1}\{c^{\dagger}_{j,\sigma}c_{j+1,\sigma}+c^{\dagger}_{j+1,\sigma}c_{j,\sigma}\}-\mu\sum_{\sigma}\sum_{j=1}^{\ell_1}c^{\dagger}_{j,\sigma}c_{j,\sigma}+\Delta\sum_{j=1}^{\ell}\{c_{j,\uparrow}c_{j,\downarrow}+c^{\dagger}_{j,\downarrow}c^{\dagger}_{j,\uparrow}\}$$
$$- \sum_{\sigma}\tau\{c^{\dagger}_{1,\sigma}c_{\ell,\sigma}e^{\frac{i}{2}\Phi}+c^{\dagger}_{\ell,\sigma}c_{1,\sigma}e^{-\frac{i}{2}\Phi}\} \tag{4.73}$$

The transfer matrix derived from Eqs.(4.72,4.73) can therefore be simply expressed in terms of the ones we provide in section 4.2.3 by simply setting one of the two lengths (say ℓ_2) to 0. We therefore obtain

$$\mathcal{M}_{p-w}[E;\ell;\Phi]=[\Upsilon(E)]^{-1}\cdot\Sigma^{-1}[2\Phi]\cdot\Omega[2\Phi]\cdot[\Upsilon(E)]\cdot\mathbf{T}[E;\ell] \tag{4.74}$$

and, similarly

$$\mathcal{M}_{s-w}[E;\ell;\Phi]=[\tilde{\Upsilon}(E)]^{-1}\cdot\tilde{\Sigma}^{-1}[2\Phi]\cdot\tilde{\Omega}[2\Phi]\cdot[\tilde{\Upsilon}(E)]\cdot\mathbf{T}[E;\ell] \tag{4.75}$$

To compute the current, let us start with the ring described by the TM in Eq.(4.74). In Fig. 4.8, we plot $I[\Phi]$ *vs.* Φ for the values of the parameters reported in the caption, particularly for a chemical potential $\mu = 0$. At zero chemical potential, the p-wave superconductor lies well within the topological region, with two MFs γ_L, γ_R localized at its endpoints. This allows us to provide a simple interpretation of the curves we draw in Fig. 4.8 at different values of the length ℓ of the superconductor. The key parameter here is the "hybridization length" ℓ_M between γ_L and γ_R, which we estimate according to the derivation of Appendix C. At $\mu = 0$ and for the values of the parameters we used, from Eq.(3.23) we obtain $\ell_M \sim 5$. Therefore, when considering the largest ring ($\ell = 40$), we may safely neglect the overlap between γ_L and γ_R across the superconducting region and accordingly describe the low-energy excitations of the system by approximating the fermion operators in the tunneling term of the total Hamiltonian (second row of Eq.(4.72)) by means of the truncated mode expansion in Eq.(3.29). As a result, we obtain the effective low-energy Hamiltonian $H_{p;Eff}$ for the ring, given by

$$H_{p;Eff}\approx-\epsilon_0\,\cos\left(\frac{\Phi}{2}\right)\left\{2\Gamma^{\dagger}\Gamma-1\right\} \tag{4.76}$$

with $\epsilon_0 \propto \tau$ and the Dirac fermion operator Γ related to γ_L, γ_R by means of Eqs.(3.32). We now use Eq.(4.76) as a main reference to discuss the behavior of the current for large-ℓ. Indeed, while one should, in principle, consider the contributions arising from all the populated single-quasiparticle states at any energy (which is exactly done in the calculation we performed based on our TM approach), based upon arguments similar to the ones provided in Refs.(155; 156), in the large-ℓ limit we expect that the result for $I[\Phi]$ can be safely recovered by taking into account only low-energy states of the system. Before spelling this point out, let us also stress that, within our formalism, we do not assume Fermion parity conservation (which can be thought of in terms of a nonnegligible single-electron tunneling rate between the ring and e.g. a backgate

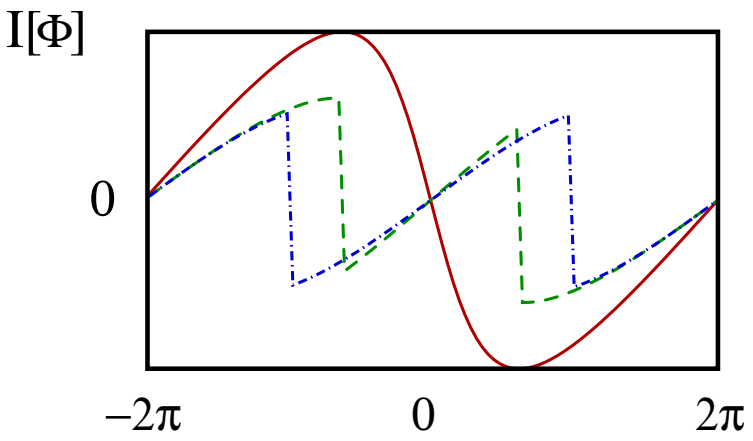

Figure 4.8: Plot of the persistent current $I[\Phi]$ *vs.* Φ (in units of Φ_0) for the p-wave mesoscopic ring with a weak link described by Eq.(4.72). The parameters are chosen so that $\mu = 0$, $\Delta = 0.2$ and $\tau = 0.5$ (in units of w), while $\ell = 4$ (red curve), $\ell = 4$ (full red curve), $\ell = 8$ (dashed green curve), $\ell = 40$ (dot-dashed blue curve). The estimated Majorana hybridization length in this case is $\ell_M \approx 5$.

used to tune from the outside the chemical potential of the system. While, within our formalism, one might in principle account for fermion parity conservation, as well, by implementing some pertinent adapted version of the approach presented in (162), we will not address this point in this work.) Now, let us first of all note that, for $-\pi < \Phi < \pi$, Eq.(4.76) tells us that the ground state has the Γ-level populated. As Φ crosses π, there is a crossing between the filled- and the empty-Γ state which, in the absence of constraints on fermion parity conservation, makes the system "jump" from the populated to the empty Γ-fermion state, with the corresponding jump in the current evidenced at $\Phi = \pi$ in the blue curve of Fig. 4.8 corresponding to $\ell = 40$. By symmetry $\Phi \to -\Phi$, an analogous jump is observed at $\Phi = -\pi$. The total current is periodic, with period equal to 2π, due to the sequential level crossings at $\Phi = 2\pi k + \pi$, with integer k (144).
At variance, as $\ell = 4$, the hybridization between the Majorana modes across the topological superconductor is no longer negligeable. As a result, at low energy the system is described by an effective Hamiltonian such as the one in Eq.(3.34), with a modulation with Φ of the energy splitting between the empty- and the filled-state, which never closes (avoided level crossing). In this case, the persistent current is only supported by Cooper pair tunneling across the weak link, which restores a 4π-periodicity in Φ (144). Again, this is consistent with our plot in Fig. 4.8 for $\ell = 4$, with the intermediate case $\ell = 8$ lying in between the two "asymptotic"cases. As a further check, we report in Fig.4.3.1 the plots of $I[\Phi]$ generated by keeping $w = 1, \Delta = 0.2, \tau = 0.5$ and varying μ, with $\ell = 16$ (Fig. 4.9 **a**) and $\ell = 40$ (Fig. 4.9 **b**) (note that $\ell_M \sim 5$, as estimated above). From the plots we draw for $\mu = 0.0, 0.9, 1.5$, we see that, incresing μ toward the critical value $\mu = 2$ at which the topological phase transition takes place (142),

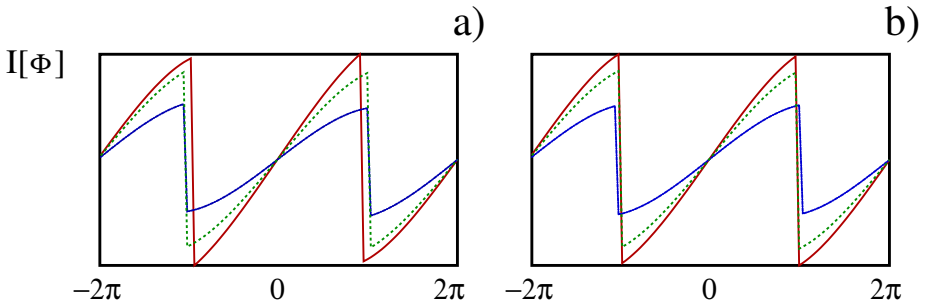

Figure 4.9: Plot of the persistent current $I[\Phi]$ *vs.* Φ (in units of Φ_0) for the p-wave mesoscopic ring with a weak link described by Eq.(4.72). The parameters are chosen so that $\Delta = 0.2$ and $\tau = 0.5$ (in units of w). The curves are plotted for various values of μ at fixed ℓ. Specifically:
a) $\ell = 16$, $\mu = 0.0$ (full red curve), $\mu = 0.9$ (dashed green curve), $\mu = 1.5$ (dot-dashed blue curve);
b) $\ell = 40$, $\mu = 0.0$ (full red curve), $\mu = 0.9$ (dashed green curve), $\mu = 1.5$ (dot-dashed blue curve).

effectively corresponds to increasing ℓ_M. This is expected from the results of Appendix C, where we show that the hybridization between γ_L and γ_R scales as $e^{-\ell/\ell_M}$. Thus, again our results appear to be consistent with the low-energy dynamics of our system as inferred from Appendix C and from the discussion reported in (144).
By contrast, we now discuss the current across an s-wave ring. Despite the lack of low-energy Majorana fermion modes in such a system, the crossover in the periodicity of $I[\Phi]$ from 4π to 2π is known to take place as the length ℓ_S of the superconducting region crosses over from values lower than the coherence length ξ_0 to values higher than ξ_0 (141). Such a crossover corresponds to a crossover in the "physical nature" of $I[\Phi]$: from a 4π-persistent current in a mesoscopic, effectively normal, system to a 2π-periodic current, analogous to the Josephson supercurrent in an SNS-junction (141; 140). In Fig. 4.10, we plot the exact results for $I[\Phi]$ obtained using our TM-approach for the system parameters $w = 1, \Delta = 0.2, \mu = 0, \tau = 0.5$ and for various values of ℓ. In our specific case, having as model Hamiltonian the one in Eq.(4.73), as we are setting to 1 the lattice step, an acceptable estimate for ξ_0 is $\xi_0 \sim 2w/\Delta$. For the numerical values of the parameters we chose to generate Fig. 4.10, this implies $\xi_0 \sim 10$. Such an estimate is definitely consistent with our results: on increasing ℓ from $\ell = 4$ to $\ell = 40$, we ultimately see a crossover in the periodicity of $I[\Phi]$ definitely similar to the one we found for the p-wave superconducting ring with a weal link, though without the jumps in the current due to the Γ-fermion level crossings. To conclude this section, let us stress once more that our technique does provide us with the exact result for $I[\Phi]$ at a generic value of the system parameters, whether the superconductor is p-wave, or s-wave, etc. To recover the final result one just needs to construct the appropriate TM and to numerically compute a single integral for various values of Φ. Using the standard

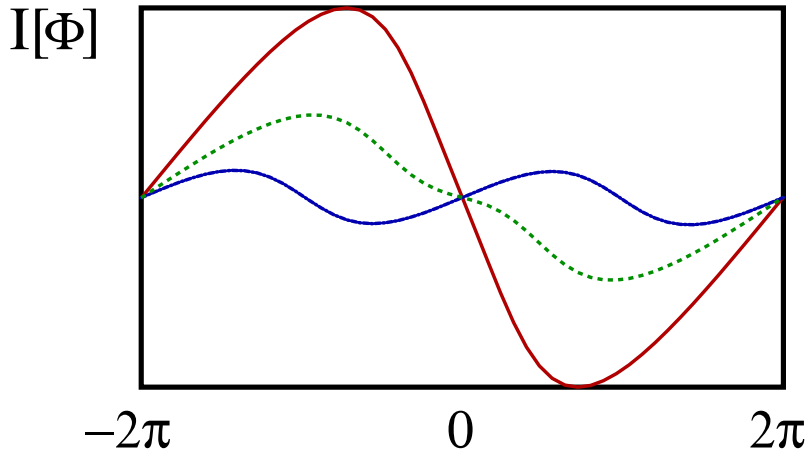

Figure 4.10: Plot of the persistent current $I[\Phi]$ *vs.* Φ (in units of Φ_0) for the s-wave mesoscopic ring with a weak link described by Eq.(4.73). The parameters are chosen so that $\Delta = 0.2$ and $\tau = 0.5$ (in units of w). The curves are plotted for various values of ℓ at $\mu = 0$. Specifically: $\ell = 4$ (full red curve), $\ell = 16$ (dashed green curve), $\ell = 40$ (dot-dashed blue curve). The crossover from a 4π periodicity for $\ell < \xi_0 \sim 10$ (see text) to a 2π-periodicity for $\ell > \xi_0$ is apparent.

approach, based on the solution of the secular equations for the allowed values of the momenta at fixed Φ, and eventually taking the derivative with respect to Φ to obtain the current is, in general, much less straightforward and, typically, exact results cannot be provided and different approximations must be implemented to attack different regimes such as the short-ring, or the long-ring limit (see, for instance, Ref.(140) for a careful and valuable discussion about this point). At variance, as we are showing here, our approach applies to any speficic case, with potentially no limitations at all. To discuss a further application of our technique, we now consider a hybrid ring, made by a p-wave superconducting segment of length ℓ_S and a normal segment of length ℓ_N: this can be regarded as a generalization of the ring with a weak link we discuss above with no imposed constraints on ℓ_N which, as we are going to discuss, opens the way to a number of interesting physical effects.

4.3.2 Persistent current across a hybrid N-S ring

In this section we discuss the persistent current across a hybrid ring, composed of a superconducting segment of length ℓ_S and of a normal segment of length ℓ_N. Such a system can be regarded as a generalization of the ring interrupted by a weak link discussed in [(159)], in which one induced superconductivity by proximity only in a part of the ring, leaving a finite normal region of length ℓ_N. In Fig.4.11 we provide a sketch of the system we discuss here. Again, for comparison, we consider both cases of a p-wave and of an s-wave superconducting region. The corresponding model Hamiltonian

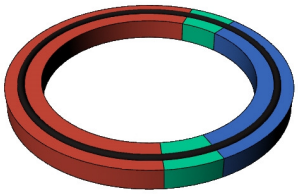

Figure 4.11: Sketch of the hybrid N-S ring with the two regions (red and blue, respectively) separated by two a weak links. A possible practical realization of such a system is the same as discussed before for the superconducting ring interrupted by a weak link.

can then be obtained from H in Eq.(4.46) by setting $\ell_1 \to \ell_S$, $\ell_2 \to \ell_N$, $\Delta_1 \to \Delta, \Delta_2 = 0$ and from H in Eq.(A.1), taken in the same limit. To spell out the behavior of $I[\Phi]$ in the various regimes of interest, let us first focuse onto the p-wave case. Specifically, we compute $I[\Phi]$ at given τ and Δ for $w_1 = w_2 \equiv w$ and for various values of $\ell_S = \ell_N \equiv \ell$. To further simplify the calculation we restricted ourselves to the particle-hole symmetric case, $\mu = 0$. Remarkably, on one hand, all the assumption are effective in simplifying the calculations of the transfer matrix, on the other hand, they do not particularly affect the important physical content of the final result. In Fig. 4.12**a)**, we plot $I[\Phi]$ *vs.* Φ for $\ell = 4, 16, 40$, with the values for the system's parameters chosen as in the caption. The behaviour of $I[\Phi]$ depends on the system size in relation to the length scales determined by the system parameters. At $\mu = 0$ the p-wave superconductor lies within its topological phase, with corresponding localized Majorana modes emerging at its edges. In this case, the important length scale is the Majorana hybridization length ℓ_M. When $\ell \leq \ell_M$, the two MFs are hybridized into a Dirac mode Γ. Since in this case the energy splitting between the empty- and the filled-Γ-state is modulated with Φ, but never closes, the persistent current is only supported by Cooper pair tunneling across the weak link and, therefore, it is periodic, with period equal to 4π (144). On increasing ℓ, when $\ell > \ell_M$, the hybridization between the Majorana modes becomes negligible and, accordingly, in the absence of fermion parity conservation, $I[\Phi]$ becomes 2π-periodic, with jumps at $\Phi = \pi + 2\pi k$. In addition to the periodicity, also the shape of $I[\Phi]$ depends on ℓ. This is due to the Kondo-like hybridization between the MFs and the excitation modes within the normal region of the ring, which takes place when $\ell \geq \xi_{K,M}$, with the Kondo-Majorana hybridization (KMH) length $\xi_{K,M} \sim [(2w)^2/\tau^2]$ (161). At the onset of KMH, $I[\Phi]$ is expected to cross from a discontinuous sinusoidal dependence on Φ to a sawtooth-like shape (161). Physically, this can be understood by recalling that, as ℓ becomes large, the systematic cancellation of contributions from high-energy states makes only low-energy states in the normal region next to the Fermi level contribute to $I[\Phi]$. The physical processes at the SN-interfaces that determine these states can be inferred from Fig.4.12, where, as

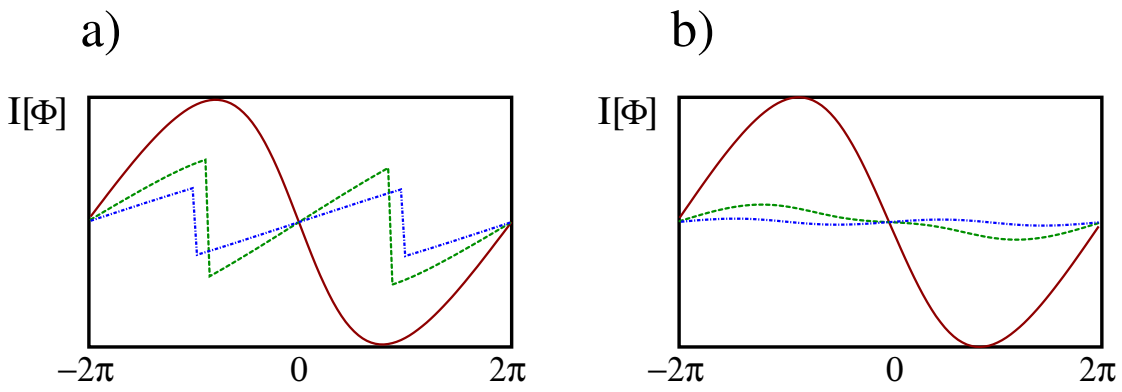

Figure 4.12: Plot of $I[\Phi]$ *vs.* Φ for a hybrid normal - superconducting ring. **a)** Plot of $I[\Phi]$ *vs.* Φ for a hybrid normal-p-wave superconducting ring for $w_1 = w_2 = 1$, $\Delta = 0.2$, $\tau = 0.5$, $\mu = 0$, which corresponds to $\ell_M \approx 6$, $\xi_{K,M} \approx 16$, for $\ell_S = \ell_N = 4$ (solid red curve), $\ell_S = \ell_N = 16$ (dashed green curve), $\ell_S = \ell_N = 40$ (dot-dashed blue curve). The crossover to a sawtooth behaviour is evident for $\ell = 40$; **b)**. Plot of $[\Phi]$ *vs.* Φ for a hybrid normal-s-wave superconducting ring for $w_1 = w_2 = 1$, $\Delta = 0.2$, $\tau = 0.5$, for $\ell_S = \ell_N = 4$ (solid red curve), $\ell_S = \ell_N = 16$ (dashed green curve), $\ell_S = \ell_N = 40$ (dot-dashed blue curve). There is no crossover in the functional form of $I[\Phi]$, but a mere scaling of $I[\Phi]$ that is $\sim \ell_N^{-1}$.

a function of ℓ_S, we plot the scattering coefficients across the superconducting regions corresponding to normal reflection at the SN-interfaces and to normal transmission across the superconducting region, as well as the coefficients corresponding to Andreev reflection (AR) at the interfaces and to "crossed Andreev reflection" (CAR) across the superconducting region (163; 158). As it clearly appears from Fig.4.12, as soon as $\ell_S > \ell_M$, all the coefficients drop to 0 but the one corresponding to AR, which saturates to 1. This evidences that, as $\ell > \ell_S$, AR is the only physical process that takes place at low energy, which implies the sawtooth behavior in $I[\Phi]$ evidenced in Fig. 4.12**a)**. By comparison, in Fig. 4.12**b)**, we plot $I[\Phi]$ *vs.* Φ for the same values of the various parameters as in Fig.4.12**a)**, but for an s-wave superconductor. Here we see that, on increasing ℓ. the current still shows the crossover from a 4π-periodic curve to a 2π-periodic curve, but that the absence of low-energy Majorana modes eventually hybridizing with the modes in the normal region as $\ell \geq \xi_{K,M}$ yields no crossover in the functional form of $I[\Phi]$ from a sinusoidal to a sawtooth behaviour. The only relevant additional feature that takes place on varying ℓ is, indeed, the expected scaling of $I[\Phi]$ $\sim \ell^{-1}$ (see discussion in the next section). Thus, the crossover in the functional form of $I[\Phi]$ can actually be regarded as a direct evidence for the existence of low-energy Majorana modes at the endpoints of the topological superconductor in the p-wave hybrid ring.

In drawing Fig4.13, we hold $\ell_N = \ell_S$ fixed at 40 (with Δ and w chosen so that $\ell_M \sim 6$), as well as the chemical potential within the normal region $\mu_N = 0$. At vari-

ance, we vary the chemical potential within the superconducing region μ_S starting from $\mu_S = 0$ till $\mu_S/w \sim 1.95$ (after which the loss of numerical precision appears not to give us reliable results). As highlighted by Kitaev (142), as $\mu_S/w = 2$ the p-wave superconductor undergoes a (topological) quantum phase transition, characterized by the disappearance (for $\mu_S/w > 2$) of the localized MFs at the endpoints of the superconductor. On approaching the phase transition from within the topological region, the closer the system is to the quantum critical point, the larger is the effective ℓ_M. While the actual numerical estimate of ℓ_M as a function of e.g. μ_S/w at fixed Δ can in principle be provided From Eq.(3.15) of Appendix C, here we just focus on the consistency of our exact results with the expectation one gets from the above discussion. Indeed, the estimated KMH-length for the system used to derive $I[\Phi]$ in Fig.4.13**a)** is $\xi_{K,M} \approx 16$ (see the discussion at the caption of Fig.4.11**a)**, which is drawn at the same values of w and τ). As in Fig. 4.13**a)** we plot $I[\Phi]$ for $\ell_S = \ell_N = 40$, we see full KMH in the normal region for $\mu_N = 0$, as evidenced by the sawtooth behavior of the current and by the corresponding 2π-periodicity in Φ. On increasing μ_S towards the critical value corresponding to the topological quantum phase transition, the nonnegligible hybridization between the MFs across the superconduting region is expected to compete with KMH and eventually to suppress it (Indeed, this can be regarded as a "Majorana analog" of the competition between Kondo effect and RKKY-interaction in the two-impurity Kondo model (164; 165; 166; 167), just as the KMH can be regarded as the Majorana analog of the onset of the Kondo cloud in a Kondo system (161)). Consistently with the expectation, we see that, on increasing μ_S, the sawtooth is smoothed (with a sizeable reduction in the critical current) and clearly evolves back towards a restoration of the 4π-periodicity that characterizes the regime $\ell_S \leq \ell_M$ (see discussion above). For comparison, in Fig.4.13**b)** we draw similar plots generated in the s-wave case. No particular changes in the functional form the current appear, except the reduction in the value of the current at a given Φ. In our view, this result do actually enforce the reliability of a persistent current measurement as a tool to detect the presence of Majorana modes at the endpoints of a p-wave superconductor in the topological phase.
Besides the possibility of exactly computing the current in a number of different physical systems by simply evaluating the integral in Eq.(4.45) for different values of Φ, our approach also provide a remarkable tool to write, for large enough systems, $I[\Phi]$ in a power series of the inverse system size which, as we are going to discuss in the following, greatly simplifies the various calculations, by even allowing for providing explicit analytic results for the current, in some simple cases.

4.4 The large-ring limit and the finite temperature case

As the ring size goes large, one may recast the integral formula for $I[\Phi]$, Eq.(4.45), in an expansion in inverse powers of the length that gets large. As we discuss in the following, this leads to a number of remarkable simplifications in the calculation of the

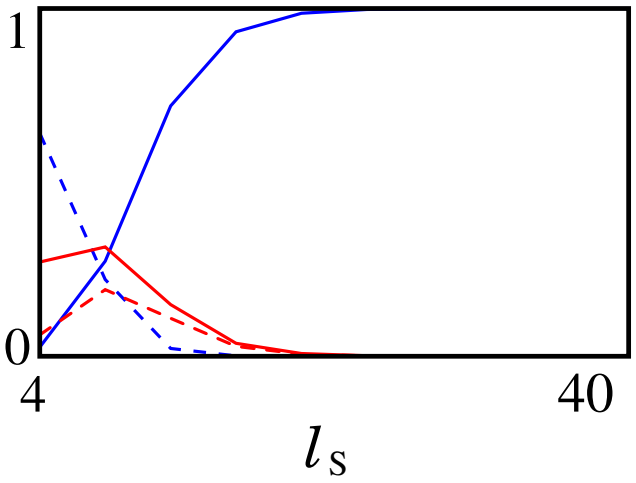

Figure 4.13: Plot of the normal and Andreev reflection coefficients at the SN-interface and of the normal transmission and CAR coefficients for the p-wave superconductor-normal hybrid ring discussed in section discussed in section 4.3.2 as a function of ℓ_S. To generate the plot we have chosen the system's parameters so that $w_1 = w_2 = 1$, $\Delta = 0.2$, $\tau = 0.5$, which corresponds to $\ell_M \approx 6$. The various curves correspond to the coefficients as
- Full blue curve: Andreev reflection coefficient at the SN-interface;
- Dashed blue curve: Normal reflection coefficient at the SN-interface;
- Full red curve: Normal transmission across the superconducting region;
- Dashed red curve: Crossed Andreev reflection across the superconducting region.
Apparently, for $\ell_S > \ell_M$ all the processes are suppressed, except the Andreev reflection at the SN-interface, with the corresponding coefficient saturating to 1.

current, similar to the ones implemented in Refs.(155; 156), even leading, in some cases, to closed a closed-form analytic formula for $I[\Phi]$ *vs.* Φ at given system parameters. In the following, we discuss a few examples of calculation of the persistent current in the large-size limit, also showing how a number of known results can be easily recovered within our formalism, once the appropriate limit is taken.

4.4.1 The limit of long superconducting region

The limit of long superconducting region is defined by sending $\ell_2 \to \infty$ in the system described by the model Hamiltonian in Eq.(4.46) (p-wave case), or by the Hamiltonian in Eq.(A.1) (s-wave case), after setting $\Delta_1 = 0$, so that region-1 is normal, and by keeping ℓ_1 finite. In this limit one expects to recover the results for a the Josephson current across an SNS-hybrid junction. To show that this is, Indeed, the case, we start by rewriting $\det\{\mathcal{M}_{p-wave}[E;\Phi;\ell_1;\ell_2]-\mathbf{I}\}$ as

$$\det\{\mathcal{M}_{p-wave}[E;\Phi;\ell_1;\ell_2]-\mathbf{I}\} = c\,\det\{\mathbf{T}_2^{-1}(E;\ell_2) - [\Upsilon^{(2)}(E)]^{-1}\cdot\Sigma_2^{-1}[\Phi]\cdot\Omega_1[\Phi]\cdot \\ \cdot[\Upsilon^{(1)}(E)]\cdot\mathbf{T}_1(E;\ell_1)\cdot[\Upsilon^{(1)}(E)]^{-1}\cdot\Sigma_1^{-1}[\Phi]\cdot\Omega_2[\Phi]\cdot[\Upsilon^{(2)}(E)] \tag{4.77}$$

with c being an over-all factor independent of Φ and, similarly, by rewriting $\det\{\mathcal{M}_{s-wave}[E;\Phi;\ell_1;\ell_2]-\mathbf{I}\}$ as

$$\det\{\mathcal{M}_{s-wave}[E;\Phi;\ell_1;\ell_2]-\mathbf{I}\} = c'\,\det\{\mathbf{T}_2^{-1}(E;\ell_2) - [\tilde{\Upsilon}^{(2)}(E)]^{-1}\cdot\tilde{\Sigma}_2^{-1}[\Phi]\cdot\tilde{\Omega}_1[\Phi]\cdot \\ \cdot[\tilde{\Upsilon}^{(1)}(E)]\cdot\mathbf{T}_1(E;\ell_1)\cdot[\tilde{\Upsilon}^{(1)}(E)]^{-1}\cdot\tilde{\Sigma}_1^{-1}[\Phi]\cdot\tilde{\Omega}_2[\Phi]\cdot[\tilde{\Upsilon}^{(2)}(E)]\} \tag{4.78}$$

with, again, c' being a constant independent of Φ. As a next step, we define the matrix $\mathbf{M}_p$ as

$$\mathbf{M}_p = [\Upsilon^{(2)}(E)]^{-1}\cdot\Sigma_2^{-1}[\Phi]\cdot\Omega_1[\Phi]\cdot[\Upsilon^{(1)}(E)]\cdot\mathbf{T}_1(E;\ell_1)\cdot[\Upsilon^{(1)}(E)]^{-1}\cdot\Sigma_1^{-1}[\Phi]\cdot\Omega_2[\Phi]\cdot[\Upsilon^{(2)}(E)] \tag{4.79}$$

for the p-wave hybrid ring, and

$$\mathbf{M}_s = [\tilde{\Upsilon}^{(2)}(E)]^{-1}\cdot\tilde{\Sigma}_2^{-1}[\Phi]\cdot\tilde{\Omega}_1[\Phi]\cdot[\tilde{\Upsilon}^{(1)}(E)]\cdot\mathbf{T}_1(E;\ell_1)\cdot[\tilde{\Upsilon}^{(1)}(E)]^{-1}\cdot\tilde{\Sigma}_1^{-1}[\Phi]\cdot\tilde{\Omega}_2[\Phi]\cdot[\tilde{\Upsilon}^{(2)}(E)] \tag{4.80}$$

for the s-wave hybrid ring. From Eqs.(4.79,4.80), we see that the current in the p-wave and the s-wave hybrid ring, $I_{p,s}[\Phi]$, can respectively be written as

$$I_{p,s}[\Phi] = -\frac{1}{2\pi i}\int_\Gamma d\epsilon\partial_\Phi \ln[\Psi_{p,s}[\epsilon;\Phi]] = -\frac{1}{4\pi i}\int_\Gamma d\epsilon\partial_\Phi\left\{\ln[\mathbf{T}_2^{-1}(\epsilon;\ell_2)-\mathbf{M}_{p,s}]-[\ln[\mathbf{T}_2^{-1}(\epsilon;\ell_2)-\mathbf{M}_{p,s}]]^*\right\} \tag{4.81}$$

where we have used the reality of the persistent current to go through the last step in Eq.(4.81). In order to systematically take the $\ell_2 \to \infty$-limit, we recall that one has eventually to deform the integrals over Γ in Eq.(4.81) into integrals over the imaginary axis, which corresponds to $\epsilon \to i\omega$. Along the imaginary axis, from the dispersion relations for particle- and hole-like excitations within the superconducting region, one obtains that the corresponding momenta are defined by

$$\begin{aligned} \cos[k_p^{(2)}] &= -\frac{\mu_2 w_2}{2(w_2^2-\Delta_2^2)} - \frac{i}{2}\sqrt{\frac{\omega^2+\Delta_w^2}{w_2^2-\Delta_2^2}} \\ \cos[k_h^{(2)}] &= -\frac{\mu_2 w_2}{2(w_2^2-\Delta_2^2)} + \frac{i}{2}\sqrt{\frac{\omega^2+\Delta_w^2}{w_2^2-\Delta_2^2}} \end{aligned} \tag{4.82}$$

in the p-wave case, and

$$\begin{aligned} \cos[k_p^{(2)}] &= -\frac{\mu_2}{2w_2} - \frac{i}{2}\sqrt{\frac{\omega^2+\Delta_2^2}{w_2^2}} \\ \cos[k_h^{(2)}] &= -\frac{\mu_2}{2w_2} + \frac{i}{2}\sqrt{\frac{\omega^2+\Delta_2^2}{w_2}} \end{aligned} \tag{4.83}$$

in the s-wave case. To solve Eqs.(4.82) we therefore set

$$k_p^{(2)} = \frac{\pi}{2} + q_p \quad , \quad k_h^{(2)} = \frac{\pi}{2} + q_p^* \tag{4.84}$$

with

$$\sin[q_p] = \frac{\mu_2 w_2}{2(w_2^2-\Delta_2^2)} + \frac{i}{2}\sqrt{\frac{\omega^2+\Delta_w^2}{w_2^2-\Delta_2^2}} \tag{4.85}$$

while, to solve Eqs.(4.83), we set

$$k_p^{(2)} = \frac{\pi}{2} + q_s \quad , \quad k_h^{(2)} = \frac{\pi}{2} + q_s^* \tag{4.86}$$

with

$$\sin[q_s] = \frac{\mu_2}{2w_2} + \frac{i}{2}\sqrt{\frac{\omega^2+\Delta_2^2}{w_2}} \tag{4.87}$$

From the explicit formula for $\mathbf{T}^{-1}_{2;(p,s)}(E \to i\omega; \ell_2)$ along the imaginary axis in the p-wave and in the s-wave case, respectively given by

$$\mathbf{T}^{-1}_{2;(p,s)}(E \to i\omega;\ell_2) = \begin{bmatrix} i^{-\ell_2} e^{iq^{(2)}_{p,s}\ell_2} & 0 & 0 & 0 \\ 0 & i^{\ell_2} e^{-iq^{(2)}_{p,s}\ell_2} & 0 & 0 \\ 0 & 0 & i^{\ell_2} e^{-i[q^{(2)}_{p,s}]^*\ell_2} & 0 \\ 0 & 0 & 0 & i^{-\ell_2} e^{i[q^{(2)}_{p,s}]^*\ell_2} \end{bmatrix} \tag{4.88}$$

we may readily compute the integrals in Eq.(4.81) in the limit $\ell_2 \to \infty$, obtaining

$$I_{p,s}[\Phi] = \frac{1}{2\pi} \int_{-\infty}^{\infty} d\omega\ \partial_\Phi \ln \mathcal{G}_{p,s}(\epsilon \to i\omega) \tag{4.89}$$

with $\mathcal{G}_{p,s}(\epsilon) = \mathbf{M}_{(p,s);(2,2)}(\epsilon)\mathbf{M}_{(p,s);(4,4)}(\epsilon) - \mathbf{M}_{(p,s);(2,4)}(\epsilon)\mathbf{M}_{(p,s);(4,2)}(\epsilon)$ and assuming (as done in (155; 156)) that

- All the poles of $\mathcal{G}(\epsilon)$ lie over the real axis;
- $\mathcal{G}(\epsilon)$ is real if ϵ lies over the real axis (and does not cohincide with a pole of $\mathcal{G}$),

Eq.(4.89) yields the dc-Josephson current in the infinite-ℓ_2 limit, in which the ring can be regarded as an idealized model for an SNS-junction. In the specific case of s-wave superconductors, Eq.(4.85) has been derived in (155) for a single-channel junction starting from the S-matrix approach to effectively one-dimensional SNS-junctions (153), and generalized in (156) to a multi-channel junction. Indeed, a comparison between Eq.(4.89) and Eqs.(7,9) of Ref.(155) also clarifies the identification between $\mathbf{M}_{p,s}$ in Eqs.(4.79,4.80) and the transfer matrix for the whole SNS-junction, as introduced and discussed in (155) for the s-wave case. After resorting to the effective SNS-junction model, at a second stage one may implement the technique developed in (155; 156) to write $I[\Phi]$ in a systematic expansion in inverse powers of ℓ_1. Basically, one considers that, because one has

$$\mathbf{T}_1(E \to i\omega;\ell_2) = \begin{bmatrix} i^{\ell_1} e^{-iq^{(1)}_n\ell_1} & 0 & 0 & 0 \\ 0 & i^{-\ell_1} e^{iq^{(1)}_n\ell_1} & 0 & 0 \\ 0 & 0 & i^{-\ell_1} e^{-i[q^{(1)}_n]^*\ell_1} & 0 \\ 0 & 0 & 0 & i^{\ell_1} e^{i[q^{(1)}_n]^*\ell_1} \end{bmatrix} \tag{4.90}$$

with

$$\sin[q_n] = \frac{\mu_1}{2w_1} + \frac{i}{2}\frac{\omega}{w_1} \quad , \tag{4.91}$$

then, only low-$|\omega|$ regions do effectively contribute to the integral in Eq.(4.89). As a result, one may first of all approximate $q_n \approx \bar{q} + i\sigma(\omega)$, with

$$\begin{aligned} \sin(\bar{q}) &= \frac{\mu_1}{2w_1} \\ \sigma(\omega) &= \frac{\omega}{2w_1} \quad , \end{aligned} \tag{4.92}$$

then, in integrating Eq.(4.89), one may rescale $\omega \to \omega\ell_1$ and eventually set the rescaled ω at 0 in all the contributions to the argument of the integral in which ω appears divided by ℓ_1 as ω/ℓ_1. Going along this procedure, one may compute the leading contribution to the current ($\mathcal{O}(\ell_1^{-1})$) by trading the original model Hamiltonian for a reduced boundary model, such as the one presented in Ref.(152) for the s-wave superconductors and the one used in Ref.(161) for the p-wave superconductor, which allows for recovering simple, closed-form analytical formulas for $I[\Phi]$.

4.4.2 The limit of long normal region

We have shown how our approach gives back the known result for the dc Josephson current across an SNS-junction in the limit of a long superconducting region. We now discuss the complementary limit of a long normal region, with ℓ_S less than, or comparable to, the coherence length of the superconducting region ξ_0. We first discuss the general formula and then consider the case of a hybrid s-wave superconducting ring as a specific example. In order to address the large-ℓ_N-limit, let us first of all rewrite $\det\{\mathcal{M}_{p-wave\,(s-wave)}[E;\Phi;\ell_1;\ell_2] - \mathbf{I}\}$ as

$$\det\{\mathcal{M}_{p-wave\,(s-wave)}[E;\Phi;\ell_1;\ell_2] - \mathbf{I}\} = c_{p,s}\,\det\{\mathbf{T}_1(E;\ell_1) - \mathbf{K}_{p,s}[E;\Phi;\ell_2]\} \tag{4.93}$$

with $c_{p,s}$ being constants independent of Φ, and

$$\begin{aligned} \mathbf{K}_p[E;\Phi;\ell_2] &= [\Upsilon^{(1)}(E)]^{-1}\cdot\Omega_1^{-1}[\Phi]\cdot\Sigma_2[\Phi]\cdot[\Upsilon^{(2)}(E)]\cdot\mathbf{T}_2^{-1}(E;\ell_2)\cdot \\ &\quad \cdot[\tilde{\Upsilon}^{(2)}(E)]^{-1}\cdot\Omega_2^{-1}[\Phi]\cdot\Sigma_1[\Phi]\cdot[\Upsilon^{(1)}(E)] \\ \mathbf{K}_s[E;\Phi;\ell_2] &= [\tilde{\Upsilon}^{(1)}(E)]^{-1}\cdot\tilde{\Omega}_1^{-1}[\Phi]\cdot\tilde{\Sigma}_2[\Phi]\cdot[\tilde{\Upsilon}^{(2)}(E)]\cdot\mathbf{T}_2^{-1}(E;\ell_2)\cdot \\ &\quad \cdot[\tilde{\Upsilon}^{(2)}(E)]^{-1}\cdot\tilde{\Omega}_2^{-1}[\Phi]\cdot\tilde{\Sigma}_1[\Phi]\cdot[\tilde{\Upsilon}^{(1)}(E)] \end{aligned} \tag{4.94}$$

Eqs.(4.94) correspond to the standard identification we have employed so far, that is, region-1 has to be identified with the normal region and region-2 with the (either p-wave, or s-wave) superconducting region. Therefore, $\ell_1 = \ell_N$. Now, in order to recover the large-ℓ_N-limit, we stricly follow the derivation of Refs.(155; 156), that is, once we have deformed the integration path to the imaginary axis, we assume that only low-$\omega(= -iE)$ regions do effectively contribute the integral in Eq.(4.45). This allows us first of all to approximate the inverse dispersion relation within the normal region as

$$k_{p,h} \approx k_F \pm i\lambda(\omega) \quad , \tag{4.95}$$

with $-2w_1\cos(k_F)=\mu_1$ and $\lambda(\omega)=\frac{\omega}{2w}$. On substituting Eqs.(4.95) into Eqs(4.94), we may eventually rewrite Eq.(4.45) as

$$I_{p,s}[\Phi]=-\frac{2ew_1}{2\pi\,\ell_1}\,\partial_\Phi\,\int_0^\infty\,\frac{dz}{z}\,\ln\{\Xi_{p,s}[z;\Phi;\ell_2]\}\quad , \tag{4.96}$$

with

$$\Xi_{p,s}[z;\Phi;\ell_2]=\det\left\{\left[\begin{array}{cccc} z & 0 & 0 & 0\\ 0 & z^{-1} & 0 & 0\\ 0 & 0 & z & 0\\ 0 & 0 & 0 & z^{-1}\end{array}\right]-\left[\begin{array}{cccc} e^{-ik_F\ell_1} & 0 & 0 & 0\\ 0 & e^{ik_F\ell_1} & 0 & 0\\ 0 & 0 & e^{ik_F\ell_1} & 0\\ 0 & 0 & 0 & e^{-ik_F\ell_1}\end{array}\right]\cdot\mathbf{K}_{p,s}[E=0;\Phi;\ell_2]\right\} \tag{4.97}$$

To illustrate the effectiveness of our simplified Eqs.(4.96,4.97) we now discuss the application to the case of a hybrid s-wave superconducting ring. For simplicity, we make the assumptions $w_1=w_2\equiv w$ and $\mu_1=0$. As a result, using Eqs.(4.96,4.97), we obtain the simplified expression for the current

$$I[\Phi]=-\frac{2ew_1}{2\pi\,\ell_1}\,\partial_\Phi\,\int_0^\infty\,\frac{dz}{z}\,\left\{\frac{\partial_\Phi a[\Phi;\ell_1](z^3+z)+\partial_\Phi b[\Phi;\ell_2]z^2}{z^4+1+a[\Phi;\ell_2](z^3+z)+b[\Phi;\ell_2]z^2}\right\}\quad , \tag{4.98}$$

with $a[\Phi;\ell_2],b[\Phi;\ell_2]$ being long, though straightforward to derive, functions of the matrix elements of $\mathbf{K}_s[E=0;\Phi;\ell_2]$. Eventually, by means of simple manipulations Eq.(4.98) can be expressed as a closed-form formula only of the four roots $z_j[\Phi;\ell_2]$ $(j=1,\ldots,4)$ of the polynomial equation $z^4+1+a[\Phi;\ell_2](z^3+z)+b[\Phi;\ell_2]z^2=0$, which take the generic form

$$\begin{aligned} z_j[\Phi;\ell_2] &= -\frac{a[\Phi;\ell_2]}{4}+u_j\frac{\sqrt{8+a^2[\Phi;\ell_2]-4b[\Phi;\ell_2]}}{4}\\ &+\quad v_j\frac{1}{2}\sqrt{-2+\frac{a^2[\Phi;\ell_2}{4}-b[\Phi;\ell_2]+u_j\frac{a^3[\Phi;\ell_2]+8a[\Phi;\ell_2]-4a[\Phi;\ell_2]b[\Phi;\ell_2]}{2\sqrt{8-a^2[\Phi;\ell_2]-4b[\Phi;\ell_2]b[\Phi;\ell_2]}}}\end{aligned} \tag{4,99}$$

with $u_j,v_j=\pm1$. Taking into account that $\prod_{j=1}^4 z_j[\Phi;\ell_2]=1$, one eventually obtains from Eq.(4.98)

$$I[\Phi]=-\frac{2ew_1}{4\pi\ell_1}\partial_\Phi\{\sum_{j=1}^4\ln^2[z_j[\Phi;\ell_2]]\}\quad . \tag{4.100}$$

Just as in the case of a long SNS-junction (155; 156), Eq.(4.100) only involves data at the Fermi level. This is an additional example of the remarkable simplifications to which our approach leads, in the large ring limit.

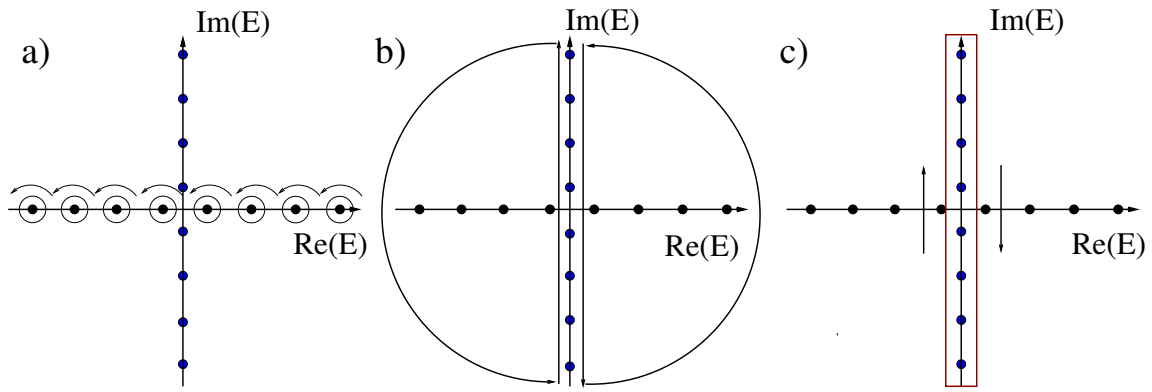

Figure 4.15: Sequence of deformations in the integration path $\tilde{\Gamma}$ eventually allowing to express $I[\Phi;T]$ as a sum over the fermionic Matsubara frequencies $\omega_m = 2\pi T\left(m+\frac{1}{2}\right)$:
a) The path $\tilde{\Gamma}$ obtained as the union of small circles, each one surrounding one, and only one, energy eigenvalue;
b) The integral over $\tilde{\Gamma}$ can be deformed to an integral over the union of the two closed path run through counterclockwisely;
c) The integral over the two closed path in **b)** is equal to the integral over a closed path surrounding the poles of the Fermi function ($i\omega_m$, displayed as blue full circles in the figure), run through clockwisely. The corresponding over-all - sign is eventually cancelled by the -1 at the residue of the Fermi function at $i\omega_m$.

4.4.3 Finite-temperature results

It is not difficult to generalize our derivation to a system at temperature T finite, though much lower than the critical temperature for the superconducting part of the ring. Indeed, at finite T, Eq.(4.45) generalizes to Eq.(4.1), with

$$F[\Phi;T] = \sum_E E f(E) \quad , \tag{4.101}$$

and $f(E) = [1+e^{E/T}]^{-1}$ being the Fermi distribution function (having set the Boltzmann constant $k = 1$. Now, the integration path Γ in Eq.(4.43) must be replaced with the integration path $\tilde{\Gamma}$ obtained as the union of small circles Γ_n, each one surrounding once one, and only one, energy eigenvalue. As illustrated in Fig.4.15, $\tilde{\Gamma}$ can be deformed to a path obtained as the union of small circles, each one surrounding once on, and only one, pole of the Fermi function, that is, a fermionic Matsubara frequency times the imaginary unit i, $i\omega_m = 2\pi T i\left(m+\frac{1}{2}\right)$. As a result, the finite-T current can be presented as

$$I[\Phi;T] = -eT\sum_{\omega_m} \partial_\Phi\{\det[\mathcal{M}[i\omega_m;\Phi] - \mathbf{I}]\} \quad , \tag{4.102}$$

that is the appropiate generalization of Eq.(4.45) to the finite-T case.

Chapter 5

Discussion and Conclusions

To conclude, we summarize the main results we got in our thesis work.

In the first chapter we provide an introduction of our work.

In the second chapter we used the scattering matrix to calculate the Anomalous Josephson current in an SNS junction with spin-orbit and electromagnetic interaction. Here the interest lies in the non-topological (or trivial) phase of the superconductor. We have seen how in the case in which the Fermi energy is such as to allow only one propagative channel, we can find the anomaly of the current (i.e. the minimu of the current is shifted from 0 or π), but the current turns out to be still symmetrical with regard to the maximum I_{0+} and the minimum I_{0+}. These results are summarized in Fig.2.7, where it was shown, on varying α' and b', how the anomaly φ_0 shifts. As for the visibility $\aleph$, instead, it remains mostly constant, excluding numerical computation errors, despite the variation of the spin-orbit interaction and of the strenght of the applied magnetic field. Instead, if we allow more propagation channels, i.e. we adequately modify the Fermi energy of the system, we can see that is not only presents the anomaly φ_0 , but also that the visibility $\aleph$ varies considerably, up to a value of 20%. The diagram in Fig.2.8 show our results for the anomaly in a two-open channel analysis, while Fig. 2.9 shows the variation of $\aleph$ in terms of α' and b'. Such effect, being tuned, for instance by varying the magnetic field, may have useful application for superconducting circuits: for example, circuits with an efficiency as high as 50% are required to realize a proper superconducting diode. In the hope to building quantum processors using Josephson junctions (21; 22; 23; 24) and the quantum computer just launched by Google (26), the possibilities for implementation are becoming increasingly tempting and likely. However, by properly engineering the interfaces and the materials we expect to achieve a wider tuneability of this value up to experimentally relevant scales. Nonetheless, we believe that the present analysis can be taken as a first example for further studies in this direction.

In the third chapter, we analytically found that a p-wave superconducting ring obtained by closing a Kitaev chain with a weak link displays, under very general conditions, two low-energy putative Majorana fermion states which, at a generic value of the applied flux Φ pearcing the ring, hybridize into a Dirac fermion of energy $\epsilon_0[\Phi]$.

We then proved that, at a certain value of $\Phi = \Phi_*$, $\epsilon_0[\Phi_*] = 0$. At $\Phi = \Phi_*$ the system exhibits two actual zero-energy Majorana modes with exactly the same properties as the Majorana modes located at the boundaries of an infinite Kitaev chain. We then investigated the modifications to this scenario implied by disorder. We found numerical evidence that, while a small amount of disorder is not sufficient to either wash out the putative Majorana modes, or the level crossing $\Phi = \Phi_*$ (though it can in principle slightly renormalize Φ_*), a strong disorder can get rid of the putative Majorana modes, thus suppressing the putative topological phase characterized by the presence of the subgap putative Majorana modes. Then, we extend the discussion on the relation between disorder and disappearance of putative Majorana modes, eventually showing how to map out the whole putative topological phase in the chemical potential-disorder plane by looking at the discontinuity of the persistent current $I[\Phi]$ at $\Phi = \Phi_*$. Fig.3.15 summarizes the key results of this subsection: on one hand, it can be regarded as a theoretical derivation of the region, in the $\sigma_V - \mu$ plane, in which it is possible to make two zero-energy Majorana modes emerge at the quantum ring by pertinently acting on the applied flux. On the other hand, the way we derived it suggests a practical tool to map it out in an experiment: to check whether, at a given values of the system parameters, zero-energy Majorana modes are recovered in the disordered one-dimensional superconducting ring, it is enough to probe the dependence of $I[\Phi]$ on Φ and to check whether, at some flux $\Phi = \Phi_*$ (with Φ_* typically being $\sim \pi$ for a not-too-short chain), $I[\Phi]$ shows a discontinuous behavior, with a finite jump when going across Φ_*. A key point of this technique is that $I[\Phi]$ can in principle be probed by means of a noninvasive magnetometer, without need for contacting the system as we have to do in a transport experiment attempting to probe Majorana modes (124), thus potentially introducing a number of potential sources of noise in the system. Moreover, we recall that the techniques so far proposed to map out the phase diagram of a disordered Kitaev-like chain, mostly rely on looking at the eigenvalues of the transfer matrix of the whole chain (110; 111): an approach rigorous and effective from the mathematical point of view, but quite unlikely to be experimentally employed. At variance, it should not be extremely difficult to implement in practice the technique we propose, as we outline above. From the physical point of view, our numerical findings prove that zero energy Majorana modes emerging in a quantum ring at $\Phi = \Phi_*$ are quite robust against disorder.

In Chapter 4, we present a technique to exactly compute the zero-temperature persistent current across a hybrid NS-mesoscopic ring pierced by a magntic flux Φ as a single integral of a known function of the system's parameters. Our approach makes use of the properties of the transfer matrix of the ring, which allows us to circumvent technical difficulties associated to the secular equation for the energy eigenvalues of the system. A straightforward generalization of the zero-temperature formalism allows us to also compute the current in a ring at a temperature T finite, though much lower than the superconducting gap. While in general one may readily numerical compute the integral/sum yielding the current at a given value of the flux Φ, a remarkable simplification takes place in the limit of a large ring size, where resorting to a systematic

expansion in inverse powers of the ring length allows for deriving the current in analytic closed-form formulas, applicable to a number of cases of physical interest.

In summary, this thesis has analyzed some phenomena inherent to currents in one-dimensional superconducting systems. We have seen how, both in the topological phase and in the trivial phase, it is possible to observe a huge amount of phenomena. The anomalies, the discontinuities, can become relevant not only for the study of the physics of the collective excitations of the system, but also provide useful tools for the physics of high energies for the study of particles not yet observed (Majorana fermions) and provide, also , to engineers, useful tools for the realization of increasingly precise, small and powerful electronic components. The road is still long and there are so many things still to be studied. For example, referring to the first Chapter, it is possible to continue to study the effects of asymmetry and anomaly in Josephson currents to build diodes and transistors for quantum processors. Furthermore, through different symmetries (such as that of the ring presented in Chapters 3 and 4 it is possible to study anions, but also the mathematical properties of the Majorana modes, creating interferometers and logic gates in the perspective of quantum computation. These are few prospects for the use of these systems, but let us not forget the basic research that can be carried out to measure the Majorana modes: indeed, to date, there is no universally accepted experimental measure of these zero-energy excitations. The systems we offer would therefore provide a starting point towards the experimental demonstration.

Appendix A

The s-wave case in the tight binding model

The tight-binding model that we are going to show in the following is appropriate to be used for studying narrow band behaviors arising from electronic correlation effects. As we will see, this kind of modelization can be useful to describe more complicated superconductors's symmetries (like the p-wave pairing symmetry). In the following, we consider a one-dimensional finite chain with an s and $p-wave$ superconducting pairing. From the model Hamiltonians, we will derive the BdG equations and the energy relation dispersions. Let us start by considering an homogeneous $s-wave$ wire; here we assume that the kinetic hopping trought sites and the chemical potential are do not change along the chain. Moreover we assume an homogeneous and real distribution for the superconducting pairing, i.e. $\Delta_j = \Delta, \forall j$ with $\Delta \in \mathcal{R}$, and define ℓ. We obtain the model Hamiltonian for a finite-lenght s-wave superconductor:

$$\begin{aligned} H &= -\sum_{j=1}^{\ell-1}\sum_{\sigma}\{w[c^{\dagger}_{j,\sigma}c_{j+1,\sigma} + c^{\dagger}_{j+1,\sigma}c_{j,\sigma}]\} - \sum_{j=1}^{\ell}\mu c^{\dagger}_{j,\sigma}c_{j,\sigma} \\ &+ \sum_{j=1}^{\ell}\{\Delta[c_{j,\uparrow}c_{j,\downarrow} + c^{\dagger}_{j,\downarrow}c^{\dagger}_{j,\uparrow}]\} \end{aligned} \tag{A.1}$$

where w is the kinetic energy hopping from the $j-th$ site to the $j\pm1-th$ one, which, as the all parameters of Eq.(A.1), is assumed to be homogeneous along the all chain, Δ is the superconducting paring and μ is the chemical potential. To find the energy spectrum of this system, we have to solve the Heisenberg equation $[\Gamma_{E,\sigma}, H] = E\Gamma_{E,\sigma}$,where $\Gamma_{E,\sigma}$ is the most generic eingenmode of our Hamiltonian and is a function of the energy E and the spin polarization σ. In this case, we can write it as follows:

$$\Gamma_{E,\sigma} = \sum_{j=1}^{\ell}\{[u_{E,\sigma}(j)]^{*}c_{j,\sigma} + [v_{E,\sigma}(j)]^{*}c^{\dagger}_{j,\bar{\sigma}}\} \tag{A.2}$$

On imposing the canonical commutation relation $[\Gamma_{E,\sigma}, H] = E\Gamma_{E,\sigma}$, we derive the Bogoliubov-de Gennes equations for the wavefunction $(u_{E,\sigma}(j), v_{E,\sigma}(j))$ in the form :

$$\begin{aligned} Eu_{E,\sigma}(j) &= -w\{u_{E,\sigma}(j+1) + u_{E,\sigma}(j-1)\} - \mu u_{E,\sigma}(j) + \sigma\Delta_j v_{E,\sigma}(j) \\ Ev_{E,\sigma}(j) &= w\{v_{E,\sigma}(j+1) + v_{E,\sigma}(j-1)\} + \mu v_{E,\sigma}(j) + \sigma\Delta_j u_{E,\sigma}(j) \end{aligned} \tag{A.3}$$

We note that an homogeneous system described by a lattice model has translational invariance symetry; therefore, we can look for solutions of the form:

$$\begin{bmatrix} u_{E,\sigma}(j) \\ v_{E,\sigma}(j) \end{bmatrix} = \begin{bmatrix} u_E \\ \sigma v_E \end{bmatrix} e^{ikj} \tag{A.4}$$

with:

$$\begin{aligned} [E + 2w\cos(k) + \mu]u_{E,\sigma} - \Delta v_{E,\sigma} &= 0 \\ -\Delta u_{E,\sigma} + [E - 2w\cos(k) - \mu]v_{E,\sigma} &= 0 \end{aligned} \tag{A.5}$$

Therefore, nontrivial solutions for $u_{E,\sigma}, v_{E,\sigma}$ are only found provided that:

$$E^2 - [2w\cos(k) + \mu]^2 - \Delta^2 = 0 \tag{A.6}$$

Now, at a given value of the energy ϵ, we may ask the question of which values of the momentum k are consistent with Eq.(A.6). Specifically, in view of the following developments of our calculations, we will set $|\epsilon| \geq \Delta$. By solving Eq.(A.6) for the momenta, we can find:

$$\begin{aligned} \cos(k_p) &= -\frac{\mu}{2w} - \frac{\sqrt{-\Delta^2 + \epsilon^2}}{2w} \\ \cos(k_h) &= -\frac{\mu}{2w} + \frac{\sqrt{-\Delta^2 + \epsilon^2}}{2w} \end{aligned} \tag{A.7}$$

where k_p identifies the quasi-particle momentum and k_h the quasi-hole one. We therefore find the following four independent solutions:

$$\begin{bmatrix} u_j \\ v_j \end{bmatrix}_{(\alpha,\pm);\sigma} = \begin{bmatrix} e^{\alpha\frac{1}{2}\xi(\epsilon)} \\ \sigma e^{-\alpha\frac{1}{2}\xi(\epsilon)} \end{bmatrix} e^{\pm ik_\alpha} \tag{A.8}$$

where we have defined:

$$\xi(\epsilon) = \text{atan}\left[\frac{\sqrt{-\Delta^2 + \epsilon^2}}{\epsilon}\right] \tag{A.9}$$

and $\alpha = 1$ if we consider the particle-like solutions and $\alpha = -1$ is we consider the hole-like solutions.

Appendix B

The p-wave case in the tight binding model

In this section we analyze the case of an open superconducting p-wave chain with ℓ sites, reviewing the derivation of the Bogolioubov-de Gennes equations and the energy spectrum . To formally describe the p-wave superconductor we use Kitaev's one-dimensional lattice model Hamiltonian (142). Indeed, despite its apparent simplicity and mathematical tractability, the Kitaev model can be regarded as an effective low-energy description of a quantum wire with a strong spin-orbit coupling and a large enough Zeeman effect, which turns into a one-dimensional p-wave superconductor by proximity to a "standard" s-wave bulk superconductor.(98; 99). Our starting Hamiltonian is:

$$H = -w \sum_{j=1}^{\ell-1} \{c_j^\dagger c_{j+1} + c_{j+1}^\dagger c_j\} - \mu \sum_{j=1}^{\ell} c_j^\dagger c_j + \Delta \sum_{j=1}^{\ell-1} \{c_j c_{j+1} + c_{j+1}^\dagger c_j^\dagger\} \tag{B.1}$$

In Eq.(B.1) the operator c_j ($c_j^\dagger$) ($j = 1, \ldots, \ell$) are single-fermion annihilation (creation) operators defined on site-j of the one-dimensional chain. They satisfy the canonical anticommutation relations $\{c_j, c_{j'}^\dagger\} = \delta_{j,j'}$, all the other anticommutators being equal to 0. Here w is the normal single-electron hopping amplitude, Δ is the p-wave superconducting pairing and μ is the chemical potential.

Now, we want to look for and analyze the exitation spetrum by setting the condition $w = \Delta$, which does not qualitatively affect the spectrum and the eigenfunctions with respect to the general case, and $\mu \geq 0$. Besides its mathematical simplifity, it is also worth noticing that the Hamiltonian in Eq.(B.1) with $w = \Delta$ takes a precise physical meaning, as it be obtained from the Hamiltonian open quantum Ising chain via Jordan-Wigner transformation (100). Technically, we diagonalize the Hamiltonian, with open boundary conditions on the single-mode wavefunction. Again, we consider the generic eigenmode of H with energy E :

$$\Gamma_E = \sum_{j=1}^{\ell} \{[u_j]^* c_j + [v_j]^* c_j^\dagger\} \tag{B.2}$$

with the wavefunctions u_j, v_j solving the appropriate Bogoliubov-de Gennes (BdG) equations obtained from the canonical commutation relation $[\Gamma_E, H] = E\Gamma_E$. These, are given by :

$$\begin{aligned} Eu_j &= -w\{u_{j+1} + u_{j-1}\} - \mu u_j + w\{v_{j+1} - v_{j-1}\} \\ Ev_j &= -w\{u_{j+1} - u_{j-1}\} + w\{v_{j+1} + v_{j-1}\} + \mu v_j \end{aligned} \tag{B.3}$$

for $1 < j < \ell$. At variance, at the endpoints ($j = 1, \ell$), the equations take the form :

$$\begin{aligned} Eu_1 &= -wu_2 + wv_2 - \mu u_1 \\ Ev_1 &= -wu_2 + wv_2 + \mu v_1 \quad , \end{aligned} \tag{B.4}$$

and:

$$\begin{aligned} Eu_\ell &= -wu_{\ell-1} - wv_{\ell-1} - \mu u_\ell \\ Ev_\ell &= wu_{\ell-1} + wv_{\ell-1} + \mu v_\ell \end{aligned} \tag{B.5}$$

Requiring that Eqs.(B.3) are satisfied, the solution for $1 < j < \ell$ takes the form :

$$\begin{bmatrix} u_j \\ v_j \end{bmatrix} = e^{ikj} \begin{bmatrix} u_k \\ v_k \end{bmatrix} \tag{B.6}$$

Imposing the wavefunctions in Eqs.(B.6) to be a solution of Eqs.(B.3), we obtain the system of equations in momentum space:

$$\begin{aligned} Eu_k &= -[2w\cos(k) + \mu]u_k + 2iw\sin(k)v_k \\ Ev_k &= -2iw\sin(k)u_k + [2w\cos(k) + \mu]v_k \end{aligned} \tag{B.7}$$

supplemented with the open boundary conditions:

$$u_0 + v_0 = u_{\ell+1} - v_{\ell+1} = 0 \tag{B.8}$$

Assuming the chemical potential be positive, i.e. $\mu > 0$, from Eqs.(B.7), we obtain the dispersion relation:

$$E = \pm\epsilon(k) = \pm\sqrt{(2w - \mu)^2 + 8w\mu\cos^2\left(\frac{k}{2}\right)} \tag{B.9}$$

Having defined the actual gap Δ_w as $\Delta_w = |2w - \mu|$, Eq.(B.9) can be inverted, yielding the momentum of an excitation with energy ϵ as :

$$\cos\left(\frac{k}{2}\right) = \pm\sqrt{\frac{\epsilon^2 - \Delta_w^2}{8w\mu}} \tag{B.10}$$

Solutions with energy $|\epsilon| > \Delta_w$ correspond to real value of momentum k. These can be readily written in a compact form; we define θ such that:

$$\begin{aligned} \cos(\theta) &= -\frac{2w\cos(k) + \mu}{\epsilon_k} \\ \sin(\theta) &= \frac{2w\sin(k)}{\epsilon_k} \end{aligned} \tag{B.11}$$

Imposing the boundary conditions in Eq.(B.8), we can find the positive-energy solutions:

$$\left[\begin{array}{c} u_j \\ v_j \end{array}\right]_+ = \sqrt{\frac{2}{\ell}} \left[\begin{array}{c} \cos\left(\frac{\theta}{2}\right)\sin\left(kj + \frac{\theta}{2}\right) \\ -\sin\left(\frac{\theta}{2}\right)\cos\left(kj + \frac{\theta}{2}\right) \end{array}\right] \tag{B.12}$$

while the corresponding negative-energy solutions are recovered by acting with τ^x on the solution in Eq.(B.12), that is:

$$\left[\begin{array}{c} u_j \\ v_j \end{array}\right]_- = \tau^x \left[\begin{array}{c} u_j \\ v_j \end{array}\right]_+ = \sqrt{\frac{2}{\ell}} \left[\begin{array}{c} -\sin\left(\frac{\theta}{2}\right)\cos\left(kj + \frac{\theta}{2}\right) \\ \cos\left(\frac{\theta}{2}\right)\sin\left(kj + \frac{\theta}{2}\right) \end{array}\right] \tag{B.13}$$

The secular equation for the allowed values of k is determined by the boundary condition at $j = \ell + 1$. It is given by:

$$\sin[k(\ell + 1) + \Psi] = 0 \tag{B.14}$$

Now we consider the case with $|\epsilon| < w$ to find the sub-gap solutions. We can recover them for comples values of the momenta k, which are fixed by the condition :

$$\cos\left(\frac{k}{2}\right) = \pm i\sqrt{\frac{\Delta_w^2 - \epsilon^2}{8w\mu}} \tag{B.15}$$

To solve Eq.(B.15), we now define the momentum for particle-like excitations as $k_p = \pi - i\delta$ and for hole-like excitations as $k_h = \pi + i\delta$, with :

$$\delta = 2\sinh^{-1}\left\{\sqrt{\frac{\Delta_w^2 - \epsilon^2}{8w\mu}}\right\} \tag{B.16}$$

As a result, the most general sub-gap eigenfunction with energy $\epsilon > 0$ is given by

$$\left[\begin{array}{c} u_j \\ v_j \end{array}\right] = c\,(-1)^j \left[\begin{array}{c} \cosh\left(\frac{\xi}{2}\right)\{\alpha e^{j\delta} + \beta e^{-j\delta}\} \\ \sinh\left(\frac{\xi}{2}\right)\{\alpha e^{j\delta} - \beta e^{-j\delta}\} \end{array}\right] \tag{B.17}$$

with ξ defined through the equations :

$$\begin{aligned} \cosh(\xi) &= \frac{2w\cosh(\delta)-\mu}{\epsilon} \\ \sinh(\xi) &= \frac{2w\sinh(\delta)}{\epsilon} \end{aligned} \tag{B.18}$$

and the coefficients α and β determined by the boundary conditions in Eqs.(B.8). Clearly, a state with energy $\epsilon > 0$ comes together with the particle-hole conjugated one, with energy $-\epsilon$ (142). In imposing the boundary conditions in Eqs.(B.8), we find that $\alpha e^{\frac{\xi}{2}} + \beta e^{-\frac{\xi}{2}} = 0$ and, more importantly, that the allowed value of ϵ must satisfy the condition:

$$\sinh[\xi - (\ell+1)\delta] = 0 \Rightarrow \xi(\epsilon) = (\ell+1)\delta(\epsilon) \tag{B.19}$$

Eq.(B.19) is a transcendent equation, whose solution can in general only be derived numerically. Yet, a simple approximate formula for the energy can be derived in the long chain limit, where we may assume that the energy is small enough to enable one to neglect the dependence of δ on ϵ and, therefore, to make the approximation:

$$\delta(\epsilon) \approx \delta_0 = 2\sinh^{-1}\left\{\sqrt{\frac{\Delta_w^2}{8w\mu}}\right\} \tag{B.20}$$

By using this result, we get:

$$\epsilon \sim \{2we^{\delta} - \mu\}e^{-\xi} \approx \{2we^{\delta_0} - \mu\}e^{-(\ell+1)\delta_0} \tag{B.21}$$

In general, even without knowing the explicit solution,we can identify the boundary of the phase characterized by the low-lying modes by noting that, in order for Eq.(B.19) to be satisfied, $\xi(\epsilon)$ must be real, which implies that $e^{-\xi(\epsilon)} > 0$. Therefore, we note that:

$$e^{-\xi(\epsilon)} = \frac{2we^{-\delta(\epsilon)} - \mu}{\epsilon} \tag{B.22}$$

which implies that $\xi(\epsilon)$ is real if, and only if:

$$\frac{2w}{\mu} > e^{\delta(\epsilon)} = \frac{\sqrt{(2w+\mu)^2-\epsilon^2} + \sqrt{(2w-\mu)^2-\epsilon^2}}{\sqrt{(2w+\mu)^2-\epsilon^2} - \sqrt{(2w-\mu)^2-\epsilon^2}} \geq 1 \tag{B.23}$$

Therefore, the phase characterized by the presence of low-lying sub-gap modes close to the Fermi level (which evolves into the topological phase with Majorana exciations at the boundary of the chain as $\ell \to \infty$) is defined by the condition $\frac{2w}{\mu} > 1$ (142) , even in the case of a finite-length chain.

Appendix C

p-wave chain with closed boundary conditions

Previously, we focused our study on one-dimensional chains with open boundary conditions. Now, we take in account the case in which our system has periodic boundary conditions and it is pierced by a magnetic flux Φ. In particular, we want to analyze a p-wave superconducting ring linked by a weak link τ. By using the BdG formalism, we derive the energy eigenvalues and the corresponding eigenmodes of the model described by the Hamiltonian, by considering, as we did in the previous section, $w = \Delta$. As we will see, by tuning the flux Φ to the special value Φ_* (which is a function of parameters of the ring), we can find zero-energy modes in the spectrum of this system. Let us start from the Hamiltonian:

$$\begin{aligned} H &= -w\sum_{j=1}^{\ell-1}\{c_j^\dagger c_{j+1} + c_{j+1}^\dagger c_j\} - \mu\sum_{j=1}^{\ell} c_j^\dagger c_j \\ &+ \Delta\sum_{j=1}^{\ell-1}\{c_j c_{j+1} + c_{j+1}^\dagger c_j^\dagger\} + -\tau\{e^{\frac{i}{2}\Phi}c_1^\dagger c_\ell + e^{-\frac{i}{2}\Phi}c_\ell^\dagger c_1\} \end{aligned} \tag{C.1}$$

To find the BdG equations, when $1 < j < \ell$, we can do the same computations did in the previous section, obtaining the results of Eq.(B.3) with the same energy-relation disperion. But when $j = 1$ and $j = \ell$ the case, differently as the previous one, is more tricky. Indeed, at variance, at $j = 1$, we get:

$$\begin{aligned} Eu_1 &= -wu_2 - \tau e^{-\frac{i}{2}\Phi}u_\ell - \mu u_1 + wv_2 \\ Ev_1 &= -wu_2 + wv_2 + \tau e^{\frac{i}{2}\Phi}v_\ell + \mu v_1 \end{aligned} \tag{C.2}$$

while at $j = \ell$, we obtain:

$$
\begin{aligned}
Eu_\ell &= -wu_{\ell-1} - \tau e^{\frac{i}{2}\Phi} u_1 - \mu u_\ell - wv_{\ell-1} \\
Ev_\ell &= wu_{\ell-1} + wv_{\ell-1} + \tau e^{-\frac{i}{2}\Phi} v_1 + \mu v_\ell
\end{aligned} \tag{C.3}
$$

In order for the conditions in Eqs.(C.2,C.3) to be satisfied, one has to modify the ansatz in Eq.(B.6). For the sake of clarity, in the following we shall use $\bar{u}_1, \bar{v}_1$ and $\bar{u}_\ell, \bar{v}_\ell$ to respectively denote the wavefunctions at $j = 1$ and at $j = \ell$. Therefore, using Eqs.(C.2,C.3), we obtain:

$$
\begin{bmatrix} (E+\mu) & \tau e^{-\frac{i}{2}\Phi} \\ \tau e^{\frac{i}{2}\Phi} & (E+\mu) \end{bmatrix} \begin{bmatrix} \bar{u}_1 \\ \bar{u}_\ell \end{bmatrix} = -w \begin{bmatrix} (u_2 - v_2) \\ (u_{\ell-1} + v_{\ell-1}) \end{bmatrix} \tag{C.4}
$$

and :

$$
\begin{bmatrix} (E-\mu) & -\tau e^{\frac{i}{2}\Phi} \\ -\tau e^{-\frac{i}{2}\Phi} & (E-\mu) \end{bmatrix} \begin{bmatrix} \bar{v}_1 \\ \bar{v}_\ell \end{bmatrix} = -w \begin{bmatrix} (u_2 - v_2) \\ -(u_{\ell-1} + v_{\ell-1}) \end{bmatrix} \tag{C.5}
$$

On inverting Eqs.(C.4), we get:

$$
\begin{bmatrix} \bar{u}_1 \\ \bar{u}_\ell \end{bmatrix} = -\left\{ \frac{w}{(E+\mu)^2 - \tau^2} \right\} \begin{bmatrix} \{(E+\mu)(u_2 - v_2) - \tau e^{-\frac{i}{2}\Phi}(u_{\ell-1} + v_{\ell-1})\} \\ \{-\tau e^{\frac{i}{2}\Phi}(u_2 - v_2) + (E+\mu)(u_{\ell-1} + v_{\ell-1})\} \end{bmatrix} \tag{C.6}
$$

while, on inverting Eqs.(C.5), one rather gets

$$
\begin{bmatrix} \bar{v}_1 \\ \bar{v}_\ell \end{bmatrix} = -\left\{ \frac{w}{(E-\mu)^2 - \tau^2} \right\} \begin{bmatrix} \{(E-\mu)(u_2 - v_2) - \tau e^{\frac{i}{2}\Phi}(u_{\ell-1} + v_{\ell-1})\} \\ \{\tau e^{-\frac{i}{2}\Phi}(u_2 - v_2) - (E-\mu)(u_{\ell-1} + v_{\ell-1})\} \end{bmatrix} \tag{C.7}
$$

Now, setting $j = 2, \ell - 1$, we get the BdG equations:

$$
\begin{aligned}
Eu_2 &= -w\{u_3 + \bar{u}_1\} - \mu u_2 + w\{v_3 - \bar{v}_1\} \\
Ev_2 &= -w\{u_3 - \bar{u}_1\} + w\{v_3 + \bar{v}_1\} + \mu v_2 \quad ,
\end{aligned} \tag{C.8}
$$

and :

$$
\begin{aligned}
Eu_{\ell-1} &= -w\{u_{\ell-2} + \bar{u}_\ell\} - \mu u_{\ell-1} + w\{\bar{v}_\ell - v_{\ell-2}\} \\
Ev_{\ell-1} &= -w\{\bar{u}_\ell - u_{\ell-2}\} + w\{\bar{v}_\ell + v_{\ell-2}\} + \mu v_{\ell-1}
\end{aligned} \tag{C.9}
$$

From Eqs.(C.8,C.9) we see that, in order for the solution in Eq.(C.18) to hold for $1 < j < \ell$, we must have:

$$\begin{aligned}\bar{u}_1 + \bar{v}_1 &= u_1 + v_1 \\ \bar{u}_\ell - \bar{v}_\ell &= u_\ell - v_\ell \end{aligned} \tag{C.10}$$

where, now, u_1, v_1 (u_ℓ, v_ℓ) denote the wavefunction u_j, v_j evaluated at $j = 1$ ($j = \ell$). By combining these equations, we can extrapolate the consistency conditions:

$$\begin{aligned}\bar{u}_1 + \bar{v}_1 &= -w \left\{ \frac{E+\mu}{(E+\mu)^2 - \tau^2} + \frac{E-\mu}{(E-\mu)^2 - \tau^2} \right\} (u_2 - v_2) + \\ &= \tau w \left\{ \frac{e^{-\frac{i}{2}\Phi}}{(E+\mu)^2 - \tau^2} + \frac{e^{\frac{i}{2}\Phi}}{(E-\mu)^2 - \tau^2} \right\} (u_{\ell-1} + v_{\ell-1}) \\ \bar{u}_\ell - \bar{v}_\ell &= -w \left\{ \frac{E+\mu}{(E+\mu)^2 - \tau^2} + \frac{E-\mu}{(E-\mu)^2 - \tau^2} \right\} (u_{\ell-1} + v_{\ell-1}) + \\ &= \tau w \left\{ \frac{e^{\frac{i}{2}\Phi}}{(E+\mu)^2 - \tau^2} + \frac{e^{-\frac{i}{2}\Phi}}{(E-\mu)^2 - \tau^2} \right\} (u_2 - v_2) \end{aligned} \tag{C.11}$$

Now, we make the ansatz that a generic solution of energy ϵ takes the form :

$$\left[\begin{array}{c} u_j \\ v_j \end{array} \right]_+ = c \left[\begin{array}{c} \cos\left(\frac{\theta}{2}\right) \{a e^{ikj} + b e^{-ikj}\} \\ -i \sin\left(\frac{\theta}{2}\right) \{a e^{ikj} - b e^{-ikj}\} \end{array} \right] \tag{C.12}$$

with c being an appropriate normalization constant. Moreover, to simplify the notation, we introduce:

$$\begin{aligned}\mathcal{A}(E) &= w \left\{ \frac{E+\mu}{(E+\mu)^2 - \tau^2} + \frac{E-\mu}{(E-\mu)^2 - \tau^2} \right\} \\ \mathcal{B}(E;\Phi) &= \tau w \left\{ \frac{e^{-\frac{i}{2}\Phi}}{(E+\mu)^2 - \tau^2} + \frac{e^{\frac{i}{2}\Phi}}{(E-\mu)^2 - \tau^2} \right\} \quad . \end{aligned} \tag{C.13}$$

Therefore, we obtain the system of algebraic equations for a and b given by :

$$\begin{aligned}&\{e^{ik - i\frac{\theta}{2}} + \mathcal{A}(E) e^{2ik + i\frac{\theta}{2}} - \mathcal{B}[E;\Phi] e^{ik(\ell-1) - i\frac{\theta}{2}}\} a + \{e^{-ik + i\frac{\theta}{2}} + \\ &\mathcal{A}(E) e^{-2ik - i\frac{\theta}{2}} - \mathcal{B}[E;\Phi] e^{-ik(\ell-1) + i\frac{\theta}{2}}\} b = 0 \\ &\{e^{ik\ell + i\frac{\theta}{2}} + \mathcal{A}(E) e^{ik(\ell-1) - i\frac{\theta}{2}} - \mathcal{B}^*[E;\Phi] e^{2ik + i\frac{\theta}{2}}\} a + \{e^{-ik\ell - i\frac{\theta}{2}} + \\ &\mathcal{A}(E) e^{-ik(\ell-1) + i\frac{\theta}{2}} - \mathcal{B}^*[E;\Phi] e^{-2ik - i\frac{\theta}{2}}\} b = 0 \end{aligned} \tag{C.14}$$

On requiring Eqs.(C.14) to provide nontrivial solutions for a and b, we readily obtain the secular equation for the allowed values of the energy $|\epsilon| > \Delta_w$ in the form :

$$
\begin{aligned}
&-\sin[k(\ell-1)+\theta]-(\mathcal{A}^2(\epsilon)-|\mathcal{B}[\epsilon;\Phi]|^2)\sin[k(\ell-3)-\theta]\\
&-2\mathcal{A}(\epsilon)\sin[k(\ell-2)]+2\Re e\mathcal{B}[\epsilon;\Phi]\sin[k+\theta]=0
\end{aligned}
\tag{C.15}
$$

Now, we consider the equation for sub-gap energies, i.e. $|\epsilon|<w$. These correspond to complex values of k satisfying :

$$
\cos\left(\frac{k}{2}\right)=\pm i\sqrt{\frac{\Delta_w^2-\epsilon^2}{8w\mu}}
\tag{C.16}
$$

To solve Eq.(C.16), we now define the momentum for particle-like excitations as $k_p=\pi-i\delta$ and for hole-like excitations as $k_h=\pi+i\delta$, with :

$$
\delta=2\sinh^{-1}\left\{\sqrt{\frac{\Delta_w^2-\epsilon^2}{8w\mu}}\right\}
\tag{C.17}
$$

As a result, we find that the positive-energy wavefunction is given by:

$$
\left[\begin{array}{c}u_j\\v_j\end{array}\right]=c\,(-1)^j\left[\begin{array}{c}\cosh\left(\frac{\xi}{2}\right)\{\alpha e^{j\delta}+\beta e^{-j\delta}\}\\ \sinh\left(\frac{\xi}{2}\right)\{\alpha e^{j\delta}-\beta e^{-j\delta}\}\end{array}\right]
\tag{C.18}
$$

with ξ defined through the equations

$$
\begin{aligned}
\cosh(\xi) &= \frac{2w\cosh(\delta)-\mu}{\epsilon}\\
\sinh(\xi) &= \frac{2w\sinh(\delta)}{\epsilon}
\end{aligned}
\tag{C.19}
$$

and the coefficients α and β determined by the appropriate boundary conditions for the allowed wavefunctions. We therefore trade Eqs.(C.11) for the following system in the unknowns α,β:

$$
\begin{aligned}
&\{e^{\delta+\frac{\xi}{2}}-e^{2\delta-\frac{\xi}{2}}\mathcal{A}(E)-e^{(\ell-1)\delta+\frac{\xi}{2}}\mathcal{B}(E;\Phi)\}\alpha+\\
&\{e^{-\delta-\frac{\xi}{2}}-e^{-2\delta+\frac{\xi}{2}}\mathcal{A}(E)-e^{-(\ell-1)\delta-\frac{\xi}{2}}\mathcal{B}(E;\Phi)\}\beta=0\\
&\{e^{\ell\delta-\frac{\xi}{2}}-e^{(\ell-1)\delta+\frac{\xi}{2}}\mathcal{A}(E)-e^{2\delta-\frac{\xi}{2}}\mathcal{B}^*(E;\Phi)\}\alpha+\\
&\{e^{-\ell\delta+\frac{\xi}{2}}-e^{-(\ell-1)\delta-\frac{\xi}{2}}\mathcal{A}(E)-e^{-2\delta+\frac{\xi}{2}}\mathcal{B}^*(E;\Phi)\}\beta=0
\end{aligned}
\tag{C.20}
$$

The system in Eq.(C.20) admits a nontrivial solution for α and β only provided that the following secular equation for the energy eigenvalue ϵ is satisfied

$$
\begin{aligned}
&-\sinh[(\ell-1)\delta-\xi]+2\mathcal{A}(\epsilon)\sinh[(\ell-2)\delta]+2\Re e(\mathcal{B}(\epsilon;\Phi))\sinh[\delta-\xi]-\\
&\{\mathcal{A}^2(\epsilon)-|\mathcal{B}(\epsilon;\Phi)|^2\}\sinh[(\ell-3)\delta+\xi]=0
\end{aligned}
\tag{C.21}
$$

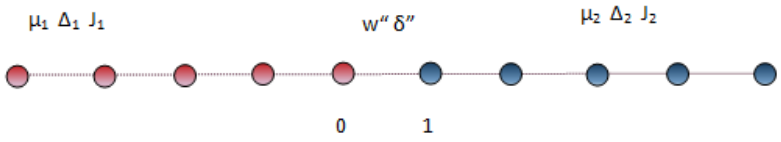

Figure C.1: Junction of two finite lenght Kitaev chains

Clearly, Eqs.(C.20,C.21) are consistent with the solution for $\tau = 0$. Indeed, as $\tau = 0$ (open chain limit), one obtains that (apart for a constant) $\alpha = e^{-\frac{\xi}{2}}$ and $\beta = -e^{\frac{\xi}{2}}$. Also, we obtain that $\mathcal{B}(E;\Phi) = 0$ and, as a result, Eqs.(C.20) take the form :

$$\begin{aligned}
&\{e^{\delta+\frac{\xi}{2}} - e^{2\delta-\frac{\xi}{2}}\mathcal{A}(\epsilon)\}\alpha + \{e^{-\delta-\frac{\xi}{2}} - e^{-2\delta+\frac{\xi}{2}}\mathcal{A}(\epsilon)\}\beta = 0 \\
&\{e^{\ell\delta-\frac{\xi}{2}} - e^{(\ell-1)\delta+\frac{\xi}{2}}\mathcal{A}(\epsilon)\}\alpha + \{e^{-\ell\delta+\frac{\xi}{2}} - e^{-(\ell-1)\delta-\frac{\xi}{2}}\mathcal{A}(\epsilon)\}\beta = 0
\end{aligned} \tag{C.22}$$

Using the explicit expression for $\mathcal{A}(\epsilon)$, Eqs.(C.22) yield:

$$\begin{aligned}
&\alpha e^{\delta+\frac{\xi}{2}} + \beta e^{-\delta-\frac{\xi}{2}} - \left[\frac{w}{\epsilon+\mu} + \frac{w}{\epsilon-\mu}\right]\{\alpha e^{2\delta-\frac{\xi}{2}} + \beta e^{-2\delta+\frac{\xi}{2}}\} = 0 \\
&\alpha e^{\ell\delta-\frac{\xi}{2}} + \beta e^{-\ell\delta+\frac{\xi}{2}} - \left[\frac{w}{\epsilon+\mu} + \frac{w}{\epsilon-\mu}\right]\{\alpha e^{(\ell-1)\delta+\frac{\xi}{2}} + \beta e^{-(\ell-1)\delta-\frac{\xi}{2}}\} = 0
\end{aligned} \tag{C.23}$$

that is :

$$\begin{aligned}
&u_1 + v_1 + \left[\frac{w}{\epsilon+\mu} + \frac{w}{\epsilon-\mu}\right]\{u_2 - v_2\} = 0 \\
&v_\ell - v_\ell + \left[\frac{w}{\epsilon+\mu} + \frac{w}{\epsilon-\mu}\right]\{u_{\ell-1} + v_{\ell-1}\} = 0
\end{aligned} \tag{C.24}$$

We now see that Eqs.(C.24) respectively imply $u_0 + v_0 = 0$, and $u_{\ell+1} - v_{\ell+1} = 0$, which are the appropriate equations for $\tau = 0$ (open chain limit). Of course, in general we have to solve Eq.(C.15,C.21) to observe the functional dependence of the energy ϵ on the flux Φ. This, how we will see in the following, allows us to obtain a signature of the presence of Majorana Modes in the system.

C.0.1 SS p-wave junctions in the lattice model

Now we are going to study the case of a junction of two homogeneous Kitaev chain.Our model Hamiltoninan is:

$$H_1 = -\sum_{j<0} \left(w_1 \left(c_j^\dagger c_{j+1} + c_{j+1}^\dagger c_j \right) - \mu_1 c_j^\dagger c_j + \Delta_1 \left(c_j a_{j+1} + c_{j+1}^\dagger c_j^\dagger \right) \right)$$

for the left chain and, similarly the hamiltoninan:

$$H_2 = -\sum_{j<0} \left(w_2 \left(d_j^\dagger d_{j+1} + d_{j+1}^\dagger d_j \right) - \mu_2 d_j^\dagger d_j + \Delta_2 \left(d_j a_{j+1} + d_{j+1}^\dagger d_j^\dagger \right) \right)$$

for the right chain. As regards the wave functions , we impose the conditions :

$$u_j = \begin{cases} u_j^{(1)} & \text{for } j \leq 0 \\ u_j^{(2)} & \text{for } j \geq 1 \end{cases}$$

$$v_j = \begin{cases} v_j^{(1)} & \text{for } j \leq 0 \\ v_j^{(2)} & \text{for } j \geq 1 \end{cases}$$

The eingenvalues equations obteined in previous equations can be rewritten for the first chain ($j < 0$):

$$\begin{aligned} c_j &: 0 = -w_1 \left(u_{j-1}^{(1)} + u_{j+1}^{(1)} \right) - \Delta_1 \left(v_{j-1}^{(1)} - v_{j+1}^{(1)} \right) - \mu_1 u_j^{(1)} - E u_j^{(1)} \\ c_j^\dagger &: 0 = +w_1 \left(v_{j+1}^{(1)} + v_{j-1}^{(1)} \right) + \Delta_1 \left(u_{j+1}^{(1)} - u_{j-1}^{(1)} \right) + \mu_1 v_j^{(1)} - E v_j^{(1)} \end{aligned} \tag{C.25}$$

and, in the same way, for the second ($j > 1$):

$$\begin{aligned} d_j &: 0 = -w_2 \left(u_{j-1}^{(2)} + u_{j+1}^{(2)} \right) - \Delta_2 \left(v_{j-1}^{(2)} - v_{j+1}^{(2)} \right) - \mu_2 u_j^{(2)} - E u_j^{(2)} \\ d_j^\dagger &: 0 = w_2 \left(v_{j+1}^{(2)} + v_{j-1}^{(2)} \right) + \Delta_2 \left(u_{j+1}^{(2)} - u_{j-1}^{(2)} \right) + \mu_2 v_j^{(2)} - E v_j^{(2)} \end{aligned} \tag{C.26}$$

As it regards instead the cases in which $j = 0$ and $j = 1$, we must consider the following junction conditions

$$\begin{aligned} c_j &: 0 = -w_1 u_{-1}^{(1)} - w" u_1^{(2)} - \Delta_1 v_{-1}^{(1)} + \delta" v_1^{(2)} - \mu_1 u_0^{(1)} - E u_0^{(1)} \\ c_j^\dagger &: 0 = w_1 v_{-1}^{(1)} + w" v_1^{(2)} - \Delta_1 u_{-1}^{(1)} + \delta" u_1^{(2)} + \mu_1 v_0^{(1)} - E v_0^{(1)} \end{aligned} \tag{C.27}$$

for $j = 0$ and

$$\begin{aligned} d_j &: 0 = -w" u_0^{(1)} - w_2 u_2^{(2)} - \delta" v_0^{(1)} + \Delta_2 v_2^{(2)} - \mu_2 u_1^{(2)} - E u_1^{(2)} \\ d_j^\dagger &: 0 = w" v_0^{(1)} + J_2 v_2^{(2)} - \Delta_2 u_2^{(2)} + \delta" u_0^{(1)} + \mu_2 v_1^{(2)} - E v_1^{(2)} \end{aligned} \tag{C.28}$$

for $j = 1$. To simplify Eq. (C.27,C.28) we can extend the solutions $u_j^{(1)}$, $v_j^{(1)}$ to site $j = 1$ and, in the same way, $u_j^{(2)}$, $v_j^{(2)}$ to site $j = 0$ as illustrated in the figure.

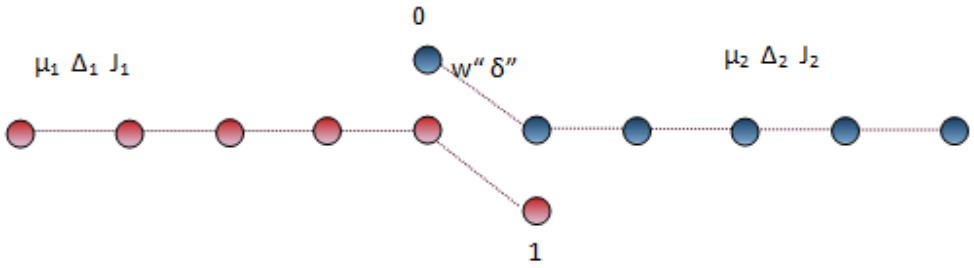

Figure C.2: Junction and ghost sites

In this way, using Eq. (C.25,C.26), we obtain:

$$\begin{aligned} c_j &: 0 = -w_1\left(u_{-1}^{(1)} + u_1^{(1)}\right) - \Delta_1\left(v_{-1}^{(1)} - v_1^{(1)}\right) - \mu_1 u_0^{(1)} - E u_0^{(1)} \\ c_j^\dagger &: 0 = w_1\left(v_1^{(1)} + v_{-1}^{(1)}\right) + \Delta_1\left(u_1^{(1)} - u_{-1}^{(1)}\right) + \mu_1 v_0^{(1)} - E v_0^{(1)} \end{aligned} \tag{C.29}$$

for $j = 0$ in the first chain, and:

$$\begin{aligned} d_j &: 0 = -w_2\left(u_0^{(2)} + u_2^{(2)}\right) - \Delta_2\left(v_0^{(2)} - v_2^{(2)}\right) - \mu_2 u_1^{(2)} - E u_1^{(2)} \\ d_j^\dagger &: 0 = w_2\left(v_2^{(2)} + v_0^{(2)}\right) + \Delta_2\left(u_2^{(2)} - u_0^{(2)}\right) + \mu_2 v_1^{(2)} - E v_1^{(2)} \end{aligned} \tag{C.30}$$

for $j = 1$. Now we subtract the results obteind in Eq. (C.29,C.30) to Eq. (C.27,C.28) to achieve:

$$\begin{aligned} c_j &: 0 = w_1 u_1^{(1)} - \Delta_1 v_1^{(1)} - w" u_1^{(2)} + \delta" v_1^{(2)} \\ c_j^\dagger &: 0 = w_1 v_1^{(1)} - \Delta_1 u_1^{(1)} - w" v_1^{(2)} + \delta" u_1^{(2)} \end{aligned} \tag{C.31}$$

for the first chain, and:

$$\begin{aligned} d_j &: 0 = w_2 u_0^{(2)} - \Delta_2 v_0^{(2)} - w" u_0^{(1)} + \delta" v_0^{(1)} \\ d_j^\dagger &: 0 = w_2 v_0^{(2)} - \Delta_2 u_0^{(2)} - w" v_0^{(1)} + \delta" u_0^{(1)} \end{aligned} \tag{C.32}$$

for the second chain.

Appendix D

Continuum model for superconductors

In this section, we want to analyze the case of an s-wave one-dimensional superconductor in a continuum space description, deriving the energy spectrum and the Bogolioubov-de Gennes equations. Differently from the lattice modellization, the continuum model is reasonable to describe weak-coupling superconductors, especially when they have a wide-band metallic normal state. Let us consider an homongeoneus real superconducting pairing, then $\Delta(x, y) = \Delta$; our model Hamiltonian is:

$$H = \int dx \sum_{\sigma} \psi^{\dagger}_{\sigma}(x) H_{\alpha} \psi_{\sigma}(x) + \Delta \int dx \left(\psi^{\dagger}_{\uparrow}(x) \psi^{\dagger}_{\downarrow}(x) + \psi_{\uparrow}(x) \psi_{\downarrow}(x) \right)$$

where m the mass of the quasi-particles, ϵ_F the Fermi energy, $\sigma = \uparrow, \downarrow$ the spin polarization, $\psi^{\dagger}_{\sigma}(x)$ and $\psi_{\sigma}(x)$, respectively, creation and annihilation fermionic operators which satisfy the anticommutators:

$$\left\{ \psi^{\dagger}_{\sigma}(x), \psi_{\sigma'}(y) \right\} \quad = \quad \delta(x - y) \delta_{\sigma\sigma'} \tag{D.1}$$

and the others are equal to zero. To obtain the eigenvalues of this Hamiltonian, we have to sole the Heisenberg commutator $[\Gamma_{n,\sigma}, H] = E\Gamma_{n,\sigma}$, where $\Gamma_{n,\sigma}$ is the most generic eigenmode which diagonalize the Hamiltonian as:

$$H_{eff} = \sum_{\sigma,n} \epsilon_n \Gamma^{\dagger}_{n,\sigma} \Gamma_{n,\sigma} \tag{D.2}$$

To obtain the Bogolioubov-de Gennes equations, we first of all write:

$$\psi_\uparrow(x) = \sum_n \left(\Gamma_{n\uparrow} u_n(x) - \Gamma^\dagger_{n\downarrow} v^*_n(x)\right) \tag{D.3}$$

$$\psi_\downarrow(x) = \sum_n \left(\Gamma_{n\downarrow} u_n(x) + \Gamma^\dagger_{n\uparrow} v^*_n(x)\right) \tag{D.4}$$

$$\psi^\dagger_\uparrow(x) = \sum_n \left(\Gamma^\dagger_{n\uparrow} u^*_n(x) - \Gamma_{n\downarrow} v_n(x)\right) \tag{D.5}$$

$$\psi^\dagger_\downarrow(x) = \sum_n \left(\Gamma^\dagger_{n\downarrow} u^*_n(x) + \Gamma_{n\uparrow} v_n(x)\right) \tag{D.6}$$

Then, we compute the commutators $[\psi_\sigma(x), H]$ and $[\psi^\dagger_\sigma(x), H]$ and compare them with:

$$[\Gamma_{E,\sigma}, H_{eff}] = \epsilon_n \Gamma_{E,\sigma} \tag{D.7}$$

$$[\Gamma^\dagger_{E,\sigma}, H_{eff}] = -\epsilon_n \Gamma^\dagger_{E,\sigma} \tag{D.8}$$

Doing this, we obtain the BdG equations:

$$\epsilon_n u_n(x) = H_\alpha u_n(x) + \Delta v_n(x) \tag{D.9}$$

$$\epsilon_n v_n(x) = -H^*_\alpha v_n(x) + \Delta u_n(x) \tag{D.10}$$

Now, we note that in the presence of an s-wave potential, both spin polarization have the same BdG equations; moreover Eqs.(D.10) are satisfied $\forall n$; for this reason, for the sake of simplicity, we can neglect the dependence on n (i.e. $u_n(x) \to u(x)$,$v_n(x) \to v(x)$ and $\epsilon_n \to E$). If we consider a complex superconducting pairing, Eqs.(D.10) must be written as:

$$Eu(x) = H_\alpha u(x) + \Delta v(x) \tag{D.11}$$

$$Ev(x) = -H^*_\alpha v(x) + \Delta^* u(x) \tag{D.12}$$

Now, to find E, we have to look for non trivial solutions of Eqs.(D.10) . To do this, let assume that :

$$\begin{pmatrix} u(x) \\ v(x) \end{pmatrix} = \begin{pmatrix} u_k \\ v_k \end{pmatrix} e^{ikx} \tag{D.13}$$

this help us to find the energy relation dispersion:

$$E = \pm\sqrt{\left(\frac{\hbar^2 k^2}{2m} + \epsilon_F\right)^2 - \Delta^2} \tag{D.14}$$

Eq.(D.14) show us an important consequence of the superconductivity in a material. First of all, the energy relation dispersion is characterized by a gap of lenght 2Δ; moreover, we can obsere the presence of the particle-hole symmetry. From the energy relation dispersion, we can easly find that:

$$k = \pm\sqrt{\frac{2m}{\hbar^2}(\epsilon_F \pm \sqrt{(E^2 - \Delta^2)})} \tag{D.15}$$

which permit us to define, respectively, the quasi-particle and the quasi-hole momenta as:

$$q_p = \sqrt{\frac{2m}{\hbar^2}(\epsilon_F + \sqrt{(E^2 - \Delta^2)})} \tag{D.16}$$

$$q_h = \sqrt{\frac{2m}{\hbar^2}(\epsilon_F - \sqrt{(E^2 - \Delta^2)})} \tag{D.17}$$

Now we fix the energy $|\epsilon| \geq \Delta$. From Eqs.(D.10,D.17) we find the explicit expression for u_k and v_k:

$$u_k = \sqrt{\frac{1}{2}\left(1 + a\frac{\xi_q}{E}\right)} = \sqrt{\frac{\Delta}{2E}}e^{\frac{1}{2}\arccos\left(i\frac{E}{\Delta}\right)} \tag{D.18}$$

$$v_k = \sqrt{\frac{1}{2}\left(1 - a\frac{\xi_q}{E}\right)} = \sqrt{\frac{\Delta}{2E}}e^{-\frac{1}{2}\arccos\left(i\frac{E}{\Delta}\right)} \tag{D.19}$$

where $\xi_q = \frac{\hbar^2}{2m}q_a^2 - \epsilon_F$ and $a = 1$ if we consider q_p and $a = -1$ if we consider q_h.

If we consider, instead, values of energy lower then the superconducting gap, i.e. $|\epsilon| < \Delta$, we find that the momenta in Eqs.(D.17) becomes complex functions. Indeed, we have:

$$q_p = \sqrt{\frac{2m}{\hbar^2}(\epsilon_F + i\sqrt{(-\epsilon^2 + \Delta^2)})} \tag{D.20}$$

$$q_h = \sqrt{\frac{2m}{\hbar^2}(\epsilon_F - i\sqrt{(-\epsilon^2 + \Delta^2)})} \tag{D.21}$$

Note that now $q_p = q_h^*$, then we can define in this case $q_p \equiv q$ and $q_h \equiv q^*$. Once we have discussed the case of homogeneous p-wave and s-wave one-dimensional systems, we want now to show how to obtain the BdG equations in the case of wire junctions.

Appendix E

Two channels scattering matrix of a normal region with $V(x) = V_0\delta(x)$

In the following, we ask how to compute the Andreev Bound States in a SNS junction in the case in which we have an harmonic potential along the wire. Because of the presence of this harmonic potential, we have compute the scattering matrix S of a process in which more energy channels are possible. Indeed, in this case, we have to consider that the harmonic potential contributes to the total energy of the system and we have to add this contribute to the free energy spectrum.

To focus on, let us consider the Hamiltonian:

$$H_0 = -\frac{\hbar^2}{2m}\frac{d^2}{dx^2} - \frac{\hbar^2}{2m}\frac{d^2}{dy^2} + \frac{1}{2}m\omega^2 y^2 + V(x,y) - E_F \tag{E.1}$$

where $V(x,y)$ is a potential barrier defined as:

$$V(x,y) = V_0\delta(x) \tag{E.2}$$

ω the frequency of the harmonic oscillator, m the mass and E_F the Fermi energy.

To build the scattering matrix of this system, let us consider, for the sake of simplicity, the case in which only two propagating channels are allowed (i.e. the total particle energy bigger than the Fermy energy plus the oscillator contribute with n=2). The most generic wave functions for the left and the right side of the barrier take the form:

$$\begin{cases} \psi_L(x,y) = \frac{a_{L,1}}{\sqrt{v_1}}\chi_1(y)e^{ik_1x} + \frac{b_{L,1}}{\sqrt{v_1}}\chi_1(y)e^{-ik_1x} + \frac{a_{L,2}}{\sqrt{v_2}}\chi_2(y)e^{ik_2x} + \frac{b_{L,2}}{\sqrt{v_2}}\chi_2(y)e^{-ik_2x} & for\ x \leq 0 \\ \psi_R(x,y) = \frac{a_{R,1}}{\sqrt{v_1}}\chi_1(y)e^{ik_1x} + \frac{b_{R,1}}{\sqrt{v_1}}\chi_1(y)e^{-ik_1x} + \frac{a_{R,2}}{\sqrt{v_2}}\chi_2(y)e^{ik_2x} + \frac{b_{R,2}}{\sqrt{v_2}}\chi_2(y)e^{-ik_2x} & for\ x > 0 \end{cases} \tag{E.3}$$

where v_1 and v_2 are the velocities, respectively, in the first and in the second scattering channel, and k_1 and k_2 are the momenta for a free particle propagating along a normal metal. $\chi_{1/2}(y)$ are the wave function contributions which have dependence from y. The energy in the first channel is given by $E_1 = \epsilon_0 + E$, where ϵ_0 is the contribution

of the first mode of the quantum oscillator along y, while E is the energy contribution of the free-motion along x. In the same way, we can define the energy of the second scattering channel as: $E_2 = \epsilon_1 + E$, where ϵ_1 is the contribution of the second mode of the quantum oscillator along y. Velocities and momenta are function of the energies.

To compute the scattering matrix, we impose the continuity of the wave function in $x = 0$ as follows:

$$\int dy \chi_1^*(y) \left\{ \psi_L(x=0,y) - \psi_R(x=0,y) \right\} = 0 \tag{E.4}$$

$$\int dy \chi_2^*(y) \left\{ \psi_L(x=0,y) - \psi_R(x=0,y) \right\} = 0 \tag{E.5}$$

Where

$$\int dy \chi_m^*(y) \chi_n(y) = \delta_{m,n} \tag{E.6}$$

By inserting Eq.(E.3) in Eqs.(E.4,E.5), we find the conditions:

$$\frac{a_{L,1}}{\sqrt{v_1}} + \frac{b_{L,1}}{\sqrt{v_1}} - \frac{a_{R,1}}{\sqrt{v_1}} - \frac{b_{R,1}}{\sqrt{v_1}} = 0 \tag{E.7}$$

$$\frac{a_{L,2}}{\sqrt{v_2}} + \frac{b_{L,2}}{\sqrt{v_2}} - \frac{a_{R,2}}{\sqrt{v_2}} - \frac{b_{R,2}}{\sqrt{v_2}} = 0 \tag{E.8}$$

which we can simply write as:

$$a_{L,1} + b_{L,1} - a_{R,1} - b_{R,1} = 0 \tag{E.9}$$

$$a_{L,2} + b_{L,2} - a_{R,2} - b_{R,2} = 0 \tag{E.10}$$

To have an equation for the derivative of the wave function, we use the trick of the integration of the Schroedinger equation from $-\epsilon$ to ϵ, and then send $\epsilon \to 0$, and to the bracket with the wave functions $\chi_{1/2}(y)$. We obtain:

$$\int dy \chi_1^*(y) \left\{ \hbar^2 \frac{\psi_L'(x=0,y) - \psi_R'(x=0,y)}{2m} + V_0 \psi_L(0,y) \right\} = 0 \tag{E.11}$$

$$\int dy \chi_2^*(y) \left\{ \hbar^2 \frac{\psi_L'(x=0,y) - \psi_R'(x=0,y)}{2m} + V_0 \psi_L(0,y) \right\} = 0 \tag{E.12}$$

This set of equations give us the conditions:

$$\frac{ik_1\hbar^2}{2m\sqrt{v_1}} \left(a_{L,1} - b_{L,1} - a_{R,1} + b_{R,1} \right) + \frac{V_0}{\sqrt{v_1}} \left(a_{L,1} + b_{L,1} \right) = 0 \tag{E.13}$$

$$\frac{ik_2\hbar^2}{2m\sqrt{v_2}} \left(a_{L,2} - b_{L,2} - a_{R,2} + b_{R,2} \right) + \frac{V_0}{\sqrt{v_2}} \left(a_{L,2} + b_{L,2} \right) = 0 \tag{E.14}$$

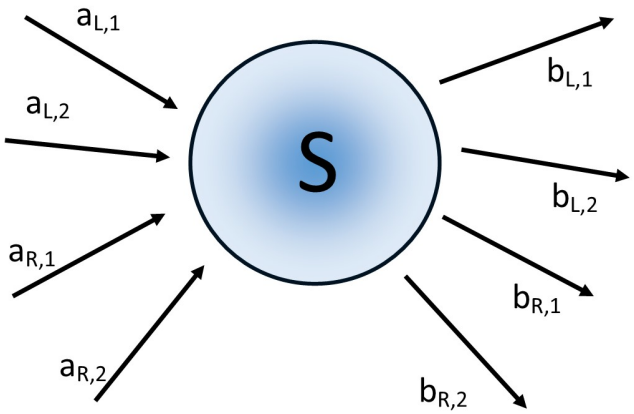

Figure E.1: Sketch of the scattering matrix S.

which we can write in the compact form:

$$(a_{L,1} - b_{L,1} - a_{R,1} + b_{R,1}) + V_1 (a_{L,1} + b_{L,1}) = 0 \tag{E.15}$$
$$(a_{L,2} - b_{L,2} - a_{R,2} + b_{R,2}) + V_2 (a_{L,2} + b_{L,2}) = 0 \tag{E.16}$$

where

$$V_1 = \left(\frac{k_1 \hbar^2}{m}\right)^{-1} V_0 \tag{E.17}$$
$$V_2 = \left(\frac{k_2 \hbar^2}{m}\right)^{-1} V_0 \tag{E.18}$$

From Eqs.(E.8,E) we obtain the system:

$$\begin{pmatrix} 1 & -1 & 0 & 0 \\ -1 + \frac{iV_1}{2} & -1 & 0 & 0 \\ 0 & 0 & 1 & -1 \\ 0 & 0 & -1 + i\frac{V_2}{2} & -1 \end{pmatrix} \begin{pmatrix} a_{L,1} \\ b_{R,1} \\ a_{L,2} \\ b_{R,2} \end{pmatrix} = \begin{pmatrix} -1 & 1 & 0 & 0 \\ -1 - i\frac{V_1}{2} & -1 & 0 & 0 \\ 0 & 0 & -1 & 1 \\ 0 & 0 & -1 - i\frac{V_2}{2} & -1 \end{pmatrix} \begin{pmatrix} b_{L,1} \\ a_{R,1} \\ b_{L,2} \\ a_{R,2} \end{pmatrix} \tag{E.19}$$

which permit us to write the scattering matrix (Fig. E.1):

$$S_e \begin{pmatrix} a_{L,1} \\ b_{R,1} \\ a_{L,2} \\ b_{R,2} \end{pmatrix} = \begin{pmatrix} b_{L,1} \\ a_{R,1} \\ b_{L,2} \\ a_{R,2} \end{pmatrix} \tag{E.20}$$

with

$$S_e = \begin{pmatrix} -i\frac{V_1}{1+iV_1} & \frac{1}{1+iV_1} & 0 & 0 \\ \frac{1}{1+iV_1} & -i\frac{V_1}{1+iV_1} & 0 & 0 \\ 0 & 0 & -i\frac{V_2}{1+iV_2} & \frac{1}{1+iV_2} \\ 0 & 0 & \frac{1}{1+iV_2} & -i\frac{V_2}{1+iV_2} \end{pmatrix} \tag{E.21}$$

Now, having the scattering matrix, we can compute the Andreev Bound States by using the secular equation Eq.(2.65) and following the steps shown in Section 1.2.2.

Bibliography

[1] H. K. Onnes (1911). "The resistance of pure mercury at helium temperatures". Commun. Phys. Lab. Univ. Leiden. 12: 120.

[2] W. Meissner, R. Ochsenfeld (1933). "Ein neuer Effekt bei Eintritt der Supraleitfähigkeit". Naturwissenschaften. 21 (44): 787–788.

[3] F. London, H. London (1935). "The Electromagnetic Equations of the Supraconductor". Proceedings of the Royal Society of London A. 149 (866): 71–88.

[4] . Bardeen; L. N. Cooper , J. R. Schrieffer (1957). "Microscopic Theory of Superconductivity". Physical Review. 106 (1): 162–164.

[5] J. Bardeen; L. N. Cooper , J. R. Schrieffer (1957). "Theory of Superconductivity". Physical Review. 108 (5): 1175–1205.

[6] V. L. Ginzburg , L.D. Landau (1950). "On the theory of superconductivity". Zhurnal Eksperimental'noi i Teoreticheskoi Fiziki. 20: 1064.

[7] E. Maxwell (1950). "Isotope Effect in the Superconductivity of Mercury". Physical Review. 78 (4): 477.

[8] C. A. Reynolds; B. Serin; W. H. Wright , L. B. Nesbitt (1950). "Superconductivity of Isotopes of Mercury". Physical Review. 78 (4): 487.

[9] J. Bardeen, Cooper, L. N. e Schrieffer, J. R., Microscopic Theory of Superconductivity, in Physical Review, vol. 106, n^o 1, April 1957, pp. 162–164.

[10] E. Majorana, Nuovo Cimento, vol.14, 1937, pp. 171–184.

[11] C. A. Reynolds; B. Serin; W. H. Wright , L. B. Nesbitt (1950). "Superconductivity of Isotopes of Mercury". Physical Review. 78 (4): 487.

[12] Castelvecchi, Davide (5 January 2017). "Quantum computers ready to leap out of the lab in 2017". Nature. pp. 9–10.

[13] https://www.microsoft.com/en-us/quantum/

[14] IBM Makes Quantum Computing Available on IBM Cloud". www-03.ibm.com. 4 May 2016.

[15] Rigetti Launches Quantum Cloud Services, Announces "1Million Challenge". HPCwire. 2018-09-07. Retrieved 2018-09-16.

[16] Oindrila Deb, K. Sengupta, and Diptiman Sen, Phys. Rev. B 97, 174518 – Published 22 May 2018.

[17] Doh Y-J, van Dam J A, Roest A L, Bakkers E P A M, Kouwenhoven L P and De Franceschi S 2005 Science 309 272.

[18] B. D. Josephson, Phys. Lett. 1 (7): 251–253,(1962).

[19] B. D. Josephson , Rev. Mod. Phys. 46 (2): 251–254, (1974).

[20] Joneckis, Lance; Koester, David; Alspector, Joshua (2014-01-01). "An Initial Look at Alternative Computing Technologies for the Intelligence Community". Institute for Defense Analyses. pp. 15–16, 24–25, 47–50.

[21] Koshelets V, Likharev K, Migulin V, Mukhanov O, Ovsyannikov G, Semenov V, Serpuchenko I, Vystavkin A (1987). "Experimental realization of a resistive single flux quantum logic circuit". IEEE Trans. Magn. 23 (2): 755–758.

[22] Tanaka M, Kondo T, Nakajima N, Kawamoto T, Yamanashi Y, Kamiya Y, Akimoto A, Fujimaki A, Hayakawa H, Yoshikawa N, Terai H, Hashimoto Y, Yorozu S (2005). "Demonstration of a single-flux-quantum microprocessor using passive transmission lines". IEEE Trans. Appl. Supercond. 15 (2): 400–404.

[23] Nobumori Y, Nishigai T, Nakamiya K, Yoshikawa N, Fujimaki A, Terai H, Yorozu S (2007). "Design and Implementation of a Fully Asynchronous SFQ Microprocessor: SCRAM2". IEEE Trans. Appl. Supercond. 17 (2): 478–481.

[24] Tanaka M, Yamanashi Y, Irie N, Park H-J, Iwasaki S, Takagi K, Taketomi K, Fujimaki A, Yoshikawa N, Terai H, Yorozu S (2007). "Design and implementation of a pipelined 8 bit-serial single-flux-quantum microprocessor with cache memories". Supercond. Sci. Technol. 20 (11).

[25] S. Boixo et all., Nature Physics, vol. 14 (2018), 595–600.

[26] Chelsea Whyte, Google claims it has finally reached quantum supremacy, New Scientist, 2019.

[27] Sand-Jespersen T, Paaske J, Andersen B M, Grove-Rasmussen K, Jørgensen H I, Aagesen M, Sørensen C B, Lindelof P E, Flensberg K and Nygård J 2007 Phys. Rev. Lett. 99 126603.

[28] van Dam J A, Nazarov Y V, Bakkers E P A M, De Franceschi S and Kouwenhoven L P 2006 Nature 442 667.

[29] Braga D, Gutirrez Lezama I, Berger H and Morpurgo A F 2012 Nano Lett. 12 5218 pMID: 22989251.

[30] Buzdin A I 2005 Rev. Mod. Phys. 77 935.

[31] Golubov A A, Kupriyanov M Y and Il'ichev E 2004 Rev. Mod. Phys. 76 411.

[32] Awschalom D D, Bassett L C, Dzurak A S, Hu E L and Petta J R 2013 Science 339 1174.

[33] Crepaldi A et al 2012 Phys. Rev. Lett. 109 096803

[34] E. Buzdin, 2008,PhysRevB.67.184505.

[35] E. Buzdin,Nat.phys.Eschrig,2008.

[36] E. Buzdin, PhysRevB.76.224525.

[37] E. Buzdin,PhysRevLett.98.077003.

[38] E. Buzdin,PhysRevLett.102.017001.

[39] A. Zazunov, A. Schulz, R. Egger, Phys. Rev. Lett. 102, 047002 (2009).

[40] Aldo Brunetti, Alex Zazunov, Arijit Kundu, and Reinhold Egger Phys. Rev. B 88, 144515 – Published 25 October 2013.

[41] A. A. Reynoso, Gonzalo Usaj, C. A. Balseiro, D. Feinberg, and M. Avignon Phys. Rev. Lett. 101, 107001 – Published 2 September 2008.

[42] Andres A. Reynoso, Gonzalo Usaj, C. A. Balseiro, D. Feinberg, M. Avignon, Phys. Rev. B 86, 214519 (2012).

[43] Tomohiro Yokoyama, Mikio Eto, Yuli V. Nazarov, J. Phys. Soc. Jpn. 82 (2013) 054703.

[44] Tomohiro Yokoyama, Mikio Eto, Yuli V. Nazarov, Phys. Rev. B 89, 195407 (2014).

[45] I.V. Krive, A.M. Kadigrobov, R.I. Shekhter, M. Jonson, 10.1103/PhysRevB.71.214516, 2004.

[46] I. V. Krive, A. M. Kadigrobov, R. I. Shekhter, and M. Jonson Phys. Rev. B 71, 214516 – Published 17 June 2005.

[47] M. A. Silaev, I. V. Tokatly, and F. S. Bergeret Phys. Rev. B 95, 184508 – Published 10 May 2017.

[48] Konstantin N. Nesterov, Manuel Houzet, and Julia S. Meyer Phys. Rev. B 93, 174502 – Published 3 May 2016.

[49] Pasquale Marra, Roberta Citro, and Alessandro Braggio Phys. Rev. B 93, 220507(R) – Published 20 June 2016.

[50] Constantin Schrade, Silas Hoffman, and Daniel Loss Phys. Rev. B 95, 195421 – Published 19 May 2017.

[51] D. B. Szombati, S. Nadj-Perge, D. Car, S. R. Plissard, E. P. A. M. Bakkers, L. P. Kouwenhoven, Nat. Phys. 12 (2016) 568.

[52] C.W.J. Beenakker, Transport Phenomena in Mesoscopic Systems, edited by H. Fukuyama and T. Ando (Springer, Berlin, 1992).

[53] G. Wendin and V. S. Shumeiko, Low Temperature Physics 33, 724 (2007).

[54] P. G. de Gennes, Superconductivity of Metals and Alloys. New York: W. A. Benjamin. ISBN 978-0-7382-0101-6, (1966).

[55] A.F. Andreev, "Thermal conductivity of the intermediate state of superconductors". Sov. Phys. JETP. 19: 1228, (1964).

[56] S. Nadj-Perge, et all, Science, 31 october 2014.

[57] J. Alicea, Y. Oreg, G. Refael, F. von Oppen, M. P. A. Fisher, Nature Physics 7, 412-417 (2011).

[58] Nayak, Chetan; Simon, Steven H.; Stern, Ady; Freedman, Michael; Das Sarma, Sankar (2008). "Non-Abelian anyons and topological quantum computation". Reviews of Modern Physics. 80 (3): 1083–1159.

[59] V. Mourik, K. Zuo, S. M. Frolov, S. R. Plissard, E. P. A. M. Bakkers and L. P. Kouwenhoven, Science 336, 1003 (2012).

[60] M. T. Deng, C. L. Yu, G. Y. Huang, M. Larsson, P. Caro, H. Q. Xu, Nano Lett. 12, 6414 (2012).

[61] A. Das, Y. Ronen, Y. Most, Y. Oreg, M. Heiblum, H. Shtrikman, Nat. Phys. 8, 887 (2012).

[62] A. D. K. Finck, D. J. Van Harlingen, P. K. Mohseni, K. Jung, X. Li, Phys. Rev. Lett. 110, 126406 (2013).

[63] H. O. H. Churchill, V. Fatemi, K. Grove-Rasmussen, M. T. Deng, P. Caro, H. Q. Xu, C. M. Marcus, arXiv:1303.2407 (2013).

[64] S. Hegde, S. Vishveshwara, Phys. Rev. B 94, 115166 (2016).

[65] W. DeGottardi, D. Sen, and S. Vishveshwara, New J. Phys. 13, 065028 (2011).

[66] J. J. M. Verbaarschot and I. Zahed, Phys. Rev. Lett. 70, 3853 ˜1993!; J. J. M. Verbaarschot, ibid. 72, 2531 (1994).

[67] R. Gade, Nucl. Phys. B 398, 499 (1993).

[68] K. Slevin and T. Nagao, Phys. Rev. Lett. 70, 635 (1993).

[69] E. P. Wigner, Proc. Cambridge Philos. Soc. 47, 790 (1951); Ann. Math. 67, 325 (1958).

[70] F. J. Dyson, J. Math. Phys. 3, 140, 1199 (1962).

[71] A.Altland and M. R. Zirnbauer, Phy Rev B, 55, 2 (1997).

[72] C.V.J. Beenakker, Rev. Mod. Phys. 87, 1037 (2015).

[73] Youla, D. C., 1961, Canad. J. Math. 13, 694.

[74] R.B.Griffiths: Nonanalytic Behavior Above Critical Point in a Random Ising Ferromagnet. Phys. Rev. Lett. 23, 17–19 (1969).

[75] T. Vojta, J. Phys. A: Math. Gen. 39 (2006) R143–R205.

[76] T. Vojta, Phases and phase transitions in disordered quantum systems (...)

[77] O. Motrunich, K. Damle, and D. A. Huse, Phys Rev B 63 ,224204, (2001).

[78] D.A. Ivanov, P.M. Ostrovsky, M.A. Skvortsov, Europhys Lett. 106, 37006, (2014).

[79] P. Schmitteckert, T. Schulze, C. Schuster, P. Schwab, and U. Eckern, Phys. Rev. B 80, 560, (2013).

[80] J. D. Sau, S. Das Sarma, Phys. Rev. B 88, 064506 (2013).

[81] Chiani M , Journal of Multivariate Analysis. 129: 69–81 (2014).

[82] A. M. Lobos, R. M. Lutchyn, S. Das Sarma, Phys. Rev. Lett. 109, 146403 (2012).

[83] P. W. Brouwer, M. Duckheim, A. Romito, and F. von Op- pen, Phys. Rev. Lett. 107, 196804 (2011).

[84] P. W.Brouwer, A. Furusaki, I. A. Gruzberg, and C. Mudry, Phys. Rev. Lett. 85, 1064 (2000).

[85] Gruzberg, I. A., N. Read, and S. Vishveshwara, Phys. 32 Rev. B 71, 245124 (2005).

[86] I. Affleck, D. Giuliano, Screening Clouds and Majorana Fermions, Journal of Statistical Physics, 1547 (4), 666-691 (2014).

[87] Y. Aharonov, Bohm D., Significance of electromagnetic potentials in quantum theory, Phys. Rev., 115, 485–491 (1959).

[88] M. Buttiker, Y. Imry, and R. Landauer, Josephson behavior in small normal one-dimensional rings , Physics Letters A, 96(7), 365-367 (1983).

[89] S. K. Maiti, Persistent Current in Metallic Rings and Cylinders , Solid State Phenomena, Vol. 155 pp. 87-104, (2009).

[90] L.P. Levy, G. Dolan, J. Dumsmuir, H. Bouchiat, Phys. Rev. Lett. 64, 2074,(1990).

[91] V. Chandrasekhar, R.A. Webb, H.J. Brandy, M. Ketchen, W.J. Gallagher, A. Kleinsasser, Phys. Rev. Lett. 67, 3578, (1991).

[92] Piet W. Brouwer, Jeroen Danon, Semiclassical theory of persistent current fluctuations in ballistic chaotic rings , NBI CMT QDEV ,(2015).

[93] G. Campagnano, R. Giuliano, D. Giuliano, P. Lucignano, A. Tagliacozzo, IEEE Transactions on Applied Superconductivity, 28, 7 , (2018).

[94] J. Bardeen, R. Kummel, A. E. Jacobs, and L. Tewordt, Phys. Rev. 187, 556 (1969).

[95] C. Beenakker, "Three "universal" mesoscopic josephson effects," in Transport phenomena in mesoscopic systems, H. Fukuyama and T. Ando, Eds. Springer, Berlin, 1992.

[96] E. Akkermans, A. Auerbach, J. E. Avron, and B. Shapiro, Phys. Rev. Lett. 66, 76 (1991).

[142] A. Y. Kitaev, Physics-Uspekhi **44**, 131 (2001).

[98] R. M. Lutchyn, J. D. Sau, and S. Das Sarma, Phys. Rev. Lett. **105**, 077001 (2010).

[99] Y. Oreg, G. Refael, and F. von Oppen, Phys. Rev. Lett. **105**, 177002 (2010).

[100] P. Jordan and E. Wigner, Z. Phys. **47**, 531 (1928).

[101] A. Nava, R. Giuliano, G. Campagnano, and D. Giuliano, Phys. Rev. B **94**, 205125 (2016).

[102] A. R. Akhmerov, J. P. Dahlhaus, F. Hassler, M. Wimmer, and C. W. J. Beenakker, Phys. Rev. Lett. **106**, 057001 (2011).

[140] J. Cayssol, T. Kontos, and G. Montambaux, Phys. Rev. B **67**, 184508 (2003).

[104] A. Nava, R. Giuliano, G. Campagnano, D. Giuliano, Phys. Rev. B 95, 155449 (2017).

[105] A. Nava, R. Giuliano, G. Campagnano, D. Giuliano, Phys. Rev. B 94, 205125 (2016).

[159] F. Pientka, A. Romito, M. Duckheim, Y. Oreg, and F. von Oppen, New Journal of Physics **15**, 025001 (2013).

[107] P. W. Brouwer, M. Duckheim, A. Romito, and F. von Oppen, Phys. Rev. B **84**, 144526 (2011).

[108] P. W. Brouwer, M. Duckheim, A. Romito, and F. von Oppen, Phys. Rev. Lett. **107**, 196804 (2011).

[109] F. Pientka, G. Kells, A. Romito, P. W. Brouwer, and F. von Oppen, Phys. Rev. Lett. **109**, 227006 (2012).

[110] N. M. Gergs, L. Fritz, and D. Schuricht, Phys. Rev. B **93**, 075129 (2016).

[111] W. DeGottardi, M. Thakurathi, S. Vishveshwara, and D. Sen, Phys. Rev. B **88**, 165111 (2013).

[112] J. D. Sau, S. Tewari, and S. Das Sarma, Phys. Rev. B **85**, 064512 (2012).

[113] J. D. Sau and S. Das Sarma, Phys. Rev. B **88**, 064506 (2013).

[114] C. W. J. Beenakker, Rev. Mod. Phys. **69**, 731 (1997).

[115] A. Altland and M. R. Zirnbauer, Phys. Rev. B **55**, 1142 (1997).

[116] S. S. Hegde and S. Vishveshwara, Phys. Rev. B **94**, 115166 (2016).

[117] O. Motrunich, K. Damle, and D. A. Huse, Phys. Rev. B **63**, 224204 (2001).

[118] M. Bocquet, D. Serban, and M. Zirnbauer, Nuclear Physics B **578**, 628 (2000), ISSN 0550-3213.

[119] M. L. Mehta, Random Matrices (Elsevier Academic Press, Amsterdam, 2004).

[120] C. W. J. Beenakker, Rev. Mod. Phys. **87**, 1037 (2015).

[121] D. Thouless, Physics Reports **13**, 93 (1974), ISSN 0370-1573.

[122] J. T. Edwards and D. J. Thouless, Journal of Physics C: Solid State Physics **5**, 807 (1972).

[123] N. M. Gergs, L. Fritz, and D. Schuricht, Phys. Rev. B **93**, 075129 (2016).

[124] V. Mourik, K. Zuo, S. M. Frolov, S. R. Plissard, E. P. A. M. Bakkers, and L. P. Kouwenhoven, Science **336**, 1003 (2012).

[125] G. D. Affleck Ian, Journal of Statistical Physics **157**, 666 (2014).

[126] S. D. S. J. D. Sau, Phys. Rev. B **88**, 064506 (2013).

[127] M. Thinkam, Introduction to Superconductivity (Dover, New York, 2004).

[128] Y. Imry, Introduction to Mesoscopic Physics (Oxford University Press, London, 2002).

[129] J. File and R. G. Mills, Phys. Rev. Lett. **10**, 93 (1963).

[130] M. Büttiker, Y. Imry, and M. Landauer, Phys. Lett. A **96**, 365 (1983).

[131] H. Bluhm, N. C. Koshnick, J. A. Bert, M. E. Huber, and K. A. Moler, Phys. Rev. Lett. **102**, 136802 (2009).

[132] A. C. Bleszynski-Jayich, W. E. Shanks, B. Peaudecerf, E. Ginossar, F. von Oppen, L. Glazman, and J. G. E. Harris, **326**, 272 (2009).

[133] H.-F. Cheung, Y. Gefen, E. K. Riedel, and W.-H. Shih, Phys. Rev. B **37**, 6050 (1988).

[134] G. Montambaux, H. Bouchiat, D. Sigeti, and R. Friesner, Phys. Rev. B **42**, 7647 (1990).

[135] D. Loss and P. Goldbart, Phys. Rev. B **43**, 13762 (1991).

[136] A. Müller-Groeling, H. A. Weidenmüller, and C. H. Lewenkopf, EPL (Europhysics Letters) **22**, 193 (1993).

[137] J. Splettstoesser, M. Governale, and U. Zülicke, Phys. Rev. B **68**, 165341 (2003).

[138] B. J. Ferry D. K., Goodnick S. M., Transport in Nanostructures (Cambridge University Press, Cambridge, 2009).

[139] F. V. M., Physics of Quantum Rings (Springer-Verlag, Berlin, 2014).

[140] J. Cayssol, T. Kontos, and G. Montambaux, Phys. Rev. B **67**, 184508 (2003).

[141] M. Büttiker and T. M. Klapwijk, Phys. Rev. B **33**, 5114 (1986).

[142] A. Y. Kitaev, Physics-Uspekhi **44**, 131 (2001).

[143] R. M. Lutchyn, J. D. Sau, and S. Das Sarma, Phys. Rev. Lett. **105**, 077001 (2010).

[144] Y. Oreg, G. Refael, and F. von Oppen, Phys. Rev. Lett. **105**, 177002 (2010).

[145] V. Mourik, K. Zuo, S. M. Frolov, S. R. Plissard, E. P. A. M. Bakkers, and L. P. Kouwenhoven, **336**, 1003 (2012).

[146] J. Liu, A. C. Potter, K. T. Law, and P. A. Lee, Phys. Rev. Lett. **109**, 267002 (2012).

[147] E. Dumitrescu, B. Roberts, S. Tewari, J. D. Sau, and S. Das Sarma, Phys. Rev. B **91**, 094505 (2015).

[148] F. Dessotti, L. Ricco, Y. Marques, L. Guessi, M. Yoshida, M. Figueira, M. de Souza, P. Sodano, and A. Seridonio (arXiv:1605.04325).

[149] P. Lucignano, F. Tafuri, and A. Tagliacozzo, Phys. Rev. B **88**, 184512 (2013).

[150] P. Jacquod and M. Büttiker, Phys. Rev. B **88**, 241409 (2013).

[151] G. E. Blonder, M. Tinkham, and T. M. Klapwijk, Phys. Rev. B **25**, 4515 (1982).

[152] I. Affleck, J.-S. Caux, and A. M. Zagoskin, Phys. Rev. B **62**, 1433 (2000).

[153] C. W. J. Beenakker, Phys. Rev. Lett. **67**, 3836 (1991).

[154] A. Furusaki and M. Tsukada, Solid State Communications **78**, 299 (1991).

[155] I. Affleck and D. Giuliano, Journal of Statistical Physics **157**, 666 (2014).

[156] D. Giuliano and I. Affleck, Phys. Rev. B **90**, 045133 (2014).

[157] K. A. Matveev, A. I. Larkin, and L. I. Glazman, Phys. Rev. Lett. **89**, 096802 (2002).

[158] M. Lee, H. Khim, and M. Choi, Phys. Rev. B **89**, 035309 (2014).

[159] F. Pientka, A. Romito, M. Duckheim, Y. Oreg, and F. von Oppen, New Journal of Physics **15**, 025001 (2013).

[160] C. W. J. Beenakker, D. I. Pikulin, T. Hyart, H. Schomerus, and J. P. Dahlhaus, Phys. Rev. Lett. **110**, 017003 (2013).

[161] I. Affleck and D. Giuliano, Journal of Statistical Physics **157**, 666 (2014), ISSN 1572-9613.

[162] C. W. J. Beenakker, D. I. Pikulin, T. Hyart, H. Schomerus, and J. P. Dahlhaus, Phys. Rev. Lett. **110**, 017003 (2013).

[163] K. T. Law, P. A. Lee, and T. K. Ng, Phys. Rev. Lett. **103**, 237001 (2009).

[164] C. Jayaprakash, H. R. Krishna-murthy, and J. W. Wilkins, Phys. Rev. Lett. **47**, 737 (1981).

[165] B. A. Jones, C. M. Varma, and J. W. Wilkins, Phys. Rev. Lett. **61**, 125 (1988).

[166] I. Affleck and A. W. W. Ludwig, Phys. Rev. Lett. **68**, 1046 (1992).

[167] I. Affleck, A. W. W. Ludwig, and B. A. Jones, Phys. Rev. B **52**, 9528 (1995).

[168] K. A. Matveev, D. Yue, and L. I. Glazman, Phys. Rev. Lett. **71**, 3351 (1993).

[169] D. Yue, L. I. Glazman, and K. A. Matveev, Phys. Rev. B **49**, 1966 (1994).

[170] S. Lal, S. Rao, and D. Sen, Phys. Rev. B **66**, 165327 (2002).

[171] D. Giuliano and A. Nava, Phys. Rev. B **92**, 125138 (2015).